2017-04-01

Full-Scale Pavement Testing of Aggregate Base Material Stabilized with Triaxial Geogrid

Shaun Todd Hilton
Brigham Young University

Full-Scale Pavement Testing of Aggregate Base Material Stabilized with Triaxial Geogrid

Shaun Todd Hilton

A thesis submitted to the faculty of
Brigham Young University
in partial fulfillment of the requirements for the degree of

Master of Science

W. Spencer Guthrie, Chair
Grant G. Schultz
E. James Nelson

Department of Civil and Environmental Engineering

Brigham Young University

ABSTRACT

Full-Scale Pavement Testing of Aggregate Base
Material Stabilized with Triaxial Geogrid

Shaun Todd Hilton
Department of Civil and Environmental Engineering, BYU
Master of Science

The objective of this research was to investigate the structural capacity of aggregate base materials stabilized with triaxial geogrid placed in a full-scale pavement involving control, or unstabilized, sections. Field testing was performed on a roadway in northeastern Utah that was 16 km (10 miles) long and included 10 test sections, seven stabilized sections and three control sections, each having five test locations. The pavement structure was comprised of a hot mix asphalt layer overlying an untreated aggregate base layer of varying thickness, depending on the test section. Except for the control sections, one or two layers of geogrid were incorporated into portions of the pavement structure at different locations.

Falling-weight deflectometer testing and dynamic cone penetrometer testing were used to evaluate the structural capacity of the aggregate base layer in each pavement section. For data analysis, the Rohde's method was applied in conjunction with the 1993 American Association of State Highway and Transportation Officials pavement design guide methodology, and the Area under the Pavement Profile (AUPP) method was applied in conjunction with a mechanistic-empirical pavement analysis. Statistical analyses were then performed to enable comparisons of the test sections.

Field results indicated that the asphalt layer thickness was consistently 140 mm (5.5 in.) at all 10 test sections, and the base layer thickness varied from 360 mm (14 in.) to 510 mm (20 in.). The results of the statistical analyses indicated that the majority of the 45 possible pairwise comparisons among the test sections were not statistically significant, meaning that variations in the presence and position of triaxial geogrid at those sections did not appear to affect the structural capacity. The remaining comparisons, however, were statistically significant and involved the test sections with the highest structural capacity. While one of these was unexpectedly an unstabilized control section, the others were constructed using one or two layers of geogrid in the base layer. In addition to being statistically significant, the observed differences were also practically important. Increases in the observed base layer coefficient from 0.12 to 0.18 correspond to an increase in the allowable number of equivalent single axle loads (ESALs) from 5.9 million to 19.2 million at the research site, while decreases in the observed AUPP value from 340 mm (13.37 in.) to 213 mm (8.38 in.) correspond to an increase in the allowable number of ESALs from 3.7 million to 17.3 million at the research site. These results indicate that, when geogrid reinforcement is compatible with the given aggregate base material and proper construction practices are followed, statistically significant and practically important increases in pavement design life can be achieved.

Key words: aggregate base material, Area under the Pavement Profile method, Rohde's method, structural capacity, triaxial geogrid

ACKNOWLEDGEMENTS

Tensar International Corporation provided funding and technical support for this research. The Utah Department of Transportation performed falling-weight deflectometer testing at the research site, and Jones and DeMille Engineering provided helpful pavement construction information. I acknowledge and greatly appreciate the assistance of Brigham Young University students Jared Baxter, Katri Clay, Cameron Lusvardi, Mercedes Richardson, Rawley Selk, Elizabeth Smith, Robert Stevens, Eric Sweat, Callie Vogel, and Tenli Waters with the field and laboratory testing and data analysis required for this research. I also appreciate Eric Sweat's assistance with the literature review completed for this research. I acknowledge Dr. Dennis L. Eggett of the Brigham Young University Center for Collaborative Research and Statistical Consulting, who assisted with the statistical analyses. I appreciate the support, guidance, and mentorship given by Dr. Grant G. Schultz and Dr. E. James Nelson as members of my graduate advisory committee. I am especially grateful for Dr. W. Spencer Guthrie, who has spent countless hours working with and aiding me throughout my scholastic endeavors; his friendship and tutelage have taught me valuable life lessons, specifically caring for the individual, respect, diligence, and hard work. Lastly, and most importantly, I thank my wife, McKell. All of my success and accomplishments can certainly be attributed to the wonderful love, support, and never-ending encouragement that she always gives to me.

TABLE OF CONTENTS

LIST OF TABLES

LIST OF FIGURES

1 INTRODUCTION

1.1 Problem Statement

Using geogrid reinforcement in pavement construction has become an increasingly common practice within the past decade. Geogrid reinforcement, available in both biaxial and triaxial configurations as shown in Figure 1-1, is typically positioned beneath and/or within an aggregate base layer and is designed to prevent lateral spreading of the individual aggregate particles comprising that layer (Aran 2006, Kwon et al. 2008, Kwon and Tutumluer 2009, Moayedi et al. 2009). Thus, to the extent that the given geogrid and aggregate base material are compatible (Knighton 2015), inter-particle friction can be increased among the individual aggregate particles above and potentially below the geogrid. When this occurs, the result is an

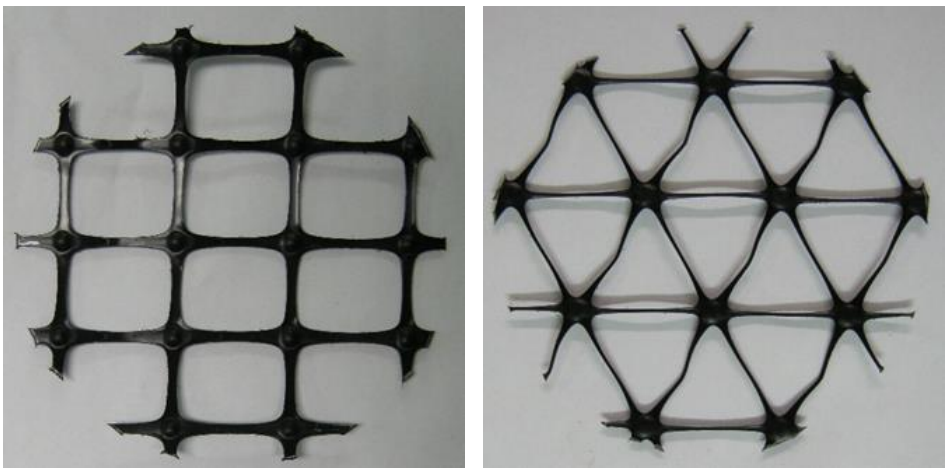

(a) (b)

Figure 1-1: Examples of (a) biaxial and (b) triaxial geogrid.

increase in the stiffness of the aggregate base layer that leads to a greater load-carrying capacity of the pavement (Henry et al. 2011, Kwon and Tutumluer 2009, Schuettpelz et al. 2009, Tingle and Jersey 2009).

Several laboratory and field studies have been performed to characterize the properties of aggregate base materials stabilized with geogrid. While many of these studies focused mainly on biaxial geogrid (Al-Qadi et al. 2008, Hufenus et al. 2006, Joshi and Zornberg 2011, Kwon and Tutumluer 2009, Reck 2009), others have included triaxial geogrid (Nelson et al. 2012, Wayne 2016, Wayne et al. 2011a, Wayne et al. 2011b, Wayne et al. 2011c, White et al. 2011). Selected studies have also been performed to investigate differences in the behavior of aggregate base materials stabilized with biaxial and triaxial geogrid (Jas et al. 2015). While these studies have advanced understanding of the potential benefits associated with using geogrid stabilization, the results have typically been limited in their application to specific geogrid products, specific aggregate base materials, and/or specific conditions. The Federal Highway Administration (FHWA) has explained that developing a generic specification for geogrid reinforcement for use in pavements has been difficult, in part, because of the proprietary nature of geogrid products and a lack of performance documentation (FHWA 2008); for these reasons, well designed field experiments are an especially valuable part of continuing research on the use of geogrid for stabilizing aggregate base materials in pavement structures. To further investigate the efficacy of triaxial geogrid for stabilizing aggregate base materials, Tensar International Corporation, a leading manufacturer of geogrid, requested full-scale field testing of a roadway constructed in northeastern Utah.

1.2 Research Objective and Scope

The objective of this research was to investigate the structural capacity of aggregate base materials stabilized with triaxial geogrid (Tensar TX140) placed in a full-scale pavement involving control, or unstabilized, sections. The scope of this research included evaluation of 10 test sections along an approximately 16-km (10-mile) roadway in northeastern Utah, where the test sections were distinguished by base layer thickness and the presence and position of triaxial geogrid. The results of this study provide additional information about the ability of triaxial geogrid to improve the mechanical properties of aggregate base layers in pavement structures.

1.3 Outline of Report

This report contains five chapters. This chapter introduces the research, defines the problem statement, and states the research objective and scope. Chapter 2 provides background information obtained from a literature review about the use of geogrid-stabilized aggregate base materials in flexible pavements. Chapters 3 and 4 detail the procedures and results of this research, respectively. Chapter 5 provides a summary together with conclusions and recommendations resulting from this research.

2 BACKGROUND

2.1 Overview

This chapter provides background information obtained from a literature review about the use of geogrid-stabilized aggregate base materials in flexible pavements. A brief description of geogrids and a discussion of their use are presented in the following sections.

2.2 Geogrid Description

Geogrid is a high-strength extruded geosynthetic material consisting of connected sets of tensile ribs with apertures that can be penetrated by surrounding aggregate particles (Aran 2006, Reck 2009). Characteristics of geogrid differ due to varying geometric, mechanical, and durability properties (Hanes Geo Components 2015, Tensar International Corporation 2016). Geometric properties include aperture shapes and sizes along with rib spacing, depth, width, length, and shape. Biaxial geogrids, which have square or rectangular aperture shapes, provide tensile strength in two directions, while triaxial geogrids, which have triangular aperture shapes, provide tensile strength in three directions. The aperture size directly determines the degree to which aggregate particles can penetrate the geogrid. A general recommendation is that the minimum aperture size of the geogrid should be at least equal to the particle size corresponding to 50 percent passing (D_{50}) of the aggregate being placed on the geogrid, but not less than 13 mm (0.5 in.), and the maximum aperture size should be less than or equal to twice the particle

diameter corresponding to 85 percent passing (D_{85}), but not greater than 76 mm (3 in.) (FHWA 2008). Mechanical properties include tensile strength, radial stiffness, aperture stability, and flexural rigidity of the geogrid. Durability is a measure of the resistance of geogrid to ultraviolet degradation, installation damage, and chemical damage (Hanes Geo Components 2015, Tensar International Corporation 2016).

2.3 Geogrid Use in Pavement Structures

Many field and laboratory studies regarding geogrid reinforcement and pavement performance have been conducted to investigate the benefits of geogrid-stabilized aggregate base materials in flexible pavements (Al-Qadi et al. 2008, Haas et al. 1988, Huntington and Ksaibati 2000, Kwon and Tutumluer 2009, Tingle and Jersey 2009). Although the general consensus is that geogrid can be beneficial, quantifying the effect of including geogrid reinforcement in pavement structures has proven to be difficult (Aran 2006, Hall et al. 2004). Because laboratory evaluations of geogrid reinforcement do not usually account for environmental, trafficking, and subgrade capacity variations associated with actual pavement structures in the field, full-scale field studies of geogrid-stabilized pavement structures are often preferred for evaluating potential benefits of geogrid (Al-Qadi et al. 2008, Barksdale et al. 1989, Brandon et al. 1996, Helstrom et al. 2006, Joshi and Zomberg 2011). Furthermore, the use of control, or unstabilized, sections is critical in such investigations (Holder and Andrae 2004).

As discussed in the following sections, previous studies have incorporated full-scale experimentation and testing to evaluate performance, stiffness, and strength improvements in geogrid-stabilized aggregate base materials. Specifically, researchers have explored the possible requirement for a conditioning period, identified a zone of influence resulting from geogrid

reinforcement, and investigated the effects of different geogrid positions within pavement structures.

2.3.1 Conditioning Period

Research suggests that a sufficient conditioning period may be required before the full effects of geogrid reinforcement on pavement performance can be observed (Kwon and Tutumluer 2009). A sufficient conditioning period has been defined as the time required for the geogrid and surrounding aggregate particles to fully interlock (Tingle and Jersey 2009). For a given geogrid and aggregate base material, the length of the conditioning period is presumed to vary depending on the amount of trafficking, where higher traffic loads and/or volumes are expected to aid in the densification of the aggregate base material and its interlock with the geogrid (Hall et al. 2004, Helstrom et al. 2006).

In full-scale pavement testing conducted in Mississippi (Tingle and Jersey 2009), researchers showed that an adequate trafficking and densification period was required before optimal geogrid performance was achieved. As summarized in Table 2-1, eight 3.7-m by 7.3-m (12-ft by 24-ft) full-scale pavement sections were constructed for testing. Each pavement section

Table 2-1: Experimental Design for Mississippi Study

Test Section	Base Material	Base Thickness, mm (in.)	Geogrid Reinforcement Present	Geotextile Present
1	Crushed Aggregate	150 (6)	No	No
2	Clay Gravel	150 (6)	No	No
3	Crushed Limestone	150 (6)	No	No
4	Crushed Limestone	150 (6)	No	Yes
5	Crushed Limestone	150 (6)	Yes	Yes
6	Crushed Limestone	150 (6)	Yes	No
7	Clay Gravel	150 (6)	Yes	No
8	Crushed Aggregate	150 (6)	Yes	No

was constructed on native silty clay subgrade material that was surfaced with a 610-mm (24-in.) layer of high-plasticity clay and an unsurfaced 150-mm (6-in.) base layer comprised of crushed aggregate, crushed limestone, or clay gravel. The high-plasticity clay layer was specified to ensure consistency in the underlying base layer support across all eight pavement sections. Each test section was trafficked with a dual-wheel tandem-axle truck loaded to 19.8 metric tons (21.8 tons), and falling-weight deflectometer (FWD) testing was performed after different numbers of total truck passes, specifically 0, 1,000, 5,500, and 10,000, to quantify the structural capacity of each section. From the FWD data, the highest backcalculated modulus values of the base layer were observed at 5,500 passes of the truck, and the increase in stiffness was attributed to the development of progressively greater aggregate interlock with the geogrid. In this study, the modulus values of the geogrid-stabilized base layers were generally lower than those of the unstabilized base layers in two of the comparisons for which FWD data were presented in this study; however, three of the four geogrid-stabilized sections did not exhibit rutting failure, which was defined as more than 75 mm (3 in.) of permanent deformation after 10,000 truck passes, while only two of the unstabilized sections, including one with a geotextile, did not fail in rutting. Overall, despite having lower average base layer stiffness, the geogrid-stabilized test sections demonstrated an improved resistance to rutting in comparison to the unstabilized sections.

Research performed in Wyoming compared the performance of two pavement sections; one was an unstabilized section with a 430-mm (17-in.) conventional granular base layer, and the other was a geogrid-stabilized section with a 280-mm (11-in.) base layer (Huntington and Ksaibati 2000). Testing consisting of FWD measurements, rutting evaluations, and pavement condition surveys was performed shortly after construction of the roadway and again after three

years of trafficking to evaluate the performance of the sections. The results of the FWD testing indicated that the stiffness of the geogrid-stabilized section was initially lower than that of the unstabilized section but increased during the three-year period to a level equal to or surpassing that of the unstabilized section by the end of the study. The rutting evaluations indicated that the unstabilized and geogrid-stabilized test sections were equivalent after three years of service. In the pavement condition surveys, no other distresses were identified in either section of the pavement. The researchers concluded that a 150-mm (6-in.) reduction in base thickness, in this case from 430 mm (17 in.) to 280 mm (11 in.), was possible with the inclusion of geogrid (Huntington and Ksaibati 2000).

These field studies substantiate the idea that quantifying the benefit of geogrid reinforcement in a pavement section requires an adequate conditioning period, which allows the geogrid and surrounding aggregate base material to fully interlock. Although exact predictions of the length of the conditioning period are probably not possible, several months or even a few years may be required in some cases.

2.3.2 Zone of Influence

The spatial extent of increased stiffness in the immediate vicinity of geogrid reinforcement can be quantified in terms of a zone of influence. The zone of influence may or may not extend through the entire base course layer, depending on the degree of interlock between the geogrid and aggregate and the thickness of the base layer (Edil et al. 2007, Tutumluer et al. 2009). Therefore, when the degree of interlock is lower and/or the base layer is thicker, increases in stiffness can be more difficult to detect (Schuettpelz et al. 2009).

In a study performed in California (Kwon and Tutumluer 2009), researchers investigated aggregate interlock associated with geogrid-stabilized base layers in pavements along with the

increase in stiffness in the vicinity of the geogrid. Geogrid was placed at the base-subgrade interface in pavements with varying cross sections and trafficked for five years. Two geogrid-stabilized sections included 150 mm (6 in.) of base and 280 mm (11 in.) of hot mix asphalt (HMA), while two unstabilized sections consisted of either 460 mm (18 in.) or 480 mm (19 in.) of base and 230 mm (9 in.) of HMA. The study lacked a proper control section, such that the higher stiffness of the 150 mm (6 in.) of base material in the stabilized section compared to the upper 150 mm (6 in.) of base material in the unstabilized section could not be clearly attributed to only the presence of geogrid; however, the results of dynamic cone penetrometer (DCP) testing indicated a uniform stiffness throughout the full depth of the stabilized 150-mm (6-in.) base layers. This result suggests that the zone of influence of the geogrid may have extended 150 mm (6 in.) above the geogrid in the stabilized sections.

In a study performed in Illinois (Kwon et al. 2008), nine full-scale pavement test sections were constructed with varying cross sections, as shown in Table 2-2, to evaluate the effectiveness of geogrid reinforcement. The pavement sections were subjected to accelerated

Table 2-2: Experimental Design for Illinois Study

Section	HMA Thickness, mm (in.)	Base Thickness, mm (in.)	Geogrid or Control	Position of Reinforcement
A-1	75 (3)	200 (8)	Geogrid	Base-subgrade interface
A-2	75 (3)	200 (8)	Geogrid	Base-subgrade interface
A-3	75 (3)	200 (8)	Control	-
B-1	75 (3)	300 (12)	Control	-
B-2	75 (3)	300 (12)	Geogrid	Base-subgrade interface
C-1	75 (3)	300 (12)	Control	-
D-1	75 (3)	460 (18)	Geogrid	6 in. below HMA
D-2	75 (3)	460 (18)	Geogrid	6 in. below HMA and at base-subgrade interface
D-3	75 (3)	460 (18)	Control	-

loading using a dual-tire assembly with an applied load of 40.0 kN (9,000 lb), a tire inflation pressure of 690 kPa (100 psi), and a traverse speed of 8 kph (5 mph). Numbers of passes ranging from 3,300 to 89,000 were applied to the test sections until failure, which was defined as 25 mm (1 in.) of rutting, or until a terminal number of passes was reached. Although the exact spatial extent was not quantified, the researchers cited a region of increased stiffness immediately above the geogrid reinforcement that was attributed to aggregate interlock with the geogrid; this conclusion was supported by rutting profiles observed through open trenches excavated after the testing was complete. The stabilized sections exhibited less rutting in the base layers and/or sustained greater numbers of load repetitions before failure than the unstabilized sections (Kwon et al. 2008).

Laboratory testing performed in Montana addressed the presence of a zone of influence in geogrid-stabilized aggregate base material specimens (Perkins et al. 2004). In this testing, a circle of geogrid was positioned horizontally at the center of 300-mm by 610-mm (12-in. by 24-in.) specimens during the compaction process. Results from repeated load permanent deformation testing showed that the geogrid reinforcement restrained radial movement of the aggregate within a region that extended approximately one radius of the laboratory specimen being tested, or 150 mm (6 in.) in this case, above and below the reinforcement (Perkins et al. 2004).

The field and laboratory studies presented in this section demonstrate the occurrence of a zone of influence in the immediate vicinity of geogrid reinforcement. Although exact measurements of the extent of the zone of influence have not been commonly reported, values approaching 150 mm (6 in.) may be possible in some cases.

2.3.3 Optimal Geogrid Position

Several studies have been performed to identify the optimal position for geogrid reinforcement in a pavement structure. Researchers in Illinois (Al-Qadi et al. 2008) tested pavement sections, previously shown in Table 2-2, to evaluate the effects of geogrid reinforcement with respect to geogrid position in a pavement structure. Results from performance testing under accelerated trafficking, including rutting, cracking, and visual observation, indicated that the optimal geogrid reinforcement position in thin base layers is at the base-subgrade interface. Thin base layers for this research consisted of layers in the range of 200 mm (8 in.) to 460 mm (18 in.) thick. For thicker base layers, greater than 460 mm (18 in.), the researchers suggested installing geogrid at two positions, one at the base-subgrade interface and the other at the upper one-third position within the base layer. Pavement sections were constructed over a weak subgrade with a California bearing ratio (CBR) value of 4.

Laboratory testing performed in Canada (Haas et al. 1988) on full-scale pavement sections involved varying subgrade strengths (CBR values ranging from 1 to 8), varying thicknesses of stabilized and unstabilized granular base layers (100 mm (4 in.) to 300 mm (12 in.)), and varying HMA thicknesses (50 mm (2 in.) to 100 mm (4 in.)) in order to evaluate different geogrid positions in pavement structures. Single layers of geogrid reinforcement were placed in the upper, middle, or bottom portions of the base layers, and a single test section including two layers of geogrid reinforcement placed at the middle and bottom of the base layer was also evaluated. Based on stress, strain, and deflection data obtained in the testing, the conclusion of this work was that the optimum geogrid position was at the base-subgrade interface. However, for very thick base layers, the researchers stated that the use of two layers of

geogrid reinforcement, one placed at the base-subgrade interface and the other at the middle of the base layer, may help delay permanent deformation within the pavement.

In one laboratory study in Louisiana (Chen and Abu-Farsakh 2012), geogrid reinforcement was placed at one of three positions, including the base-subgrade interface, the middle of the base layer, or the upper one-third position within the base layer, in full-scale pavement sections constructed in a 2.0-m by 2.0-m by 1.7-m (6.5-ft by 6.5-ft by 5.5-ft) test box. The aggregate base layer was 300 mm (12 in.) thick and was surfaced with a 19-mm (0.75-in.)-thick HMA layer. A 40.0-kN (9,000-lb) load was applied through a single wheel with a tire pressure of 550 kPa (80 psi). The number of load cycles recorded for each pavement section was used in backcalculating effective base resilient modulus values using the Mechanistic-Empirical Pavement Design Guide software with a failure criterion of 19 mm (0.75 in.) of rutting. The backcalculated effective base resilient modulus values were compared to base resilient modulus values estimated from DCP testing of the corresponding unstabilized sections to quantify the effect of the geogrid reinforcement. The researchers showed that geogrid reinforcement placed at the upper one-third position within the base layer performed best in increasing the effective base resilient modulus values in this case, followed by geogrid reinforcement placed at the base-subgrade interface and, after that, geogrid reinforcement placed at the middle of the base layer (Chen and Abu-Farsakh 2012).

In a laboratory study in Montana (Perkins 1999), geogrid reinforcement was placed at either the base-subgrade interface or the lower one-third position of the base layer in pavement sections constructed in a 2.0-m by 2.0-m by 1.5-m (6.5-ft by 6.5-ft by 5.0-ft) test box. The base layer thickness varied from 200 mm (8 in.) to 380 mm (15 in.), and the HMA layer was 75 mm (3 in.) thick. In conjunction with stress and strain measurements obtained from instrumentation

embedded in the pavement layers, the results of cyclic plate load testing indicated that geogrid reinforcement placed at the base-subgrade interface limits the amount of lateral spreading that occurs in both the bottom of the base layer and the top of the subgrade. In this study, pavement performance was defined by surface rutting, which was lower in the sections where reinforcement was placed in the lower one-third position than in the sections where reinforcement was placed at the base-subgrade interface, although both performed better than unstabilized sections (Perkins 1999).

These field and laboratory studies confirm that geogrid reinforcement position within a pavement section can affect the ability of the reinforcement to provide improved pavement performance. Several studies have been completed to investigate the effects of different geogrid positions, and the optimal position appears to vary based on many factors. However, the general consensus is that, for thin base layers, placing geogrid reinforcement at the base-subgrade interface is a good approach, while thick base layers may warrant placing a second layer of geogrid reinforcement at the middle or upper one-third position within the base layer.

2.4 Summary

This chapter provides background information obtained from a literature review about the use of geogrid-stabilized aggregate base materials in flexible pavements. A brief description of geogrids and a discussion of their use are presented. Many field and laboratory studies regarding geogrid reinforcement and pavement performance have been conducted to investigate the benefits of geogrid-stabilized aggregate base materials in flexible pavements. Previous studies have incorporated full-scale experimentation and testing to evaluate performance, stiffness, and strength improvements in geogrid-stabilized aggregate base materials. Specifically, researchers have explored the possible requirement for a conditioning period, identified a zone of influence

resulting from geogrid reinforcement, and investigated the effects of different geogrid positions within pavement structures.

Field studies substantiate the idea that quantifying the benefit of geogrid reinforcement in a pavement section requires an adequate conditioning period, which allows the geogrid and surrounding aggregate base material to fully interlock. Although exact predictions of the length of the conditioning period are probably not possible, several months or even a few years may be required in some cases.

Field and laboratory studies demonstrate the occurrence of a zone of influence in the immediate vicinity of geogrid reinforcement. Although exact measurements of the extent of the zone of influence have not been commonly reported, values approaching 150 mm (6 in.) may be possible in some cases.

Both field and laboratory studies confirm that geogrid reinforcement position within a pavement section can affect the ability of the reinforcement to provide improved pavement performance. The optimal position appears to vary based on many factors. However, the general consensus is that, for thin base layers, placing geogrid reinforcement at the base-subgrade interface is a good approach, while thick base layers may warrant placing a second layer of geogrid reinforcement at the middle or upper one-third position within the base layer.

3 PROCEDURES

3.1 Overview

This research consisted of field testing and data analyses performed to investigate the structural capacity of aggregate base materials stabilized with triaxial geogrid placed in a full-scale pavement involving control, or unstabilized, sections. This chapter describes the field testing procedures and data analysis methods utilized in this research.

3.2 Field Testing

Field testing was performed on a roadway in northeastern Utah that was 16 km (10 miles) long and included 10 test sections, as displayed in Figure 3-1, that were each 152 m (500 ft) long; seven were stabilized sections, and three were control sections. With reference to construction notes prepared by the contractor, the researchers selected test sections distinguished by base layer thickness and the presence and position of triaxial geogrid (Tensar TX140). Each test section included five test locations that were spaced 30 m (100 ft) apart in the right wheel path of the northbound lane and centered longitudinally within the section. At the time of testing, which was performed in fall 2015, the pavement was approximately 3.5 years old; given that the roadway had been frequently trafficked by heavy trucks in support of the local oil industry during this period, the researchers were optimistic that the required conditioning period was already complete.

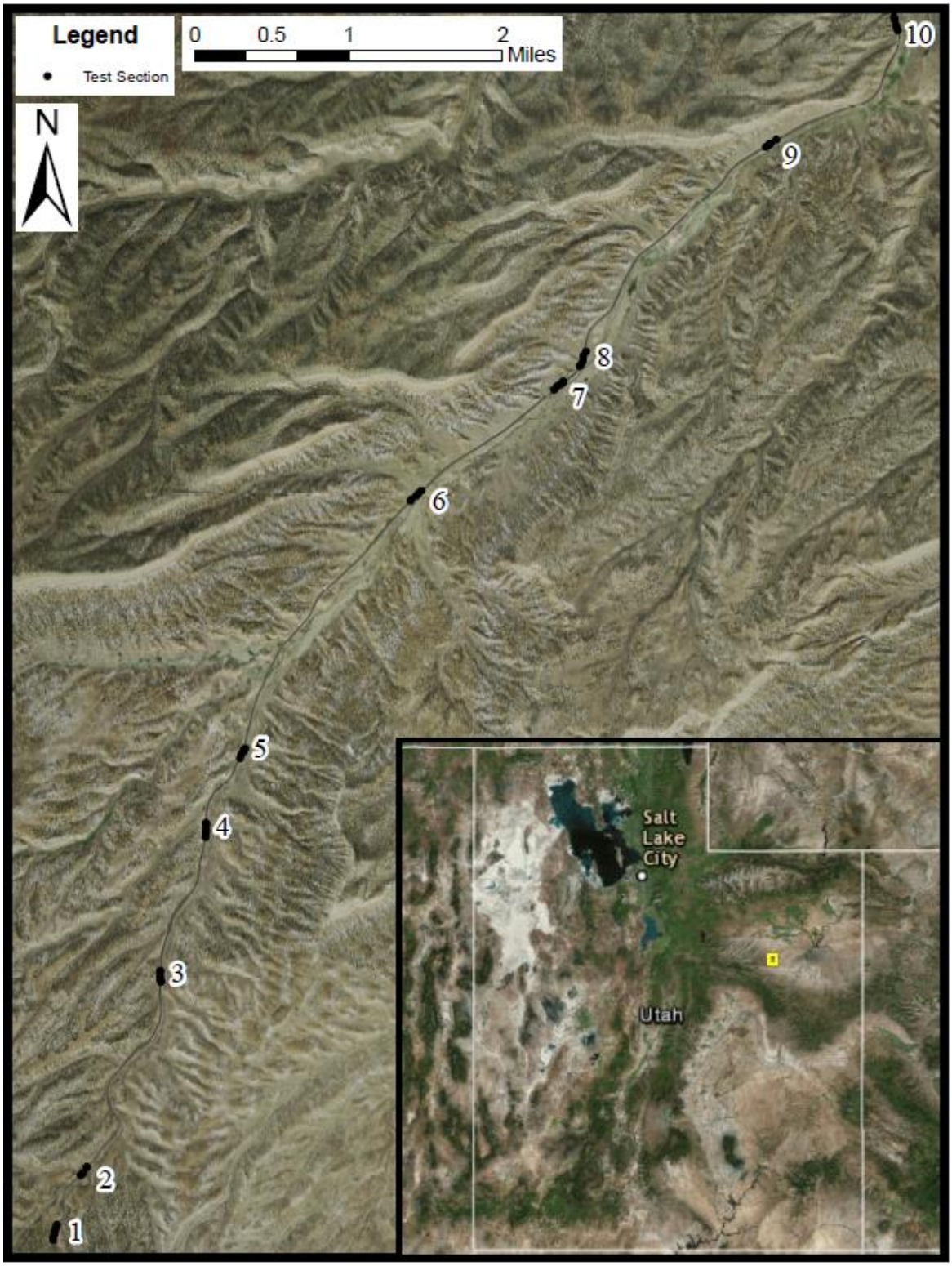

Figure 3-1: Arial view of pavement sections with test locations marked.

The pavement structure was comprised of an HMA layer overlying an untreated aggregate base layer of varying thickness, depending on the test section. Except for the control sections, one or two layers of geogrid were incorporated into portions of the pavement structure at different locations. The researchers bored holes along the shoulder of the pavement to a depth of 760 mm (30 in.) to verify the presence and depth of geogrid at both ends of each test section. The asphalt thickness, base layer thickness, and depth of geogrid, when present, were all measured from the bore holes.

According to the American Association of State Highway and Transportation Officials (AASHTO) and Unified soil classification methods, the native subgrade material was classified as A-4(0) and silty sand with gravel (SM), respectively, with an average plasticity index (PI) of 5, and the aggregate base material was classified as A-1-a and poorly graded gravel with silt and sand (GP-GM), respectively, with a PI of 1.5. Based on gradation information, the particle diameters corresponding to 85 and 50 percent finer (D_{85} and D_{50}, respectively) for the base material were determined to be approximately 19 mm (0.75 in.) and 5 mm (0.2 in.), respectively. Therefore, based on FHWA guidelines (FHWA 2008), the minimum recommended geogrid aperture size was 13 mm (0.5 in.), and the maximum recommended geogrid aperture size was 38 mm (1.5 in.). Because the maximum aperture size of the geogrid utilized in this research was 38 mm (1.5 in.), it met the FHWA recommendations for the aggregate base material specified for this project.

In this research, two field testing procedures were used to evaluate the structural capacity of the aggregate base layer in each pavement section. FWD testing was performed in general accordance with American Society for Testing and Materials (ASTM) D4694 (Standard Test Method for Deflections with a Falling-Weight-Type Impulse Load Device), and DCP testing was

performed in general accordance with ASTM D6951 (Standard Test Method for Use of the Dynamic Cone Penetrometer in Shallow Pavement Applications). The pavement surface temperature ranged from approximately 17°C to 24°C (63°F to 76°F) during the testing.

FWD testing was conducted by Utah Department of Transportation personnel. Depicted in Figure 3-2, the FWD consists of a set of weights mounted on a truck and dropped from various heights onto a 300-mm (12-in.)-diameter load plate to achieve desired loads up to 71.2 kN (16,000 lb) in this research. Nine sensors were used to measure the pavement deflection at radial distances of -300 mm (-12 in.), 0 mm (0 in.), 200 mm (8 in.), 300 mm (12 in.), 460 mm (18 in.), 610 mm (24 in.), 910 mm (36 in.), 1,220 mm (48 in.), and 1,520 mm (60 in.) from the point of impact. FWD testing was performed at each of the five test locations within each test section, specifically at 15 m (50 ft), 46 m (150 ft), 76 m (250 ft), 107 m (350 ft), and 137 m (450 ft), for a total of 50 test locations. Four drops were applied at each test location at target load

Figure 3-2: FWD testing of pavement structure.

levels of 35.6 kN (8,000 lb), 44.5 kN (10,000 lb), 53.4 kN (12,000 lb), 62.3 kN (14,000 lb) and 71.2 kN (16,000 lb). Interpolating specifically between the 35.6-kN (8,000-lb) and 44.5-kN (10,000-lb) load levels allowed for analysis of an exactly 40.0-kN (9,000-lb) load, which corresponds to an equivalent single axle load (ESAL). The first drop at each load level was a seating load and was not used in the analysis. After FWD testing was completed, one DCP test was performed at three test locations in each test section, specifically at 15 m (50 ft), 76 m (250 ft), and 137 m (450 ft), for a total of 30 test locations. The DCP consists of a 12-mm (0.47-in.)-diameter metal rod fitted with a standard metal cone at the end. As shown in Figure 3-3, an 8.0-kg (17.6-lb) slide hammer was repeatedly dropped 570 mm (22.5 in.), and the penetration rate, measured in mm/blow, of the DCP into the tested layers was recorded. Changes in DCP

Figure 3-3: DCP testing of pavement structure.

penetration rates with depth together with measurements obtained from the bore holes were used to estimate the pavement layer thicknesses. DCP penetration rates were also used to estimate the CBR of both the subgrade and base layers as shown in Equation 3-1 (Webster et al. 1992):

$$CBR = \frac{292}{DCP^{1.12}} \quad (3\text{-}1)$$

where:

CBR = California bearing ratio, %

DCP = penetration rate, mm/blow

3.3 Data Analysis

After the field testing was complete, two methods of data analysis were used to investigate the structural capacity of each test section, including the Rohde's method and the Area under the Pavement Profile (AUPP) method. These analysis approaches were used instead of a traditional backcalculation approach because the latter, which was initially attempted in this research, consistently yielded unrealistic results in comparison to the DCP data and based on the researchers' experience with similar materials. In both the Rohde's method and the AUPP method, interpolated deflections corresponding to an exactly 40.0-kN (9,000-lb) load were analyzed at each test location, as required; linearly interpolated deflections were computed from the average deflections associated with three drops at each of the target load levels of 35.6 kN (8,000 lb) and 44.5 kN (10,000 lb). This process yielded one deflection basin per test location. The following sections describe the procedures for the Rohde's method, AUPP method, and statistical analysis used in this research.

3.3.1 Rohde's Method

The Rohde's method was applied in conjunction with the 1993 AASHTO pavement design guide methodology in several steps. First, from the collected data, an asphalt modulus value was calculated for each test location using a relationship between the surface curvature index, base damage index, and asphalt modulus as shown in Equations 3-2, 3-3, and 3-4 (Xu et al. 2002):

$$SCI = D_0 - D_{300} \tag{3-2}$$

where:

SCI = surface curvature index (mm)

D_0 = peak deflection measured under a standard 40.0-kN (9,000-lb) FWD load (mm)

D_{300} = surface deflection occurring under a standard 40.0-kN (9,000-lb) FWD load at a radial distance of 300 mm (12 in.) from the center of the loading plate (mm)

$$BDI = D_{300} - D_{600} \tag{3-3}$$

where:

BDI = base damage index (mm)

D_{300} = surface deflection occurring under a standard 40.0-kN (9,000-lb) FWD load at a radial distance of 300 mm (12 in.) from the center of the loading plate (mm)

D_{600} = surface deflection occurring under a standard 40.0-kN (9,000-lb) FWD load at a radial distance of 600 mm (24 in.) from the center of the loading plate (mm)

$$log(E_{ac}) = -1.7718 * log(SCI) + 0.8395 * log(BDI) - 2.5124 * log(H_{ac}) + 0.0030 * H_{ac} + 7.7696 \quad (3\text{-}4)$$

where:

E_{ac} = asphalt modulus (MPa)

SCI = surface curvature index (mm) determined from Equation 3-2

BDI = base damage index (mm) determined from Equation 3-3

H_{ac} = asphalt concrete thickness (mm)

Second, from the asphalt modulus value calculated for each test location, an asphalt layer coefficient was determined using a standard correlation chart available in the literature (Huang 2004). Third, subgrade modulus values were calculated using Rohde's method as shown in Equations 3-5 and 3-6 (Crook et al. 2012, Rohde 1994):

$$SIS = D_{1.5Hp} - D_s \quad (3\text{-}5)$$

where:

SIS = structural index for the subgrade

Hp = total pavement thickness (mm)

$D_{1.5Hp}$ = surface deflection occurring under a standard 40.0-kN (9,000-lb) FWD load at a radial distance of 1.5Hp from the center of the loading plate (microns), estimated as necessary through interpolation from measured deflections at fixed sensor positions

D_s = surface deflection occurring under a standard 40.0-kN (9,000-lb) FWD load at a radial distance of 1.5Hp + 450 mm (18 in.) from the center of the loading plate

(microns), estimated as necessary through interpolation from measured deflections at fixed sensor positions

$$E_{sg} = 10^{k_4} * SIS^{k_5} * Hp^{k_6} \quad (3\text{-}6)$$

where:

E_{sg} = subgrade modulus (MPa)

SIS = structural index for the subgrade determined from Equation 3-5

Hp = total pavement thickness (mm)

$k_4, k_5, and\ k_6$ = coefficients determined from Table 3-1

Table 3-1: Coefficients for Calculating Subgrade Stiffness from SIS

Total Pavement Thickness	k_4	k_5	k_6
Hp ≤ 380 mm	9.138	-1.236	-1.903
380 mm < Hp ≤ 525 mm	8.756	-1.213	-1.780
525 mm < Hp	10.655	-1.254	-2.453

Fourth, the Rohde's method was used to calculate a structural number using Equations 3-7 and 3-8 (Crook et al. 2012, Rohde 1994), and, fifth, base layer coefficients (a_2 values) were computed using Equation 3-9 (Huang 2004):

$$SIP = D_0 - D_{1.5Hp} \quad (3\text{-}7)$$

where:

SIP = structural index of the pavement (microns)

D_0 = peak deflection measured under a standard 40.0-kN (9,000-lb) FWD load (microns)

Hp = total pavement thickness (mm)

$D_{1.5Hp}$ = surface deflection occurring under a standard 40.0-kN (9,000-lb) FWD load at a radial distance of 1.5Hp from the center of the loading plate (microns), estimated as necessary through interpolation from measured deflections at fixed sensor positions

$$SN = k_1 * SIP^{k_2} * Hp^{k_3} \quad (3\text{-}8)$$

where:

SN = structural number

SIP = structural index of the pavement (microns) determined from Equation 3-7

Hp = total pavement thickness (mm)

$k_1, k_2, and\ k_3$ = coefficients determined from Table 3-2

Table 3-2: Coefficients for Determining SN from SIP

Surface Type	k_1	k_2	k_3
Surface Seal	0.1165	-0.3248	0.8241
Asphalt Concrete	0.4728	-0.481	0.7581

$$a_2 = \frac{SN - a_1 \frac{D_1}{25.4}}{\frac{D_2}{25.4} m_2} \quad (3\text{-}9)$$

where:

a_2 = base layer coefficient

SN = structural number determined from Equation 3-8

a_1 = asphalt layer coefficient determined using a standard correlation chart from the results of Equation 3-4

D_1 = asphalt layer thickness (mm)

D_2 = base layer thickness (mm)

m_2 = base layer drainage coefficient, which was assumed to be 1.0

3.3.2 Area under the Pavement Profile Method

The AUPP method was applied in conjunction with a mechanistic-empirical pavement analysis in several steps. First, from the collected FWD data, an AUPP value was computed using Equation 3-10 (Alvarez and Thompson 1998, Thompson 1999, Xu et al. 2002):

$$AUPP = \frac{(5*D0)-(2*D1)-(2*D2)-D3}{2} \quad (3\text{-}10)$$

where:

$AUPP$ = area under pavement profile (mm)

$D0$ = surface deflection occurring under a standard 40.0-kN (9,000-lb) FWD load at the center of the loading plate (microns)

$D1$ = surface deflection occurring under a standard 40.0-kN (9,000-lb) FWD load at a radial distance of 300 mm (12 in.) from the center of the loading plate (microns)

$D2$ = surface deflection occurring under a standard 40.0-kN (9,000-lb) FWD load at a radial distance of 600 mm (24 in.) from the center of the loading plate (microns)

$D3$ = surface deflection occurring under a standard 40.0-kN (9,000-lb) FWD load at a radial distance of 900 mm (36 in.) from the center of the loading plate (microns)

Second, the AUPP value was used to compute an asphalt strain value using Equation 3-11 (Alvarez and Thompson 1998):

$$log\left(\frac{\varepsilon_{HMA}}{1{,}000{,}000}\right) = 1.00 + 1.01 * log(\frac{AUPP}{25.4}) \quad (3\text{-}11)$$

where:

ε_{HMA} = HMA flexural strain at bottom of HMA layer (strain)

$AUPP$ = area under pavement profile (mm) determined from Equation 3-10

Third, from the HMA flexural strain value calculated for each test location, the allowable number of ESALs until HMA fatigue cracking failure was calculated using Equation 3-12 (Huang 2004):

$$N_f = 0.0796 * \varepsilon_{HMA}^{-3.291} * (\frac{E_{ac}}{145.04})^{-0.854} \quad (3\text{-}12)$$

where:

N_f = allowable number of 80.1 kN (18-kip) ESALs until HMA fatigue cracking failure

ε_{HMA} = HMA flexural strain at bottom of HMA layer (strain) determined from Equation 3-11

E_{ac} = asphalt modulus (MPa) determined from Equation 3-4

3.3.3 Statistical Analysis

After application of both the Rohde's method and the AUPP method, an analysis of covariance (ANOCOVA) was conducted on the computed base layer coefficients and AUPP values. This statistical analysis was performed to enable comparisons of the test sections after

adjusting for potential variation in the subgrade modulus and base layer thickness values. In the ANOCOVA model, all 10 test sections were evaluated simultaneously. The dependent variable was base layer coefficient or AUPP value, the covariate was subgrade modulus and/or base layer thickness, and the independent variable was test section. *P*-values were calculated for the independent variable and covariate, and the coefficient of determination, or R^2 value, was computed for the model. In addition, least squares means were computed for the independent variable, and Tukey's mean separation procedure was applied to evaluate all possible pairwise comparisons of the 10 test sections to determine which test sections were different from other test sections. In this research, a *p*-value less than or equal to 0.05 indicated statistical significance.

3.4 Summary

This chapter describes the field testing and data analyses performed to investigate the structural capacity of aggregate base materials stabilized with triaxial geogrid placed in a full-scale pavement involving control, or unstabilized, sections. Field testing was performed on a roadway in northeastern Utah that was 16 km (10 miles) long and included 10 test sections, seven stabilized sections and three control sections, that were each 152 m (500 ft) long. Each test section included five test locations that were spaced 30 m (100 ft) apart in the right wheel path of the northbound lane and centered longitudinally within the section. The pavement structure was comprised of an HMA layer overlying an untreated aggregate base layer of varying thickness, depending on the test section. Except for the control sections, one or two layers of geogrid were incorporated into portions of the pavement structure at different locations.

In this research, two field testing procedures were used to evaluate the structural capacity of the aggregate base layer in each pavement section, including FWD testing and DCP testing.

FWD testing was performed at each of the five test locations within each test section, specifically at 15 m (50 ft), 46 m (150 ft), 76 m (250 ft), 107 m (350 ft), and 137 m (450 ft), for a total of 50 test locations. DCP testing was performed at each of three test locations in each test section, specifically at 15 m (50 ft), 76 m (250 ft), and 137 m (450 ft), for a total of 30 test locations. After the field testing was complete, two methods of data analysis were used to investigate the structural capacity of each test section, including the Rohde's method and the AUPP method. The Rohde's method was applied in conjunction with the 1993 AASHTO pavement design guide methodology, and the AUPP method was applied in conjunction with a mechanistic-empirical pavement analysis.

After application of both the Rohde's method and the AUPP method, an ANOCOVA was conducted on the computed base layer coefficients and AUPP values. This statistical analysis was performed to enable comparisons of the test sections after adjusting for potential variation in the subgrade modulus and base layer thickness values.

4 RESULTS AND ANALYSIS

4.1 Overview

This chapter presents the results of field testing and data analyses performed for this research. All results developed in this research are limited in their application to the material types, pavement designs, construction techniques, environmental conditions, and trafficking levels associated with this study.

4.2 Results

Field results included measurements obtained using the FWD and DCP; individual test values for each test section are provided in Appendices A and B, respectively. A complete overview of layer thicknesses and mechanical properties for each layer, including the subgrade, in each of the 10 test sections is shown in Table 4-1. The presence of a hyphen in Table 4-1 indicates that the given measurement was not applicable to the given layer or was not determined. The asphalt layer thickness was consistently 140 mm (5.5 in.) at all 10 test sections, while the base layer thickness varied from 360 mm (14 in.) to 510 mm (20 in.). The CBR values presented in Table 4-1 are average values computed from only the test locations at which the base layer was fully penetrated by the DCP; in many cases, the base layer was too stiff to be fully penetrated, resulting in refusal that was defined in this research as less than 30 mm (1.2 in.) of penetration after 30 blows, even after several attempts to deepen the test hole using a bull pick

Table 4-1: Layer Thicknesses and Mechanical Properties of Test Sections

Test Section	Layer Description	Layer Thickness, mm (in.)	CBR (from DCP)	Modulus, MPa (ksi) (from FWD)	Layer Coefficient (from FWD)	AUPP, mm (in.) (from FWD)	Geogrid Position
1	Asphalt	140 (5.5)	-	6410 (929)	0.56	248 (9.77)	Geogrid at depth of 600 mm (23.5 in.) below asphalt surface
	Base	460 (18.0)	237	-	0.14		
	Subgrade	-	34	80 (11)	-		
2	Asphalt	140 (5.5)	-	6050 (878)	0.55	277 (10.90)	Geogrid at depth of 600 mm (23.5 in.) below asphalt surface
	Base	460 (18.0)	106	-	0.13		
	Subgrade	-	21	90 (13)	-		
3	Asphalt	140 (5.5)	-	6110 (886)	0.55	225 (8.87)	Geogrid at depths of 340 mm (13.5 in.) and 600 mm (23.5 in.) below asphalt surface
	Base	460 (18.0)	278	-	0.16		
	Subgrade	-	18	100 (15)	-		
4	Asphalt	140 (5.5)	-	5430 (788)	0.54	257 (10.13)	Geogrid at depth of 320 mm (12.5 in.) below asphalt surface
	Base	460 (18.0)	197	-	0.15		
	Subgrade	-	26	120 (17)	-		
5	Asphalt	140 (5.5)	-	6100 (885)	0.56	215 (8.47)	No geogrid
	Base	460 (18.0)	255	-	0.18		
	Subgrade	-	41	130 (18)	-		
6	Asphalt	140 (5.5)	-	6110 (886)	0.56	197 (7.74)	Geogrid at depths of 360 mm (14.0 in.) and 600 mm (23.5 in.) below asphalt surface
	Base	460 (18.0)	-	-	0.19		
	Subgrade	-	-	140 (20)	-		
7	Asphalt	140 (5.5)	-	4820 (699)	0.52	292 (11.51)	No geogrid
	Base	510 (20.0)	172	-	0.14		
	Subgrade	-	66	80 (11)	-		
8	Asphalt	140 (5.5)	-	5920 (859)	0.55	235 (9.26)	Geogrid at depths of 320 mm (12.5 in.) and 650 mm (25.5 in.) below asphalt surface
	Base	510 (20.0)	231	-	0.16		
	Subgrade	-	93	100 (15)	-		
9	Asphalt	140 (5.5)	-	4960 (720)	0.52	320 (12.58)	Geogrid at depth of 500 mm (19.5 in.) below asphalt surface
	Base	360 (14.0)	120	-	0.12		
	Subgrade	-	43	80 (12)	-		
10	Asphalt	140 (5.5)	-	4340 (630)	0.50	291 (11.46)	No geogrid
	Base	360 (14.0)	164	-	0.15		
	Subgrade	-	51	190 (28)	-		

and 4.5-kg (10-lb) sledgehammer. Specifically, the CBR values shown for test sections 2, 3, 4, and 5 are based on one DCP test; the CBR values shown for test sections 8, 9, and 10 are based on two tests; and the CBR values shown for test sections 1 and 7 are based on three DCP tests. A CBR value for test section 6 could not be determined due to refusal at all attempted testing locations within that section. Therefore, for most of the sections, the CBR value presented in

Table 4-1 for the base layer, which ranges from 106 to 278, is lower than the hypothetical CBR value that may have been obtained if refusal had not occurred in so many of the test locations. Furthermore, the CBR data presented for a given test section may not be representative of the entire test section due to a lack of data at some test locations. The following sections provide the results from both the Rohde's method and the AUPP method.

4.2.1 Rohde's Method

For the Rohde's method, the results of the ANOCOVA indicated that both test section and subgrade modulus were statistically significant, with *p*-values of less than 0.0001, and the R^2 value of the model was 0.744; base layer thickness was determined to be correlated with subgrade modulus, with a *p*-value of 0.019, and was therefore excluded from the model. The least squares means computed for the base layer coefficient are presented in Figure 4-1, in which higher values correspond to higher structural capacity. Unlike the base layer coefficients in Table 4-1, the base layer coefficients in Figure 4-1 can be compared directly, as they have been

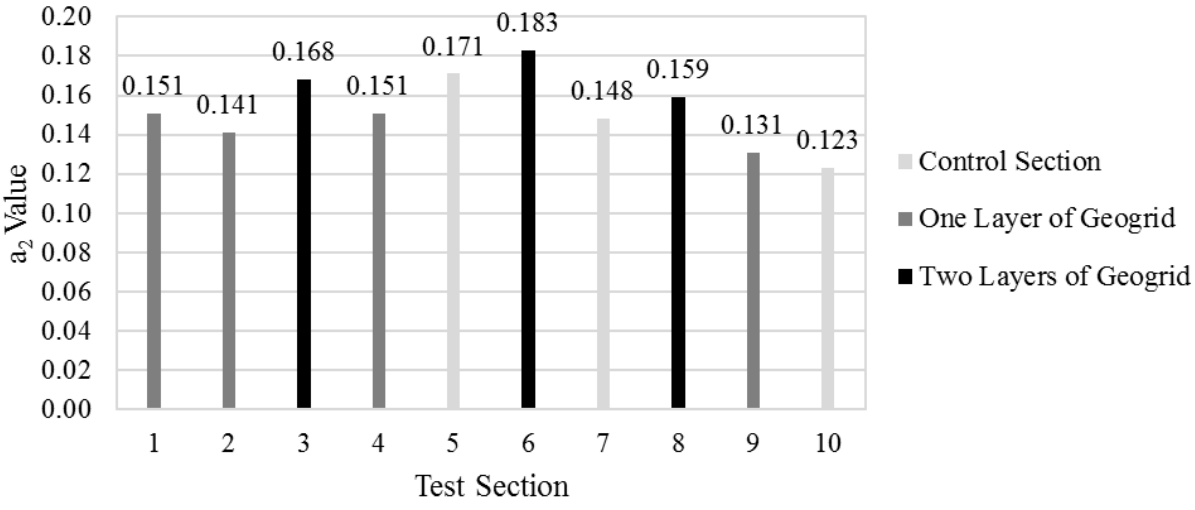

Figure 4-1: Least squares means for base layer coefficient.

adjusted for variation in the subgrade modulus value (and indirectly adjusted for variation in base layer thickness given the correlation between base layer thickness and subgrade modulus). Adjusting the base layer coefficients to a common, average subgrade modulus value enabled direct comparisons of the test sections independent of subgrade modulus, which could not be controlled in the experimentation but was shown in the analyses to be positively correlated with base layer coefficient.

The results of all possible pairwise comparisons among the 10 test sections are presented in Table 4-2, in which shading is applied where a site would be compared to itself or where a comparison would be duplicated. Among 45 total comparisons, 36 were not statistically significant, meaning that sufficient evidence was not available to identify statistically significant differences between those test sections. In other words, variations in the presence and position of triaxial geogrid at those sections did not appear to affect the base layer coefficient; indeed, differentiating between two control sections (test sections 7 and 10) and all of the test sections with one layer of geogrid, regardless of position, was not possible. The remaining nine comparisons, however, were statistically significant, meaning that sufficient evidence was

Table 4-2: Pairwise Comparisons of Base Layer Coefficients

Test Section	*P*-Values for Indicated Pairwise Comparisons								
	2	3	4	5	6	7	8	9	10
1	0.9869	0.7938	1.0000	0.6107	0.0893	1.0000	0.9975	0.5168	0.3884
2		0.1877	0.9909	0.1006	**0.0054**	0.9994	0.6767	0.9838	0.8467
3			0.7612	1.0000	0.8355	0.5804	0.9966	**0.0152**	**0.0099**
4				0.5156	**0.0477**	1.0000	0.9961	0.5770	0.2514
5					0.9541	0.3986	0.9609	**0.0079**	**0.0015**
6						**0.0414**	0.3210	**0.0003**	**0.0001**
7							0.9718	0.7411	0.5589
8								0.1268	0.0617
9									0.9994

available to identify statistically significant differences between those test sections; these are indicated by a *p*-value of less than or equal to 0.05 as presented in bold-face font in Table 4-2. (The reason that test section 6 was statistically different than test section 4 but not different than test section 1, even though test sections 1 and 4 had the same adjusted base layer coefficient, is that test section 4 had greater variability than test section 1.)

The nine statistically significant comparisons involve test sections 3, 5, and 6 as the test sections with the three highest adjusted base layer coefficients as displayed in Figure 4-1; as shown in Table 4-2, sufficient evidence was not available to differentiate among these three sections with respect to base layer coefficient. Among these, test section 5 was the only unstabilized control section. To investigate reasons for the unexpected performance of this section, the researchers contacted the engineering firm responsible for the roadway design. The engineer indicated that the base layer at that section may possibly have been underlain by relatively large, angular aggregates (some around 300 mm (12 in.) in diameter) that increased the structural capacity of the layer; however, specific construction records were not available to verify this hypothesis. The increased structural capacity of test sections 3 and 6, on the other hand, was probably associated with the presence of two layers of geogrid in the base layer. In these test sections, one geogrid layer was placed at the base-subgrade interface, while the other geogrid layer was placed approximately between the middle and upper one-third positions within the base layer, consistent with recommendations developed in previous research (Al-Qadi et al. 2008, Chen and Abu-Farsakh 2012, Haas et al. 1988). The only other test section with two layers of geogrid was section 8, which, although not involved in any statistically significant pairwise comparisons, had the fourth highest adjusted base layer coefficient, further suggesting the potential benefits of this design.

The nine statistically significant comparisons also involved test sections 2, 4, 7, 9, and 10 as the test sections with the five lowest adjusted base layer coefficients as displayed in Figure 4-1; as shown in Table 4-2, sufficient evidence was not available to differentiate among these five sections with respect to base layer coefficient. Among these, test sections 7 and 10 were unstabilized control sections, and test sections 2, 4, and 9 had one layer of geogrid. Specifically, the geogrid was placed at the base-subgrade interface at test sections 2 and 9 and in the middle of the base layer at test section 4; in this research, differentiating with respect to base layer coefficient between the two geogrid positions represented by these test sections was not possible. Differentiating with greater precision among the test sections would have required testing of a higher number of test locations.

In addition to statistical significance, the practical importance of the observed differences was also evaluated. Using the 1993 AASHTO pavement design guide methodology, the researchers computed the extension in pavement life corresponding to the increases in base layer coefficient observed in this study. For a 90 percent reliability level, an overall standard deviation of 0.45, a design serviceability loss of 1.7, an average subgrade modulus value of 110 MPa (16.0 ksi) computed from Table 4-1, a base layer thickness of 460 mm (18.0 in.), base modulus values of 170 MPa (24.0 ksi) to 280 MPa (40.0 ksi) corresponding to the measured base layer coefficients of 0.12 to 0.18 (Huang 2004), an asphalt layer thickness of 140 mm (5.5 in.), and an average a_1 value of 0.54 computed from Table 4-1, the allowable number of ESALs increases from 5.9 million to 19.2 million as shown in Appendix C; on average, the allowable number of ESALs increases by approximately 20 percent with each 0.01 increase in the base layer coefficient. Therefore, while differences among the test sections evaluated in this study were statistically significant, they were also practically important.

4.2.2 *Area under the Pavement Profile Method*

For the AUPP method, the results of the ANOCOVA indicated that both test section and subgrade modulus were statistically significant, with *p*-values of less than 0.0001, and the R^2 value of the model was 0.704; as explained previously, base layer thickness was determined to be correlated with subgrade modulus and was therefore excluded from the model. The least squares means computed for the AUPP value are presented in Figure 4-2, in which lower values correspond to higher structural capacity. Unlike the AUPP values in Table 4-1, the AUPP values in Figure 4-2 can be compared directly, as they have been adjusted for variation in the subgrade modulus value (and indirectly adjusted for variation in base layer thickness given the correlation between base layer thickness and subgrade modulus). As explained previously, adjusting the AUPP values to a common, average subgrade modulus value enabled direct comparisons of the test sections independent of subgrade modulus, which could not be controlled in the experimentation but was shown in the analyses to be negatively correlated with AUPP value.

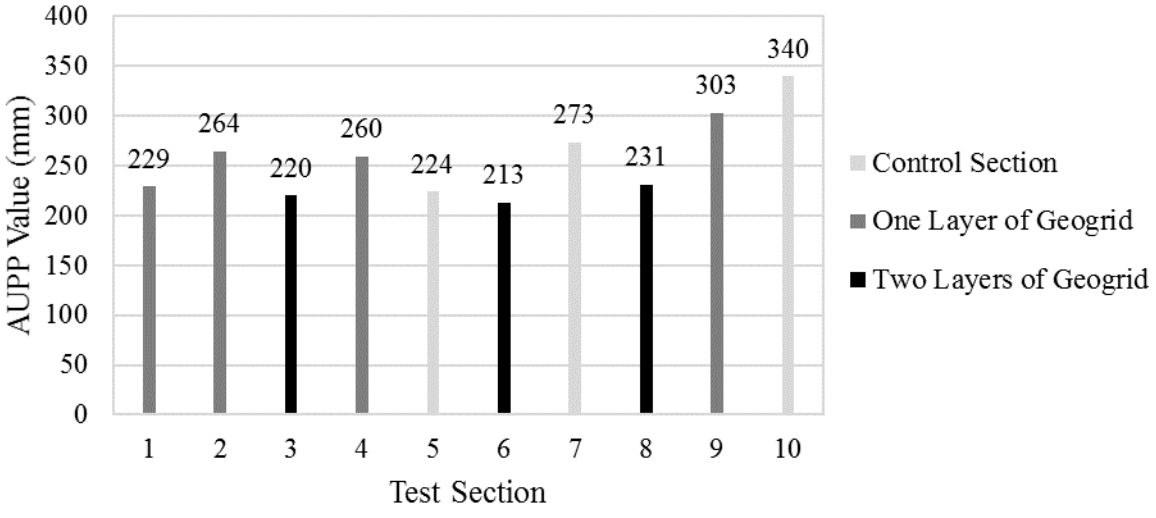

Figure 4-2: Least squares means for AUPP value.

The results of all possible pairwise comparisons among the 10 test sections are presented in Table 4-3, in which shading is applied where a site would be compared to itself or where a comparison would be duplicated. Among 45 total comparisons, 34 were not statistically significant, meaning that sufficient evidence was not available to identify statistically significant differences between those test sections. In other words, variations in the presence and position of triaxial geogrid at those sections did not appear to affect the AUPP value; indeed, differentiating between one of the control sections (test section 7) and all of the other test sections, regardless of geogrid presence or position, was not possible. The remaining 11 comparisons, however, were statistically significant, meaning that sufficient evidence was available to identify statistically significant differences between those test sections; these are indicated by a *p*-value of less than or equal to 0.05 as presented in bold-face font in Table 4-3.

The 11 statistically significant comparisons involve test sections 1, 3, 4, 5, 6, and 8 as the test sections with the six lowest AUPP values as displayed in Figure 4-2; as shown in Table 4-3, sufficient evidence was not available to differentiate among these six sections with respect to AUPP value. Among these, test section 5 was the only unstabilized control section; as explained

Table 4-3: Pairwise Comparisons of AUPP Values

Test Section	*P*-Values for Indicated Pairwise Comparisons								
	2	3	4	5	6	7	8	9	10
1	0.7122	1.0000	0.8664	1.0000	0.9984	0.407	1.0000	**0.0136**	**0.0025**
2		0.4086	1.0000	0.5756	0.2786	1.0000	0.7795	0.5913	0.0793
3			0.5639	1.0000	1.0000	0.1914	0.9998	**0.0040**	**0.0003**
4				0.6947	0.3465	0.9940	0.8928	0.4672	**0.0244**
5					0.9999	0.3287	1.0000	**0.0104**	**0.0001**
6						0.1377	0.9941	**0.0031**	**0.0000**
7							0.4992	0.8629	0.2198
8								**0.0204**	**0.0010**
9									0.8854

previously, the base layer at that section may possibly have been underlain by relatively large, angular aggregates that increased the structural capacity of the layer. The increased structural capacity of test sections 1, 3, 4, 6, and 8, on the other hand, was probably associated with the presence of one or two layers of geogrid in the base layer. In test section 1, the geogrid layer was placed at the base-subgrade interface, while in test section 4 the geogrid layer was placed in the middle of the base layer. In test sections 3, 6, and 8, one geogrid layer was placed at the base-subgrade interface, while another geogrid layer was placed approximately between the middle and upper one-third positions within the base layer, consistent with recommendations developed in previous research (Al-Qadi et al. 2008, Chen and Abu-Farsakh 2012, Haas et al. 1988). In this research, differentiating with respect to AUPP value between the three geogrid positions represented by these test sections was not possible.

The 11 statistically significant comparisons also involved test sections 9 and 10 as the test sections with the two highest adjusted AUPP values as displayed in Figure 4-2; as shown in Table 4-3, sufficient evidence was not available to differentiate among these two sections with respect to AUPP value. Among these, test section 10 was an unstabilized control section, and test section 9 had one layer of geogrid. Specifically, the geogrid was placed at the base-subgrade interface. As explained previously, differentiating with greater precision among the test sections would have required testing of a higher number of test locations.

In addition to statistical significance, the practical importance of the observed differences was also evaluated. Using correlations between AUPP, strain at the bottom of the asphalt layer, and allowable number of ESALs until HMA fatigue cracking failure, the researchers computed the extension in pavement life corresponding to the decreases in AUPP value observed in this study. For AUPP values decreasing from 340 mm (13.37 in.) to 213 mm (8.38 in.) and an

average asphalt modulus value of 5625 MPa (816 ksi) computed from Table 4-1, the allowable number of ESALs increases from 3.7 million to 17.3 million as shown in Appendix C; on average, the allowable number of ESALs increases by approximately 35 percent with each 25 mm (1.0 in.) decrease in the AUPP value. Therefore, while differences among the test sections evaluated in this study were statistically significant, they were also practically important.

4.3 Summary

This chapter presents the results of field testing and data analyses performed for this research. Field results included measurements obtained using the FWD and DCP. The asphalt layer thickness was consistently 140 mm (5.5 in.) at all 10 test sections, and the base layer thickness varied from 360 mm (14 in.) to 510 mm (20 in.). In many cases, the base layer was too stiff to be fully penetrated by the DCP, resulting in refusal. Thus, for most of the sections, the CBR value of the base layer, which ranged from 106 to 278, is lower than the hypothetical CBR value that may have been obtained if refusal had not occurred in so many of the test locations. Furthermore, the CBR data presented for a given test section may not be representative of the entire test section due to a lack of data at some test locations.

For the Rohde's method, the results of the ANOCOVA indicated that both test section and subgrade modulus were statistically significant, with *p*-values of less than 0.0001, and the R^2 value of the model was 0.744. Among the 45 possible pairwise comparisons, 36 were not statistically significant, meaning that variations in the presence and position of triaxial geogrid at those sections did not appear to affect the base layer coefficient; indeed, differentiating between two control sections (test sections 7 and 10) and all of the test sections with one layer of geogrid, regardless of position, was not possible. The remaining nine comparisons, however, were statistically significant and involved three test sections with the highest adjusted base layer

coefficients. While one of these was unexpectedly an unstabilized control section (test section 5), both of the others were constructed using two layers of geogrid in the base layer. In these test sections, one geogrid layer was placed at the base-subgrade interface, while the other geogrid layer was placed approximately between the middle and upper one-third positions within the base layer. In addition to being statistically significant, the observed differences were also practically important; according to the 1993 AASHTO pavement design guide methodology, increasing the base layer coefficient from 0.12 to 0.18 corresponds to an increase in the allowable number of ESALs from 5.9 million to 19.2 million at the research site.

For the AUPP method, the results of the ANOCOVA indicated that both test section and subgrade modulus were statistically significant, with *p*-values of less than 0.0001, and the R^2 value of the model was 0.704. Among the 45 possible pairwise comparisons, 34 were not statistically significant, meaning that variations in the presence and position of triaxial geogrid at those sections did not appear to affect the AUPP value; indeed, differentiating between one of the control sections (test section 7) and all of the other test sections, regardless of geogrid presence or position, was not possible. The remaining 11 comparisons, however, were statistically significant and involved six test sections with the lowest adjusted AUPP values. While one of these was unexpectedly an unstabilized control section (test section 5), the others were constructed using one or two layers of geogrid in the base layer. In these test sections, one geogrid layer was placed either at the base-subgrade interface or in the middle of the base layer, or one geogrid layer was placed at the base-subgrade interface while another geogrid layer was placed approximately between the middle and upper one-third positions within the base layer; in this research, differentiating with respect to AUPP value between the three geogrid positions represented by these test sections was not possible. In addition to being statistically significant,

the observed differences were also practically important; according to a mechanistic-empirical pavement analysis, decreasing the AUPP value from 340 mm (13.37 in.) to 213 mm (8.38 in.) corresponds to an increase in the allowable number of ESALs from 3.7 million to 17.3 million at the research site.

5 CONCLUSION

5.1 Summary

The objective of this research was to investigate the structural capacity of aggregate base materials stabilized with triaxial geogrid (Tensar TX140) placed in a full-scale pavement involving control, or unstabilized, sections. Field testing was performed on a roadway in northeastern Utah that was 16 km (10 miles) long and included 10 test sections, seven stabilized sections and three control sections, that were each 152 m (500 ft) long. Each test section included five test locations that were spaced 30 m (100 ft) apart in the right wheel path of the northbound lane and centered longitudinally within the section. The pavement structure was comprised of an HMA layer overlying an untreated aggregate base layer of varying thickness, depending on the test section. Except for the control sections, one or two layers of geogrid were incorporated into portions of the pavement structure at different locations.

In this research, two field testing procedures were used to evaluate the structural capacity of the aggregate base layer in each pavement section, including FWD testing and DCP testing. FWD testing was performed at each of the five test locations within each test section, for a total of 50 test locations, and DCP testing was performed at each of three test locations in each test section, for a total of 30 test locations. After the field testing was complete, two methods of data analysis were used to investigate the structural capacity of each test section, including the Rohde's method and the AUPP method. The Rohde's method was applied in conjunction with

the 1993 AASHTO pavement design guide methodology, and the AUPP method was applied in conjunction with a mechanistic-empirical pavement analysis. After application of both the Rohde's method and the AUPP method, an ANOCOVA was conducted on the computed base layer coefficients and AUPP values. This statistical analysis was performed to enable comparisons of the test sections after adjusting for potential variation in the subgrade modulus and base layer thickness values.

5.2 Findings

Field results included measurements obtained using the FWD and DCP. The asphalt layer thickness was consistently 140 mm (5.5 in.) at all 10 test sections, and the base layer thickness varied from 360 mm (14 in.) to 510 mm (20 in.). In many cases, the base layer was too stiff to be fully penetrated by the DCP, resulting in refusal. Thus, for most of the sections, the CBR value of the base layer, which ranged from 106 to 278, was lower than the hypothetical CBR value that may have been obtained if refusal had not occurred in so many of the test locations.

For the Rohde's method, the results of the ANOCOVA indicated that both test section and subgrade modulus were statistically significant, and the R^2 value of the model was 0.744. Among the 45 possible pairwise comparisons, 36 were not statistically significant, meaning that variations in the presence and position of triaxial geogrid at those sections did not appear to affect the base layer coefficient; indeed, differentiating between two control sections (test sections 7 and 10) and all of the test sections with one layer of geogrid, regardless of position, was not possible. The remaining nine comparisons, however, were statistically significant and involved three test sections with the highest adjusted base layer coefficients. While one of these was unexpectedly an unstabilized control section (test section 5), both of the others were constructed using two layers of geogrid in the base layer. In these test sections, one geogrid layer

was placed at the base-subgrade interface, while the other geogrid layer was placed approximately between the middle and upper one-third positions within the base layer.

For the AUPP method, the results of the ANOCOVA indicated that both test section and subgrade modulus were statistically significant, and the R^2 value of the model was 0.704. Among the 45 possible pairwise comparisons, 34 were not statistically significant, meaning that variations in the presence and position of triaxial geogrid at those sections did not appear to affect the AUPP value; indeed, differentiating between one of the control sections (test section 7) and all of the other test sections, regardless of geogrid presence or position, was not possible. The remaining 11 comparisons, however, were statistically significant and involved six test sections with the lowest adjusted AUPP values. While one of these was unexpectedly an unstabilized control section (test section 5), the others were constructed using one or two layers of geogrid in the base layer. In these test sections, one geogrid layer was placed either at the base-subgrade interface or in the middle of the base layer, or one geogrid layer was placed at the base-subgrade interface while another geogrid layer was placed approximately between the middle and upper one-third positions within the base layer; in this research, differentiating with respect to AUPP value between the three geogrid positions represented by these test sections was not possible.

In addition to being statistically significant, the observed differences were also practically important. According to the 1993 AASHTO pavement design guide methodology, increasing the base layer coefficient from 0.12 to 0.18 corresponds to an increase in the allowable number of ESALs from 5.9 million to 19.2 million at the research site, while, according to a mechanistic-empirical pavement analysis, decreasing the AUPP value from 340 mm (13.37 in.) to 213 mm (8.38 in.) corresponds to an increase in the allowable number of ESALs from 3.7 million to 17.3

million at the research site. These research results indicate that, when geogrid reinforcement is compatible with the given aggregate base material and proper construction practices are followed, statistically significant and practically important increases in pavement design life can be achieved.

5.3 Recommendations

In order to achieve a statistically significant improvement in the structural capacity of an aggregate base material stabilized with triaxial geogrid, FHWA guidelines specifying the minimum and maximum recommended geogrid aperture size for a given aggregate base material should be followed, and use of two layers of geogrid is recommended for material types, pavement designs, construction techniques, environmental conditions, and trafficking levels similar to those associated with this study. One geogrid layer should be placed at the base-subgrade interface, while the other geogrid layer should be placed approximately between the middle and upper one-third positions within the base layer, consistent with recommendations developed in previous research. Further research is recommended to investigate potential improvement in the structural capacity of an aggregate base material resulting from the use of only one layer of geogrid, as well as the optimum position of the geogrid within the base layer. Lastly, the Rohde's method and the AUPP method are both recommended for analyzing FWD data collected on flexible pavements with geogrid-stabilized aggregate base layers.

REFERENCES

Al-Qadi, I. L., Dessouky, S. H., Kwon, J., and Tutumluer, E. (2008). "Geogrid in flexible pavements: validated mechanism." Transportation Research Record: Journal of the Transportation Research Board, 2045, 102-109.

Alvarez, C., and Thompson, M. R. (1998). "Mechanistic-empirical evaluation of the Mn/Road mainline flexible pavement sections." Report No. FHWA-IL-UI-263, FHWA, U. S. Department of Transportation, McLean, VA.

Aran, S. (2006). "Base reinforcement with biaxial geogrid: long-term performance." Transportation Research Record: Journal of the Transportation Research Board, 1975, 115-123.

Barksdale, R. D., Brown, S. F., and Chan, F. (1989). "Potential benefits of geosynthetics in flexible pavement systems." National Cooperative Highway Research Program Report 315, Transportation Research Board, Washington, DC.

Brandon, T. L., Al-Qadi, I. L., Lacina, B. A., and Bhutta, S. A. (1996). "Construction and instrumentation of geosynthetically stabilized secondary road test sections." Transportation Research Record: Journal of the Transportation Board, 1534, 50-57.

Chen, Q., and Abu-Farsakh, M. (2012). "Structural contribution of geogrid reinforcement in pavement." Proceedings of GeoCongress 2012: State of the Art and Practice in Geotechnical Engineering, ASCE, Reston, VA, 1468-1475.

Crook, A. L., Montgomery, S. R., and Guthrie, W. S. (2012). "Using falling-weight deflectometer data for network-level flexible pavement management." Transportation Research Record: Journal of the Transportation Research Board, 2304, 75-85.

Edil, T., Kim, W., Benson, C., and Tanyu, B. (2007). "Contribution of geosynthetic reinforcement to granular layer stiffness." Proceedings of Geo-Denver 2007: New Peaks in Geotechnics, ASCE, Reston, VA, 1-10.

Federal Highway Administration (FHWA). (2008). "Geosynthetic design and construction guidelines." Report No. FHWA NHI-07-092, FHWA, U. S. Department of Transportation, McLean, VA.

Haas, R., Walls, J., and Carroll, R. G. (1988). "Geogrid reinforcement of granular bases in flexible pavements." Transportation Research Record: Journal of the Transportation Research Board, 1188, 19-27.

Hall, K. D., Warren, K. A., and Howard, I. L. (2004). "Low volume flexible pavement roads reinforced with geosynthetics." Final Report AHTD TRC-0406, Planning and Research Division, Arkansas State Highway and Transportation Department, Little Rock, AR.

Hanes Geo Components. (2015). "Terragrid RX 1200 product data sheet." <http://hanesgeo.com/Catalog/Product?id=1704> (July, 2016).

Helstrom, C. L., Humphrey, D. N., and Hayden, S. A. (2006). "Geogrid reinforced pavement structure in a cold region." Proceedings of the 13th International Conference on Cold Regions Engineering, ASCE, Reston, VA, 1-12.

Henry, K. S., Clapp, J., Davids, W. G., and Barna, L. (2011). "Back-calculated pavement layer modulus values of geogrid reinforced test sections." Proceedings of Geo-Frontiers: Advances in Geotechnical Engineering, ASCE, Reston, VA, 4673-4682.

Holder, W. H., and Andreae, J. (2004). "Geogrid reinforcement to reduce pavement section thickness: a case study." Proceedings of Geo-Trans 2004: Geotechnical Engineering for Transportation Projects, ASCE, Reston, VA, 1006-1013.

Huang, Y. (2004). Pavement Analysis and Design, 2nd Ed., Pearson Education, Upper Saddle River, NJ.

Hufenus, R., Rueegger, R., Banjac, R., Mayor, P., Springman, S. M., and Brönnimann, R. (2006). "Full-scale field tests on geosynthetic reinforced unpaved roads on soft subgrade." Geotextiles and Geomembranes, 24(1), 21-37.

Huntington, G., and Ksaibati, K. (2000). "Evaluation of geogrid-reinforced granular base." Geotechnical Fabrics Report, 18(1), 22-28.

Jas, H., Stahl, M., Konietzky, H., te Kamp, L., and Oliver, T. (2015). "Discrete element modeling of a trafficked sub-base stabilized with biaxial and multi-axial geogrids to compare stabilization mechanisms." Proceedings of Geosynthetics 2015, Industrial Fabrics Association International, Roseville, MN, 245-254.

Joshi, R. V., and Zornberg, J. G. (2011). "Use of falling weight deflectometer data to quantify the relative performance of reinforced pavement sections." Proceedings of Geo-Frontiers: Advances in Geotechnical Engineering, ASCE, Reston, VA, 4713-4722.

Knighton, J. T. (2015). "Investigation of laboratory test procedures for assessing the structural capacity of geogrid-reinforced aggregate base materials." M.S. thesis, Department of Civil and Environmental Engineering, Brigham Young University, Provo, UT.

Kwon, J., and Tutumluer, E. (2009). "Geogrid base reinforcement with aggregate interlock and modeling of associated stiffness enhancement in mechanistic pavement analysis." Transportation Research Record: Journal of the Transportation Research Board, 2116, 85-95.

Kwon, J., Tutumluer, E., Al-Qadi, I., and Dessouky, S. (2008). "Effectiveness of geogrid base-reinforcement in low-volume flexible pavements." Proceedings of GeoCongress 2008: Geosustainability and Geohazard Mitigation, ASCE, Reston, VA, 1057-1064.

Moayedi, H., Kazemian, S., Prasad, A., and Huat, B. B. K. (2009). "Effect of geogrid reinforcement location in paved road improvement." Electronic Journal of Geotechnical Engineering, 14.

Nelson, L., Fountain, G. B., and Wayne, M. H. (2012). "Performance verification of a geogrid mechanically stabilized layer flexible pavement design as part of the La Media Road widening project." Proceedings of GeoCongress 2012: State of the Art and Practice in Geotechnical Engineering, ASCE, Reston, VA, 1391-1399.

Perkins, S. W. (1999). "Geosynthetic reinforcement of flexible pavements: laboratory based pavement test sections." Report No. FHWA/MT-99-001/8138, FHWA, U. S. Department of Transportation, Washington, DC.

Perkins, S. W., Christopher, B. R., Cuelho, E. L., Eiksund, G. R., Hoff, I., Schwartz, C. W., Svano, G., and Watn, A. (2004). "Development of design methods for geosynthetic-reinforced flexible pavements." Report No. DTFH61-01-X-00068, FHWA, U. S. Department of Transportation, Washington, DC.

Reck, N. C. (2009). "Mechanistic empirical design of geogrid reinforced paved flexible pavements." Proceedings of Jubilee Symposium on Polymer Geogrid Reinforcement, Institute of Civil Engineers, London, England.

Rohde, G. T. (1994). "Determining pavement structural number from FWD testing." Transportation Research Record: Journal of the Transportation Research Board, 1448, 61-68.

Schuettpelz, C., Fratta, D., and Edil, T. B. (2009). "Evaluation of the zone of influence and stiffness improvement from geogrid reinforcement in granular materials." Transportation Research Record: Journal of the Transportation Research Board, 2116, 76-84.

Tensar International Corporation. (2016). "Tensar triax (TX) geogrids." < http://www.tensarcorp.com/Systems-and-Products/Tensar-geogrids/Tensar-Triax-geogrid > (January 2017).

Thompson, M. (1999). "Hot-mix asphalt overlay design concepts for rubblized Portland cement concrete pavements." Transportation Research Record: Journal of the Transportation Research Board, 1684, 147-155.

Tingle, J. S., and Jersey, S. R. (2009). "Full-scale evaluation of geosynthetic-reinforced aggregate roads." Transportation Research Record: Journal of the Transportation Research Board, 2116, 96-107.

Tutumluer, E., Huang, H., and Bian, X. (2009). "Research on the behaviour of geogrids in stabilisation applications." Proceedings of Jubilee Symposium on Polymer Geogrid Reinforcement, Institute of Civil Engineers, London, England.

Wayne, M. H., Boudreau, R. L., and Kwon, J. (2011a). "Characterization of a mechanically stabilized layer using resilient modulus and permanent deformation testing." Proceedings of the 10th International Conference on Low-Volume Roads, Transportation Research Board, Washington, DC, 76-82.

Wayne, M. H., Kwon, J., and Boudreau, R. L. (2011b). "Resilient modulus, repeated load permanent deformation and plate load testing of a mechanically stabilized crushed miscellaneous base material." Proceedings of 90th Annual Meeting, Transportation Research Board, Washington, DC.

Wayne, M. H., White D. J., and Kwon, J. (2011c). "Field and laboratory evaluation of a mechanically stabilized salvaged base course used in the construction of US 12 Marmarth, North Dakota." Proceedings of 2011 Mid-Continent Transportation Research Symposium, Iowa State University, Ames, IA.

Wayne, M. H. (2016). "The use of geogrids for the development of mechanically stabilized layers." Proceedings of Geo-Chicago: Sustainability, Energy, and the Geoenvironment, ASCE, Reston, VA, 49-60.

Webster, S. L., Grau, R. H., and Williams, T. P. (1992). "Description and application of dual mass dynamic cone penetrometer." Report GL-92-3, Department of the Army, Washington, DC.

White, D. J., Vennapusa, P. K. R., Gieselman, H. H., Douglas, S. C., Zhang, J., and Wayne, M. H. (2011). "In-ground dynamic stress measurements for geosynthetic reinforced subgrade/subbase." Proceedings of Geo-Frontiers: Advances in Geotechnical Engineering, ASCE, Reston, VA, 4663-4672.

Xu, B., Ranjithan, S. R., and Kim, Y. R. (2002). "New relationships between falling weight deflectometer deflections and asphalt pavement layer condition indicators." Transportation Research Record: Journal of the Transportation Research Board, 1806, 48-56.

APPENDIX A FALLING-WEIGHT DEFLECTOMETER DATA

Table A-1 presents the individual FWD test values collected in this research. The 910-mm (36-in.) sensor appears to have malfunctioned for some tests. Although the sensor typically malfunctioned when the drop load was 53.4 kN (12,000 lb) or higher, the deflections presented in Table A-1 for the 910-mm (36-in.) sensor were consistently disregarded in this research and replaced with values computed through linear interpolation from the deflections measured using the 610-mm (24-in.) and 1220-mm (48-in.) sensors.

Table A-1: FWD Data for October 6, 2015, at Wells Draw Road

Test Section	Test Location	HMA Thickness (in.)	Base Thickness (in.)	Pavement Surface Temperature (°F)	Drop	Load (1000 lb)	Deflection (mils)								
							0 in.	8 in.	12 in.	18 in.	24 in.	36 in.	48 in.	60 in.	-12 in.
1	1	5.5	18.0	64.0	1	8.03	8.28	6.90	5.99	4.95	4.18	3.07	2.26	1.72	6.22
					2	8.03	8.19	6.82	5.94	4.92	4.15	2.99	2.23	1.70	6.15
					3	8.11	8.20	6.86	5.97	4.94	4.20	2.98	2.35	1.72	6.17
					4	8.01	8.11	6.78	5.89	4.90	4.15	2.97	2.29	1.70	6.07
					1	9.99	10.01	8.44	7.35	6.12	5.11	5.72	2.75	2.12	7.52
					2	9.96	10.01	8.45	7.35	6.13	5.13	3.80	2.77	2.12	7.49
					3	10.08	10.09	8.54	7.46	6.17	5.20	6.06	2.78	2.16	7.56
					4	10.13	10.03	8.50	7.43	6.15	5.17	3.79	2.78	2.15	7.52
					1	12.06	12.17	10.17	8.85	7.37	6.16	4.43	3.29	2.53	8.92
					2	12.11	12.06	10.21	8.88	7.40	6.18	6.85	3.35	2.56	8.96
					3	11.99	11.95	10.11	8.81	7.32	6.14	5.52	3.26	2.44	8.87
					4	11.89	11.80	10.06	8.76	7.31	6.10	4.98	3.26	2.50	8.82
					1	13.94	13.93	11.72	10.23	8.53	7.12	8.39	3.82	2.85	10.26
					2	13.94	13.90	11.77	10.29	8.56	7.14	10.65	3.87	2.99	10.31
					3	13.89	14.05	11.78	10.31	8.56	7.15	10.29	3.87	2.89	10.33
					4	14.01	13.92	11.85	10.31	8.59	7.16	10.20	3.88	2.98	10.35
					1	16.14	16.30	13.51	11.77	9.81	8.18	17.59	4.26	3.29	11.75
					2	16.04	15.87	13.47	11.78	9.81	8.16	10.36	4.30	3.30	11.72
					3	15.94	16.07	13.45	11.77	9.79	8.17	12.77	4.36	3.27	11.69
					4	16.06	16.04	13.54	11.84	9.84	8.20	12.91	4.36	3.30	11.78

Table A-1 Continued

Test Section	Test Location	HMA Thickness (in.)	Base Thickness (in.)	Pavement Surface Temperature (°F)	Drop	Load (1000 lb)	Deflection (mils)								
							0 in.	8 in.	12 in.	18 in.	24 in.	36 in.	48 in.	60 in.	-12 in.
1	2	5.5	18.0	62.5	1	8.06	7.98	6.39	5.43	4.34	3.57	2.67	2.13	1.52	5.94
					2	8.03	7.84	6.28	5.36	4.30	3.51	2.64	2.23	1.50	5.84
					3	8.06	7.82	6.30	5.38	4.32	3.53	2.64	2.11	1.51	5.84
					4	7.96	7.70	6.22	5.32	4.28	3.50	2.57	2.17	1.51	5.75
					1	9.94	9.62	7.84	6.72	5.40	4.41	3.30	2.56	1.87	7.16
					2	10.08	9.70	7.89	6.74	5.44	4.43	3.59	2.58	1.87	7.17
					3	10.01	9.61	7.86	6.73	5.44	4.42	3.29	2.52	1.86	7.14
					4	10.01	9.63	7.88	6.75	5.44	4.45	3.31	2.52	1.88	7.16
					1	11.96	11.56	9.45	8.09	6.57	5.32	9.57	3.21	2.34	8.52
					2	12.01	11.54	9.50	8.15	6.59	5.34	11.03	3.20	2.36	8.56
					3	11.96	11.63	9.47	8.12	6.58	5.35	12.46	3.18	2.27	8.55
					4	11.89	11.45	9.42	8.08	6.57	5.32	6.84	3.19	2.34	8.49
					1	14.21	13.53	11.12	9.56	7.73	6.24	12.95	3.66	2.66	9.94
					2	14.04	13.41	11.06	9.52	7.71	6.22	11.37	3.72	2.68	9.89
					3	13.87	13.40	11.03	9.48	7.71	6.21	16.85	3.68	2.60	9.86
					4	14.01	13.56	11.11	9.56	7.73	6.24	13.78	3.69	2.66	9.91
					1	15.97	15.23	12.56	10.81	8.73	7.06	14.11	4.11	3.03	11.19
					2	15.99	15.38	12.64	10.88	8.80	7.11	18.71	4.21	2.93	11.23
					3	16.02	15.40	12.64	10.85	8.78	7.12	15.04	4.17	2.95	11.21
					4	15.92	15.32	12.59	10.83	8.77	7.11	14.05	4.14	2.99	11.18
1	3	5.5	18.0	63.5	1	7.96	8.39	6.77	5.79	4.71	3.92	2.71	2.01	1.53	6.28
					2	8.01	8.31	6.74	5.78	4.70	3.94	2.72	2.06	1.54	6.27
					3	8.03	8.23	6.70	5.76	4.67	3.90	2.70	2.00	1.53	6.20
					4	7.98	8.17	6.65	5.74	4.67	3.90	2.71	2.05	1.53	6.15
					1	10.08	10.18	8.41	7.23	5.90	4.89	3.40	2.53	1.91	7.62
					2	10.03	10.17	8.41	7.24	5.89	4.89	3.41	2.55	1.92	7.59
					3	9.96	10.12	8.38	7.21	5.88	4.88	3.41	2.54	1.92	7.56
					4	9.94	10.13	8.37	7.22	5.89	4.89	3.41	2.52	1.92	7.54
					1	12.01	12.33	10.24	8.83	7.20	5.96	4.17	3.14	2.29	9.14
					2	12.04	12.28	10.23	8.84	7.21	5.98	4.22	3.19	2.30	9.12
					3	12.04	12.24	10.19	8.81	7.19	5.98	4.17	3.16	2.36	9.10
					4	11.91	12.19	10.17	8.79	7.16	5.95	4.16	3.15	2.28	9.07
					1	13.92	14.15	11.84	10.23	8.39	6.91	4.82	3.66	2.65	10.50
					2	13.96	14.32	11.89	10.26	8.43	6.93	4.89	3.69	2.74	10.53
					3	13.77	14.24	11.86	10.25	8.40	6.93	4.88	3.69	2.67	10.50
					4	13.89	14.34	11.90	10.29	8.43	6.98	4.92	3.68	2.66	10.53
					1	15.92	16.27	13.55	11.71	9.59	7.91	6.61	4.22	3.05	11.94
					2	15.92	16.40	13.64	11.81	9.67	7.98	5.48	4.28	3.05	12.02
					3	16.04	16.43	13.73	11.88	9.76	8.03	5.49	4.24	3.07	12.10
					4	15.92	16.40	13.70	11.82	9.68	7.99	5.60	4.24	3.05	12.07

Table A-1 Continued

Test Section	Test Location	HMA Thickness (in.)	Base Thickness (in.)	Pavement Surface Temperature (°F)	Drop	Load (1000 lb)	Deflection (mils)								
							0 in.	8 in.	12 in.	18 in.	24 in.	36 in.	48 in.	60 in.	-12 in.
1	4	5.5	18.0	64.0	1	8.18	7.74	6.29	5.37	4.42	3.73	2.69	1.99	1.56	5.86
					2	7.93	7.49	6.08	5.20	4.28	3.66	2.60	1.91	1.54	5.72
					3	7.96	7.52	6.11	5.23	4.32	3.63	2.66	1.91	1.51	5.70
					4	7.98	7.53	6.11	5.24	4.31	3.65	2.65	1.93	1.52	5.72
					1	9.99	9.35	7.63	6.56	5.43	4.50	3.29	2.42	1.89	7.07
					2	10.01	9.39	7.68	6.61	5.46	4.52	3.32	2.45	1.89	7.07
					3	9.94	9.35	7.66	6.60	5.44	4.56	3.26	2.42	1.92	7.06
					4	9.96	9.41	7.67	6.62	5.47	4.54	3.30	2.45	1.91	7.06
					1	12.11	11.51	9.40	8.11	6.69	5.61	4.04	3.05	2.36	8.58
					2	12.04	11.44	9.40	8.09	6.68	5.59	4.03	3.04	2.34	8.55
					3	12.04	11.39	9.40	8.09	6.69	5.59	4.06	3.03	2.33	8.55
					4	11.84	11.23	9.28	7.98	6.61	5.49	3.91	3.00	2.32	8.41
					1	14.01	13.82	11.07	9.54	7.92	6.55	4.74	3.61	2.69	10.02
					2	14.01	15.04	11.09	9.54	7.92	6.55	4.75	3.62	2.74	10.01
					3	13.96	13.50	11.10	9.57	7.93	6.58	4.79	3.62	2.71	10.02
					4	13.96	13.42	11.08	9.54	7.92	6.59	4.72	3.61	2.75	10.01
					1	16.11	15.49	12.73	10.98	9.14	7.49	5.48	4.09	3.07	11.43
					2	15.87	18.96	12.70	10.94	9.12	7.52	5.53	4.11	3.05	11.39
					3	16.14	16.36	12.85	11.07	9.21	7.57	5.44	4.21	3.17	11.52
					4	16.02	16.97	12.82	11.06	9.20	7.59	5.49	4.15	3.15	11.51
1	5	5.5	18.0	62.5	1	8.13	8.06	6.73	5.85	4.84	4.03	2.97	2.45	1.72	6.28
					2	8.18	7.89	6.61	5.75	4.80	3.99	2.91	2.44	1.70	6.19
					3	8.03	7.82	6.51	5.64	4.69	3.94	2.87	2.28	1.67	6.05
					4	8.06	7.72	6.50	5.65	4.69	3.91	2.87	2.28	1.67	6.03
					1	10.13	9.77	8.29	7.24	6.02	5.02	3.73	2.78	2.13	7.61
					2	10.06	9.67	8.22	7.17	5.96	4.99	3.60	2.74	2.12	7.52
					3	9.84	9.56	8.13	7.10	5.89	4.95	3.60	2.72	2.10	7.43
					4	9.96	9.58	8.17	7.15	5.93	4.96	3.66	2.74	2.11	7.46
					1	12.16	11.72	10.04	8.76	7.31	6.08	4.45	3.41	2.57	9.08
					2	12.08	11.72	10.00	8.74	7.27	6.07	4.79	3.40	2.59	9.04
					3	11.91	11.62	9.94	8.69	7.22	6.03	4.47	3.39	2.57	9.00
					4	11.87	11.63	9.96	8.70	7.26	6.02	4.42	3.36	2.56	9.01
					1	14.09	13.68	11.74	10.29	8.57	7.07	5.20	3.90	3.00	10.57
					2	14.04	13.80	11.75	10.30	8.58	7.11	9.45	4.03	3.00	10.61
					3	13.96	13.82	11.74	10.28	8.57	7.12	11.13	4.03	3.03	10.60
					4	14.06	13.81	11.79	10.31	8.61	7.11	5.23	4.03	3.03	10.64
					1	16.09	15.78	13.49	11.83	9.85	8.18	14.95	4.60	3.44	12.11
					2	16.02	15.80	13.52	11.87	9.88	8.21	13.76	4.58	3.39	12.17
					3	16.04	15.94	13.54	11.88	9.91	8.22	12.69	4.57	3.41	12.21
					4	15.97	15.89	13.50	11.84	9.86	8.21	12.24	4.54	3.38	12.15

Table A-1 Continued

Test Section	Test Location	HMA Thickness (in.)	Base Thickness (in.)	Pavement Surface Temperature (°F)	Drop	Load (1000 lb)	Deflection (mils)								
							0 in.	8 in.	12 in.	18 in.	24 in.	36 in.	48 in.	60 in.	-12 in.
2	1	5.5	18.0	62.5	1	8.01	8.45	6.87	5.78	4.51	3.48	2.14	1.76	0.96	5.96
					2	8.01	8.28	6.76	5.70	4.47	3.43	2.10	1.47	0.94	5.85
					3	7.71	7.93	6.50	5.47	4.31	3.33	2.06	1.38	0.90	5.58
					4	7.86	8.03	6.61	5.59	4.37	3.39	2.05	1.38	0.93	5.69
					1	9.94	10.17	8.38	7.10	5.56	4.31	2.77	1.84	1.25	7.14
					2	9.89	10.15	8.40	7.11	5.58	4.32	2.75	1.83	1.22	7.14
					3	9.94	10.17	8.44	7.17	5.65	4.35	2.77	1.85	1.21	7.16
					4	9.99	10.19	8.47	7.19	5.67	4.37	2.79	1.81	1.18	7.19
					1	11.99	12.01	10.01	8.53	6.65	5.19	3.30	2.18	1.39	8.40
					2	12.01	12.05	10.05	8.55	6.74	5.18	3.32	2.20	1.49	8.45
					3	12.01	12.03	10.03	8.54	6.70	5.19	3.34	2.16	1.47	8.46
					4	11.96	12.06	10.07	8.58	6.75	5.22	3.33	2.25	1.39	8.46
					1	13.89	13.70	11.42	9.71	7.68	5.87	3.79	2.58	1.61	9.54
					2	14.04	13.87	11.56	9.84	7.73	6.00	3.88	2.59	1.61	9.66
					3	14.01	13.91	11.60	9.86	7.73	6.02	3.89	2.76	1.64	9.72
					4	14.06	13.93	11.64	9.90	7.78	6.04	3.84	2.72	1.64	9.74
					1	15.97	15.53	12.96	11.02	8.64	6.66	4.28	3.01	1.85	10.81
					2	15.97	15.59	13.01	11.07	8.70	6.72	4.27	2.90	1.85	10.87
					3	16.02	15.62	13.06	11.10	8.71	6.77	4.35	2.91	1.87	10.90
					4	16.02	15.62	13.07	11.10	8.72	6.76	4.31	2.95	1.85	10.91
2	2	5.5	18.0	66.5	1	8.03	6.81	5.32	4.39	3.39	2.57	1.54	1.51	0.79	4.70
					2	8.08	6.73	5.26	4.37	3.38	2.55	1.55	1.91	0.85	4.67
					3	7.98	6.57	5.15	4.28	3.29	2.52	1.54	1.69	0.80	4.55
					4	7.98	6.58	5.17	4.30	3.34	2.52	1.53	1.70	0.79	4.57
					1	10.06	8.31	6.60	5.49	4.26	3.22	2.04	1.40	1.01	5.69
					2	10.08	8.30	6.61	5.50	4.28	3.25	1.98	1.63	1.02	5.69
					3	10.06	8.30	6.62	5.50	4.27	3.23	2.03	1.65	1.03	5.71
					4	10.06	8.27	6.60	5.51	4.25	3.26	2.05	1.53	1.02	5.68
					1	12.01	9.85	7.88	6.58	5.12	3.90	2.43	1.74	1.22	6.73
					2	12.06	9.90	7.93	6.63	5.17	3.92	2.53	1.78	1.24	6.77
					3	12.01	9.90	7.92	6.63	5.15	3.93	2.54	1.76	1.23	6.75
					4	12.01	9.84	7.91	6.62	5.17	3.91	2.44	1.75	1.21	6.73
					1	13.99	11.39	9.15	7.67	5.97	4.56	2.87	2.05	1.44	7.75
					2	14.11	11.56	9.27	7.77	6.07	4.62	2.80	2.09	1.44	7.85
					3	13.96	11.43	9.19	7.71	6.00	4.59	2.82	2.08	1.37	7.77
					4	13.99	11.51	9.24	7.74	6.04	4.60	3.07	2.06	1.41	7.82
					1	15.94	13.00	10.45	8.78	6.82	5.19	3.15	2.32	1.56	8.82
					2	16.06	13.14	10.55	8.85	6.89	5.27	3.49	2.34	1.57	8.93
					3	16.04	13.18	10.56	8.87	6.91	5.28	3.20	2.36	1.58	8.94
					4	15.94	13.09	10.52	8.84	6.88	5.24	8.15	2.38	1.62	8.92

Table A-1 Continued

Test Section	Test Location	HMA Thickness (in.)	Base Thickness (in.)	Pavement Surface Temperature (°F)	Drop	Load (1000 lb)	Deflection (mils)								
							0 in.	8 in.	12 in.	18 in.	24 in.	36 in.	48 in.	60 in.	-12 in.
2	3	5.5	18.0	67.5	1	7.93	6.50	5.22	4.41	3.71	2.96	2.10	1.80	1.26	4.71
					2	7.91	6.38	5.20	4.40	3.70	2.96	2.16	1.64	1.28	4.65
					3	7.91	6.33	5.20	4.40	3.68	2.97	2.20	1.76	1.27	4.63
					4	7.98	6.33	5.19	4.40	3.67	2.95	2.16	1.68	1.26	4.60
					1	9.94	7.86	6.47	5.51	4.59	3.68	2.75	2.00	1.58	5.66
					2	9.99	7.86	6.54	5.53	4.57	3.71	2.74	1.98	1.57	5.69
					3	9.94	7.84	6.52	5.53	4.59	3.70	2.72	1.97	1.58	5.68
					4	10.01	7.90	6.57	5.57	4.64	3.72	3.11	2.00	1.60	5.70
					1	11.99	9.37	7.85	6.69	5.55	4.42	13.01	2.46	1.92	6.75
					2	11.96	9.07	7.87	6.72	5.56	4.43	14.62	2.45	1.92	6.76
					3	11.94	9.59	7.87	6.68	5.57	4.44	14.95	2.44	1.92	6.73
					4	11.99	9.64	7.93	6.75	5.64	4.49	14.24	2.41	1.92	6.79
					1	13.96	11.05	9.14	7.79	6.56	5.15	7.43	2.79	2.23	7.79
					2	13.99	11.03	9.20	7.86	6.56	5.17	7.32	2.86	2.27	7.82
					3	14.06	11.02	9.23	7.88	6.58	5.19	3.98	2.87	2.26	7.88
					4	13.92	11.05	9.19	7.83	6.59	5.17	3.67	2.84	2.26	7.84
					1	15.97	12.36	10.39	8.88	7.34	5.81	4.27	3.21	2.54	8.83
					2	15.92	12.38	10.41	8.90	7.35	5.83	4.27	3.25	2.53	8.85
					3	15.92	12.70	10.47	8.94	7.32	5.85	13.33	3.25	2.55	8.92
					4	15.97	12.57	10.49	8.95	7.38	5.88	10.95	3.21	2.55	8.95
2	4	5.5	18.0	68.5	1	7.96	8.14	6.36	5.22	3.90	2.93	1.77	1.59	0.71	5.73
					2	8.01	8.08	6.34	5.22	3.92	2.95	1.72	1.72	0.75	5.73
					3	8.08	8.02	6.30	5.19	3.91	2.90	1.80	1.83	0.71	5.72
					4	8.01	8.00	6.29	5.20	3.90	2.93	1.73	1.71	0.72	5.66
					1	9.86	9.82	7.78	6.43	4.86	3.66	2.29	1.36	0.91	6.94
					2	9.84	9.82	7.80	6.44	4.88	3.66	7.07	1.38	0.91	6.91
					3	9.89	9.76	7.80	6.42	4.88	3.66	6.81	1.39	0.90	6.88
					4	9.94	9.89	7.89	6.51	4.94	3.71	6.77	1.56	0.84	6.95
					1	12.04	11.81	9.45	7.85	5.97	4.46	15.26	1.71	1.03	8.22
					2	11.94	11.79	9.43	7.83	5.95	4.46	12.41	1.69	1.03	8.17
					3	11.96	11.81	9.47	7.87	5.98	4.46	13.87	1.70	1.01	8.22
					4	12.11	11.80	9.45	7.87	5.99	4.45	13.59	1.71	1.02	8.20
					1	13.96	13.54	10.80	9.00	6.83	5.12	17.76	2.00	1.20	9.34
					2	13.99	13.60	10.89	9.08	6.89	5.19	18.31	1.98	1.18	9.39
					3	14.01	13.65	10.91	9.11	6.93	5.20	19.21	2.00	1.20	9.45
					4	14.14	13.68	10.94	9.18	6.96	5.27	19.60	2.09	1.19	9.49
					1	16.04	15.39	12.33	10.28	7.79	5.87	20.60	2.34	1.37	10.66
					2	16.21	15.39	12.36	10.31	7.82	5.90	15.30	2.25	1.36	10.68
					3	15.97	15.38	12.31	10.28	7.75	5.85	15.59	2.20	1.36	10.63
					4	16.02	15.28	12.32	10.27	7.77	5.90	16.13	2.27	1.35	10.66

Table A-1 Continued

Test Section	Test Location	HMA Thickness (in.)	Base Thickness (in.)	Pavement Surface Temperature (°F)	Drop	Load (1000 lb)	Deflection (mils)								
							0 in.	8 in.	12 in.	18 in.	24 in.	36 in.	48 in.	60 in.	-12 in.
2	5	5.5	18.0	67.5	1	8.20	9.01	6.92	5.65	4.15	2.95	1.51	1.64	0.73	6.22
					2	8.13	8.77	6.76	5.54	4.09	2.89	1.51	1.61	0.76	6.08
					3	8.03	8.61	6.66	5.46	4.05	2.85	1.47	2.00	0.72	5.96
					4	8.13	8.67	6.72	5.51	4.08	2.86	1.42	2.14	0.71	6.00
					1	10.11	10.74	8.34	6.81	5.06	3.55	1.85	2.22	0.92	7.33
					2	10.03	10.55	8.30	6.78	5.02	3.54	4.00	2.18	0.82	7.30
					3	10.03	10.51	8.25	6.76	5.01	3.53	8.30	1.97	0.82	7.26
					4	10.03	10.54	8.30	6.80	5.04	3.55	1.82	2.28	0.82	7.29
					1	11.91	12.44	9.88	8.09	5.93	4.21	5.15	1.83	0.95	8.47
					2	12.04	12.55	9.98	8.15	6.01	4.27	4.94	1.92	0.95	8.54
					3	11.91	12.50	9.92	8.12	5.99	4.25	7.58	1.55	0.96	8.51
					4	11.94	12.50	9.94	8.15	6.01	4.26	2.26	1.89	0.96	8.50
					1	13.96	14.51	11.56	9.43	6.89	4.88	9.54	2.05	1.11	9.81
					2	13.92	14.53	11.57	9.48	6.95	4.91	10.40	1.93	1.12	9.86
					3	13.96	14.64	11.68	9.53	6.99	4.97	7.72	1.88	1.12	9.93
					4	14.11	14.78	11.75	9.62	7.05	5.00	10.82	2.04	1.13	9.96
					1	15.84	16.38	13.15	10.69	7.82	5.57	9.20	1.96	1.23	11.14
					2	15.99	16.68	13.30	10.82	7.89	5.62	8.04	2.00	1.23	11.24
					3	15.87	16.59	13.24	10.81	7.89	5.65	11.41	2.01	1.25	11.23
					4	16.04	16.75	13.39	10.93	7.95	5.67	12.07	2.38	1.27	11.31
3	1	5.5	18.0	76.0	1	7.93	5.95	4.81	4.11	3.35	2.84	2.11	2.24	1.32	4.21
					2	8.06	5.98	4.82	4.10	3.37	2.86	2.14	2.14	1.31	4.25
					3	8.13	6.01	4.86	4.15	3.40	2.88	2.11	2.00	1.31	4.28
					4	8.15	5.99	4.85	4.15	3.40	2.87	2.14	2.04	1.30	4.26
					1	10.06	7.42	6.05	5.17	4.26	3.57	2.72	2.15	1.65	5.29
					2	10.13	7.51	6.11	5.22	4.28	3.62	2.68	2.16	1.67	5.36
					3	10.16	7.46	6.08	5.18	4.26	3.58	2.68	2.15	1.68	5.31
					4	10.01	7.38	6.02	5.14	4.21	3.53	2.64	2.13	1.64	5.24
					1	11.99	8.85	7.22	6.19	5.05	4.26	3.12	2.53	1.97	6.25
					2	12.04	8.94	7.29	6.24	5.11	4.31	3.20	2.57	1.99	6.32
					3	12.06	8.90	7.29	6.25	5.12	4.30	3.13	2.51	2.00	6.31
					4	12.01	8.93	7.29	6.23	5.10	4.32	3.15	2.53	2.00	6.29
					1	14.09	10.39	8.47	7.27	5.96	5.00	3.91	3.06	2.31	7.29
					2	14.18	10.47	8.56	7.33	5.97	5.03	3.68	2.96	2.31	7.39
					3	14.09	10.46	8.51	7.30	6.01	5.02	3.81	2.98	2.32	7.33
					4	14.04	10.41	8.52	7.30	5.99	5.03	3.69	2.92	2.32	7.32
					1	16.21	11.87	9.73	8.38	6.85	5.71	4.32	3.37	2.66	8.38
					2	16.11	11.86	9.72	8.35	6.82	5.72	4.37	3.37	2.63	8.38
					3	16.02	11.81	9.70	8.33	6.84	5.71	4.48	3.38	2.65	8.36
					4	16.11	11.85	9.71	8.35	6.80	5.71	4.17	3.33	2.64	8.38

Table A-1 Continued

Test Section	Test Location	HMA Thickness (in.)	Base Thickness (in.)	Pavement Surface Temperature (°F)	Drop	Load (1000 lb)	Deflection (mils)								
							0 in.	8 in.	12 in.	18 in.	24 in.	36 in.	48 in.	60 in.	-12 in.
3	2	5.5	18.0	74.5	1	8.03	7.94	6.54	5.66	4.73	3.95	3.20	2.29	1.73	5.98
					2	7.91	7.74	6.38	5.53	4.63	3.87	3.16	2.24	1.71	5.85
					3	8.18	7.88	6.49	5.65	4.73	4.01	3.26	2.32	1.76	5.95
					4	8.08	7.82	6.48	5.63	4.69	3.97	3.26	2.29	1.75	5.92
					1	9.96	9.73	8.09	7.01	5.88	4.93	7.22	2.87	2.17	7.32
					2	9.99	9.70	8.08	7.03	5.87	4.90	8.41	2.84	2.18	7.25
					3	10.01	9.75	8.12	7.07	5.93	4.94	9.13	2.90	2.19	7.30
					4	9.94	9.71	8.10	7.03	5.88	4.93	9.83	2.84	2.16	7.28
					1	11.91	11.58	9.71	8.46	7.03	5.90	10.18	3.43	2.62	8.60
					2	11.84	11.63	9.73	8.48	7.08	5.91	8.79	3.41	2.63	8.66
					3	12.01	11.83	9.84	8.60	7.17	5.97	11.78	3.46	2.66	8.74
					4	12.08	11.76	9.86	8.59	7.15	5.99	10.67	3.43	2.65	8.75
					1	13.96	13.59	11.42	9.97	8.27	6.93	12.90	3.97	3.06	10.08
					2	14.01	13.60	11.49	10.01	8.34	6.99	7.61	3.98	3.08	10.13
					3	14.01	13.65	11.51	10.04	8.33	6.98	12.32	3.98	3.06	10.16
					4	13.94	13.61	11.48	10.02	8.31	6.96	13.13	3.98	3.07	10.12
					1	15.94	15.51	13.09	11.43	9.52	7.94	15.36	4.56	3.52	11.53
					2	15.89	15.51	13.11	11.44	9.53	7.96	11.42	4.63	3.53	11.53
					3	16.02	15.71	13.23	11.55	9.62	8.03	15.84	4.65	3.57	11.63
					4	16.04	15.74	13.25	11.57	9.60	8.03	11.71	4.64	3.57	11.65
3	3	5.5	18.0	73.5	1	8.13	7.17	5.91	5.11	4.23	3.67	2.68	2.08	1.71	5.27
					2	8.11	7.05	5.83	5.05	4.19	3.68	2.72	2.06	1.71	5.18
					3	8.13	7.09	5.89	5.09	4.22	3.68	2.68	2.08	1.71	5.22
					4	8.13	7.04	5.83	5.05	4.19	3.65	2.68	2.07	1.68	5.21
					1	10.13	8.77	7.29	6.32	5.19	4.50	3.35	2.55	2.10	6.42
					2	10.18	8.78	7.31	6.32	5.24	4.52	3.37	2.59	2.12	6.43
					3	10.11	8.79	7.30	6.32	5.22	4.51	3.35	2.58	2.11	6.45
					4	10.13	8.75	7.26	6.29	5.21	4.51	3.37	2.58	2.11	6.42
					1	12.13	10.55	8.83	7.65	6.32	5.46	4.11	3.10	2.55	7.71
					2	12.13	10.57	8.84	7.67	6.35	5.48	4.16	3.11	2.56	7.71
					3	12.08	10.49	8.80	7.63	6.33	5.47	4.07	3.12	2.53	7.69
					4	12.06	10.53	8.79	7.63	6.32	5.46	4.07	3.12	2.54	7.67
					1	14.21	12.33	10.34	8.97	7.42	6.36	4.79	3.60	2.98	8.99
					2	14.06	12.27	10.28	8.94	7.41	6.34	4.87	3.60	2.94	8.94
					3	14.09	12.22	10.28	8.92	7.38	6.34	4.76	3.60	2.95	8.97
					4	14.04	12.22	10.26	8.91	7.38	6.34	4.74	3.62	2.96	8.95
					1	16.19	13.94	11.67	10.16	8.39	7.18	5.67	4.05	3.38	10.17
					2	16.11	13.92	11.70	10.18	8.39	7.21	5.42	4.08	3.35	10.19
					3	16.11	13.91	11.69	10.17	8.42	7.20	7.31	4.10	3.37	10.21
					4	16.02	13.89	11.66	10.14	8.38	7.18	11.36	4.05	3.34	10.14

Table A-1 Continued

Test Section	Test Location	HMA Thickness (in.)	Base Thickness (in.)	Pavement Surface Temperature (°F)	Drop	Load (1000 lb)	Deflection (mils)								
							0 in.	8 in.	12 in.	18 in.	24 in.	36 in.	48 in.	60 in.	-12 in.
3	4	5.5	18.0	73.0	1	7.81	7.27	5.42	4.56	3.67	3.02	2.13	2.40	1.34	4.69
					2	8.01	6.60	5.51	4.65	3.75	3.11	2.20	2.12	1.37	4.79
					3	8.06	6.75	5.50	4.67	3.75	3.09	2.19	2.24	1.35	4.77
					4	7.93	6.64	5.41	4.58	3.68	3.03	2.17	2.14	1.36	4.69
					1	10.06	8.33	6.81	5.77	4.61	3.84	2.74	2.19	1.66	5.87
					2	10.03	8.38	6.85	5.80	4.64	3.83	2.69	2.19	1.68	5.87
					3	10.03	8.33	6.81	5.75	4.63	3.82	2.70	2.16	1.67	5.86
					4	9.94	8.28	6.77	5.72	4.57	3.79	2.65	2.17	1.65	5.80
					1	11.96	9.89	8.18	6.93	5.57	4.57	6.72	2.57	2.01	6.91
					2	11.94	9.94	8.18	6.95	5.56	4.57	3.23	2.65	2.03	6.96
					3	12.01	10.01	8.24	6.99	5.63	4.61	3.28	2.67	2.04	7.01
					4	12.06	10.00	8.25	6.99	5.61	4.60	3.32	2.67	2.06	6.99
					1	14.06	11.58	9.58	8.12	6.54	5.36	7.39	3.06	2.37	8.11
					2	14.16	11.72	9.66	8.21	6.60	5.37	4.25	3.11	2.39	8.19
					3	14.09	11.66	9.63	8.15	6.58	5.40	3.92	3.13	2.38	8.15
					4	14.06	11.64	9.61	8.15	6.57	5.35	3.84	3.08	2.38	8.15
					1	16.14	13.16	10.92	9.29	7.49	6.14	9.65	3.47	2.72	9.27
					2	16.04	13.21	10.91	9.27	7.46	6.13	8.09	3.44	2.72	9.25
					3	16.06	13.24	10.96	9.29	7.47	6.14	9.02	3.46	2.67	9.29
					4	15.99	13.18	10.91	9.28	7.45	6.10	9.41	3.45	2.72	9.28
3	5	5.5	18.0	71.5	1	8.01	7.34	5.55	4.64	3.72	2.95	1.99	1.91	1.05	5.32
					2	8.03	7.29	5.53	4.63	3.74	2.93	1.98	1.91	1.03	5.32
					3	7.86	7.15	5.43	4.55	3.67	2.87	1.95	1.82	1.02	5.19
					4	8.08	7.27	5.52	4.63	3.72	2.96	1.99	1.97	1.07	5.28
					1	9.94	8.98	6.91	5.80	4.62	3.71	2.60	1.99	1.33	6.50
					2	9.86	8.98	6.93	5.83	4.68	3.73	2.65	2.00	1.32	6.51
					3	9.91	8.96	6.96	5.83	4.68	3.73	2.63	1.87	1.33	6.50
					4	9.99	9.06	7.01	5.90	4.75	3.76	2.75	2.27	1.34	6.58
					1	11.77	10.75	8.43	7.11	5.72	4.54	7.70	2.53	1.61	7.74
					2	11.79	10.81	8.47	7.13	5.74	4.54	6.75	2.36	1.62	7.75
					3	11.91	10.93	8.59	7.25	5.83	4.60	9.11	2.40	1.66	7.84
					4	12.01	10.98	8.64	7.27	5.86	4.63	9.20	2.42	1.65	7.85
					1	13.84	12.72	10.02	8.46	6.79	5.39	10.94	2.91	1.92	9.07
					2	14.04	12.93	10.22	8.62	6.93	5.50	11.17	2.87	1.96	9.23
					3	13.96	12.89	10.17	8.61	6.90	5.48	14.38	2.92	1.98	9.22
					4	14.01	12.93	10.23	8.64	6.95	5.52	9.17	2.85	1.97	9.23
					1	15.87	14.65	11.65	9.84	7.89	6.27	15.37	3.31	2.25	10.47
					2	16.02	14.85	11.78	9.95	7.92	6.34	12.93	3.30	2.28	10.58
					3	15.99	14.79	11.75	9.93	7.95	6.34	14.21	3.28	2.27	10.57
					4	15.99	14.83	11.78	9.98	7.98	6.37	10.31	3.28	2.27	10.57

Table A-1 Continued

Test Section	Test Location	HMA Thickness (in.)	Base Thickness (in.)	Pavement Surface Temperature (°F)	Drop	Load (1000 lb)	Deflection (mils)								
							0 in.	8 in.	12 in.	18 in.	24 in.	36 in.	48 in.	60 in.	-12 in.
4	1	5.5	18.0	69.5	1	8.06	7.60	5.87	4.87	3.73	2.90	1.79	2.20	0.88	5.40
					2	7.84	7.27	5.65	4.70	3.62	2.77	1.70	1.60	0.86	5.19
					3	7.86	7.30	5.69	4.74	3.64	2.82	1.75	1.70	0.86	5.14
					4	7.98	7.38	5.77	4.80	3.69	2.84	1.76	2.31	0.86	5.24
					1	10.01	9.39	7.41	6.20	4.79	3.69	2.33	2.22	1.14	6.56
					2	10.06	9.44	7.47	6.24	4.86	3.71	2.43	2.24	1.14	6.61
					3	9.96	9.39	7.44	6.23	4.83	3.71	2.40	2.36	1.12	6.59
					4	10.11	9.53	7.56	6.30	4.90	3.74	2.46	1.64	1.15	6.64
					1	11.94	11.27	8.99	7.53	5.84	4.49	2.83	1.92	1.39	7.80
					2	11.96	11.35	9.05	7.60	5.90	4.52	2.87	2.08	1.40	7.86
					3	11.96	11.34	9.03	7.58	5.88	4.51	2.89	2.12	1.34	7.86
					4	11.84	11.23	8.96	7.50	5.83	4.46	6.01	1.93	1.40	7.79
					1	13.72	13.06	10.40	8.74	6.80	5.19	6.89	2.29	1.61	8.99
					2	14.06	13.32	10.72	9.00	6.99	5.34	8.75	2.37	1.65	9.26
					3	14.11	13.46	10.79	9.06	7.05	5.41	8.64	2.36	1.61	9.31
					4	14.11	13.37	10.83	9.08	7.08	5.42	3.68	2.33	1.69	9.32
					1	15.75	14.96	12.10	10.17	7.89	6.04	7.72	2.68	1.82	10.37
					2	16.06	15.23	12.37	10.39	8.09	6.23	9.70	2.71	1.93	10.59
					3	16.04	15.23	12.36	10.38	8.07	6.21	9.71	2.71	1.86	10.60
					4	15.97	15.24	12.37	10.40	8.08	6.21	9.49	2.75	1.83	10.60
4	2	5.5	18.0	69.5	1	8.06	6.61	5.06	4.15	3.11	2.46	1.54	1.51	0.91	4.57
					2	8.18	6.56	5.05	4.14	3.16	2.45	1.53	1.43	0.94	4.57
					3	8.03	6.45	4.96	4.07	3.07	2.39	1.47	1.36	0.94	4.47
					4	8.11	6.45	4.99	4.09	3.10	2.42	1.47	1.43	0.98	4.48
					1	10.03	8.09	6.35	5.24	3.98	3.09	2.04	1.43	1.12	5.57
					2	10.11	8.09	6.36	5.24	3.98	3.10	1.97	1.45	1.16	5.59
					3	9.96	8.02	6.27	5.18	3.94	3.06	1.96	1.44	1.12	5.53
					4	10.01	8.06	6.32	5.22	3.95	3.08	2.00	1.46	1.14	5.56
					1	11.91	9.59	7.60	6.28	4.81	3.68	11.52	1.69	1.36	6.55
					2	12.04	9.67	7.69	6.37	4.85	3.73	4.97	1.74	1.35	6.62
					3	12.13	9.73	7.74	6.40	4.88	3.76	10.16	1.73	1.37	6.63
					4	12.01	9.70	7.69	6.38	4.86	3.74	8.05	1.73	1.36	6.60
					1	13.96	11.19	8.92	7.41	5.65	4.34	11.89	2.00	1.51	7.60
					2	14.06	11.28	9.01	7.49	5.72	4.40	10.74	2.01	1.58	7.67
					3	14.06	11.32	9.04	7.50	5.73	4.42	5.27	2.05	1.52	7.67
					4	14.04	11.32	9.03	7.49	5.73	4.40	6.30	1.99	1.58	7.69
					1	15.89	12.72	10.17	8.45	6.47	4.96	9.43	2.29	1.78	8.66
					2	16.16	12.98	10.38	8.64	6.58	5.11	9.52	2.30	1.79	8.80
					3	16.06	12.92	10.32	8.59	6.55	5.06	9.50	2.29	1.75	8.75
					4	16.02	12.88	10.31	8.57	6.53	5.03	5.78	2.31	1.85	8.74

Table A-1 Continued

Test Section	Test Location	HMA Thickness (in.)	Base Thickness (in.)	Pavement Surface Temperature (°F)	Drop	Load (1000 lb)	Deflection (mils)								
							0 in.	8 in.	12 in.	18 in.	24 in.	36 in.	48 in.	60 in.	-12 in.
4	3	5.5	18.0	69.5	1	8.06	5.99	4.60	3.76	2.91	2.29	1.75	1.61	0.90	4.11
					2	8.11	5.96	4.57	3.73	2.88	2.28	1.77	1.84	0.96	4.10
					3	8.13	5.96	4.58	3.74	2.92	2.27	1.71	1.68	0.93	4.08
					4	8.03	5.88	4.54	3.69	2.87	2.27	1.63	1.69	0.93	4.02
					1	9.99	7.29	5.68	4.65	3.60	2.87	3.96	1.61	1.17	4.99
					2	9.91	7.30	5.67	4.66	3.62	2.86	4.65	1.68	1.15	4.98
					3	10.01	7.30	5.67	4.67	3.62	2.88	5.99	1.72	1.14	5.00
					4	10.06	7.36	5.77	4.75	3.62	2.93	2.04	1.54	1.19	4.93
					1	11.94	8.86	6.86	5.65	4.39	3.42	6.53	1.79	1.38	5.81
					2	12.16	9.04	6.98	5.72	4.45	3.52	7.57	1.82	1.41	5.93
					3	12.04	8.93	6.92	5.69	4.42	3.46	6.81	1.80	1.41	5.87
					4	12.04	8.80	6.93	5.71	4.43	3.46	5.61	1.77	1.40	5.88
					1	13.99	10.07	7.95	6.55	5.09	4.01	4.80	2.08	1.59	6.74
					2	14.09	10.37	8.05	6.61	5.13	4.03	7.56	2.08	1.63	6.76
					3	14.06	10.39	8.04	6.62	5.12	4.02	6.42	2.07	1.63	6.80
					4	14.06	10.22	8.03	6.63	5.13	4.07	6.61	2.04	1.62	6.81
					1	15.94	11.53	9.01	7.44	5.74	4.54	6.26	2.26	1.80	7.61
					2	15.99	11.55	9.09	7.49	5.78	4.56	6.96	2.34	1.83	7.71
					3	16.11	11.81	9.11	7.51	5.83	4.60	7.54	2.43	1.86	7.72
					4	16.09	11.65	9.12	7.52	5.81	4.58	6.31	2.42	1.87	7.73
4	4	5.5	18.0	69.5	1	8.06	7.50	5.77	4.78	3.68	2.94	1.99	1.89	1.39	5.17
					2	8.03	7.43	5.74	4.75	3.70	2.94	1.99	1.69	1.18	5.15
					3	8.13	7.40	5.75	4.74	3.70	2.94	2.03	1.63	1.22	5.10
					4	8.13	7.29	5.69	4.69	3.68	2.91	2.04	1.71	1.17	5.04
					1	10.06	9.24	7.27	6.04	4.67	3.75	2.62	1.95	1.57	6.42
					2	9.74	8.97	7.04	5.87	4.55	3.63	2.50	1.86	1.54	6.21
					3	9.94	9.12	7.17	5.98	4.64	3.71	2.65	1.94	1.54	6.30
					4	10.03	9.09	7.16	5.98	4.66	3.71	2.57	1.94	1.61	6.29
					1	11.96	10.90	8.68	7.22	5.66	4.45	8.19	2.30	1.89	7.46
					2	12.04	11.01	8.76	7.30	5.67	4.53	3.16	2.31	1.92	7.61
					3	12.08	11.03	8.80	7.35	5.72	4.52	8.57	2.38	1.92	7.61
					4	12.01	10.99	8.76	7.31	5.72	4.53	7.07	2.33	1.89	7.58
					1	13.87	12.66	10.12	8.47	6.62	5.19	11.42	2.72	2.24	8.73
					2	14.01	12.81	10.27	8.59	6.70	5.27	3.64	2.77	2.38	8.84
					3	13.99	12.85	10.24	8.57	6.70	5.26	7.64	2.79	2.26	8.81
					4	13.94	12.78	10.26	8.59	6.71	5.28	7.91	2.81	2.33	8.82
					1	15.82	14.52	11.55	9.67	7.57	5.96	11.66	3.12	12.94	9.95
					2	16.02	14.99	11.75	9.85	7.72	6.08	23.06	3.16	12.89	10.10
					3	15.97	14.77	11.75	9.86	7.70	6.05	15.65	3.19	11.32	10.10
					4	16.14	14.82	11.85	9.94	7.74	6.11	18.49	3.30	12.34	10.19

Table A-1 Continued

Test Section	Test Location	HMA Thickness (in.)	Base Thickness (in.)	Pavement Surface Temperature (°F)	Drop	Load (1000 lb)	Deflection (mils)								
							0 in.	8 in.	12 in.	18 in.	24 in.	36 in.	48 in.	60 in.	-12 in.
4	5	5.5	18.0	69.5	1	7.98	7.51	5.77	4.77	3.67	2.75	1.79	1.89	0.98	5.12
					2	7.98	7.42	5.71	4.71	3.64	2.73	1.80	2.14	0.96	5.12
					3	7.98	7.38	5.70	4.70	3.61	2.75	1.81	2.29	0.97	5.07
					4	8.01	7.41	5.72	4.72	3.64	2.75	1.82	2.19	0.95	5.08
					1	9.99	9.33	7.25	6.00	4.59	3.50	2.40	2.23	1.23	6.37
					2	10.08	9.29	7.29	6.04	4.62	3.55	2.39	2.04	1.25	6.34
					3	10.08	9.25	7.29	6.04	4.63	3.55	2.40	2.10	1.20	6.34
					4	10.06	9.24	7.26	6.00	4.60	3.51	2.34	2.15	1.24	6.30
					1	11.84	10.87	8.64	7.18	5.53	4.19	6.76	2.15	1.48	7.39
					2	11.99	11.09	8.77	7.26	5.64	4.25	2.94	2.53	1.50	7.47
					3	12.01	11.03	8.75	7.27	5.66	4.25	2.90	2.71	1.50	7.48
					4	11.99	11.14	8.81	7.32	5.68	4.28	2.92	2.53	1.47	7.53
					1	13.92	12.76	10.17	8.47	6.56	4.96	3.46	2.52	1.68	8.64
					2	14.06	12.92	10.31	8.60	6.65	5.05	6.32	2.60	1.80	8.76
					3	13.99	12.87	10.27	8.57	6.61	5.03	3.45	2.65	1.79	8.72
					4	13.99	13.00	10.32	8.60	6.65	5.01	3.59	2.56	1.68	8.74
					1	15.82	14.54	11.60	9.68	7.47	5.68	12.39	2.85	1.94	9.84
					2	16.11	14.87	11.82	9.88	7.57	5.80	15.08	3.01	1.98	10.02
					3	16.14	14.95	11.85	9.90	7.64	5.81	9.40	3.41	2.02	10.04
					4	16.04	14.80	11.80	9.86	7.63	5.79	14.17	2.97	1.98	10.00
5	1	5.5	18.0	67.0	1	8.11	7.18	5.64	4.76	4.00	3.28	2.38	2.06	1.50	5.09
					2	8.11	6.97	5.53	4.69	3.94	3.19	2.38	2.23	1.48	5.02
					3	8.03	6.96	5.53	4.70	3.96	3.20	2.37	2.24	1.49	4.99
					4	8.13	7.07	5.56	4.72	3.93	3.22	2.37	2.21	1.47	4.99
					1	9.96	8.71	6.95	5.87	4.94	4.02	3.01	2.37	1.84	6.19
					2	9.99	8.73	7.01	5.94	5.01	4.06	3.02	2.36	1.86	6.25
					3	9.96	8.70	7.01	5.95	4.95	4.06	3.00	2.35	1.87	6.23
					4	9.99	8.81	7.06	5.98	5.00	4.08	3.03	2.36	1.86	6.27
					1	11.94	10.39	8.48	7.19	6.05	4.89	5.48	2.86	2.24	7.40
					2	12.08	10.42	8.54	7.24	6.03	4.92	3.73	2.93	2.27	7.44
					3	12.01	10.45	8.53	7.22	6.05	4.90	3.67	2.91	2.26	7.43
					4	12.16	10.41	8.59	7.28	6.12	4.95	3.72	2.92	2.27	7.48
					1	13.92	12.08	9.88	8.41	7.05	5.71	7.63	3.40	2.59	8.57
					2	13.92	12.22	9.96	8.46	7.12	5.73	4.26	3.39	2.62	8.64
					3	13.79	12.10	9.92	8.42	7.05	5.73	7.10	3.38	2.62	8.59
					4	14.04	12.23	10.00	8.51	7.12	5.75	9.55	3.42	2.64	8.67
					1	15.99	13.88	11.39	9.71	8.12	6.60	14.04	3.89	3.00	9.84
					2	16.16	14.48	11.51	9.80	8.22	6.63	18.63	3.94	3.05	9.93
					3	16.02	14.08	11.50	9.80	8.24	6.65	14.73	3.93	3.01	9.94
					4	15.97	14.14	11.48	9.79	8.12	6.63	12.70	3.90	3.02	9.90

Table A-1 Continued

Test Section	Test Location	HMA Thickness (in.)	Base Thickness (in.)	Pavement Surface Temperature (°F)	Drop	Load (1000 lb)	Deflection (mils)								
							0 in.	8 in.	12 in.	18 in.	24 in.	36 in.	48 in.	60 in.	-12 in.
5	2	5.5	18.0	68.5	1	8.15	6.72	5.23	4.33	3.30	2.54	1.57	1.31	0.84	4.67
					2	8.06	6.52	5.11	4.24	3.24	2.50	1.53	1.46	0.83	4.55
					3	8.25	6.52	5.13	4.27	3.26	2.51	1.53	1.42	0.84	4.56
					4	7.93	6.35	5.00	4.17	3.18	2.45	1.52	1.66	0.74	4.46
					1	9.81	7.97	6.32	5.26	4.04	3.14	1.95	1.66	0.97	5.57
					2	9.96	8.07	6.42	5.35	4.12	3.20	1.97	1.43	0.97	5.63
					3	9.96	8.07	6.43	5.37	4.13	3.22	1.99	1.43	0.98	5.62
					4	9.99	8.11	6.46	5.39	4.15	3.21	2.00	1.45	0.98	5.63
					1	12.11	9.86	7.88	6.61	5.09	3.96	2.50	1.75	1.21	6.83
					2	12.06	9.87	7.90	6.62	5.10	3.98	2.48	1.77	1.20	6.84
					3	12.01	9.78	7.86	6.58	5.10	3.93	2.49	1.77	1.19	6.81
					4	11.96	9.76	7.86	6.59	5.09	3.95	2.48	1.78	1.20	6.82
					1	13.92	11.29	9.12	7.66	5.91	4.57	2.87	2.11	1.40	7.84
					2	13.96	11.46	9.20	7.73	5.99	4.62	2.92	2.10	1.41	7.92
					3	13.96	11.48	9.23	7.77	6.02	4.65	2.90	2.09	1.42	7.96
					4	13.96	11.51	9.28	7.81	6.04	4.65	2.90	2.09	1.42	7.98
					1	15.89	13.05	10.56	8.90	6.91	5.31	3.38	2.43	1.63	9.07
					2	16.19	13.31	10.77	9.07	7.03	5.47	3.51	2.50	1.65	9.24
					3	16.06	13.26	10.72	9.02	7.00	5.44	3.44	2.46	1.66	9.18
					4	15.84	13.07	10.64	8.97	6.96	5.42	3.48	2.40	1.63	9.11
5	3	5.5	18.0	68.0	1	7.81	6.87	5.29	4.40	3.42	2.69	1.88	1.48	1.06	4.87
					2	7.93	6.79	5.25	4.38	3.40	2.70	1.89	1.43	1.07	4.83
					3	8.01	6.83	5.33	4.42	3.46	2.74	1.90	1.55	1.07	4.86
					4	8.15	6.87	5.36	4.47	3.50	2.78	1.93	1.48	1.07	4.89
					1	9.94	8.54	6.75	5.63	4.39	3.49	2.49	1.77	1.37	5.98
					2	9.89	8.61	6.79	5.65	4.42	3.50	3.12	1.77	1.39	6.01
					3	9.94	8.56	6.78	5.65	4.43	3.52	2.48	1.81	1.38	6.04
					4	10.01	8.62	6.83	5.71	4.46	3.55	2.50	1.82	1.38	6.06
					1	11.87	10.22	8.18	6.87	5.38	4.27	6.25	2.14	1.68	7.11
					2	11.96	10.32	8.27	6.93	5.42	4.29	6.68	2.21	1.71	7.18
					3	11.96	10.33	8.28	6.94	5.44	4.31	6.19	2.17	1.69	7.20
					4	12.06	10.38	8.34	6.96	5.47	4.32	5.83	2.21	1.69	7.24
					1	13.89	11.99	9.61	8.06	6.35	4.98	7.58	2.55	1.97	8.29
					2	13.99	12.13	9.75	8.18	6.42	5.08	10.18	2.59	2.00	8.43
					3	14.04	12.12	9.76	8.20	6.46	5.08	9.31	2.58	1.99	8.42
					4	13.96	12.11	9.75	8.24	6.42	5.06	8.76	2.57	1.99	8.41
					1	15.70	13.60	10.98	9.22	7.24	5.71	13.57	2.82	2.25	9.42
					2	15.94	13.81	11.19	9.40	7.38	5.83	11.15	2.96	2.29	9.59
					3	15.94	13.80	11.20	9.41	7.39	5.83	13.58	2.98	2.30	9.56
					4	16.06	13.91	11.28	9.47	7.46	5.86	14.46	3.00	2.32	9.66

Table A-1 Continued

Test Section	Test Location	HMA Thickness (in.)	Base Thickness (in.)	Pavement Surface Temperature (°F)	Drop	Load (1000 lb)	Deflection (mils)								
							0 in.	8 in.	12 in.	18 in.	24 in.	36 in.	48 in.	60 in.	-12 in.
5	4	5.5	18.0	67.5	1	8.01	5.68	4.50	3.75	3.00	2.57	1.90	1.51	1.19	3.87
					2	7.89	5.50	4.34	3.66	2.91	2.51	1.81	1.71	1.15	3.76
					3	8.01	5.57	4.44	3.71	3.00	2.55	2.12	1.50	1.19	3.85
					4	8.20	5.68	4.54	3.78	3.04	2.63	2.05	1.53	1.22	3.92
					1	10.03	7.09	5.72	4.81	3.85	3.29	2.55	1.93	1.53	4.85
					2	10.01	7.07	5.71	4.79	3.83	3.26	2.41	1.92	1.54	4.87
					3	10.03	7.09	5.71	4.80	3.84	3.26	2.41	1.93	1.52	4.86
					4	10.08	7.11	5.74	4.83	3.87	3.26	2.43	1.95	1.53	4.87
					1	12.04	8.41	6.85	5.73	4.61	3.86	2.99	2.26	1.81	5.70
					2	12.04	8.47	6.88	5.76	4.62	3.90	3.06	2.31	1.82	5.76
					3	12.13	8.49	6.91	5.78	4.67	3.91	2.93	2.30	1.82	5.78
					4	11.96	8.44	6.85	5.76	4.62	3.88	2.88	2.29	1.82	5.76
					1	13.94	9.72	7.93	6.67	5.35	4.48	6.50	2.63	2.09	6.62
					2	14.11	9.90	8.09	6.79	5.46	4.54	5.64	2.63	2.14	6.75
					3	14.04	9.91	8.08	6.79	5.47	4.57	5.58	2.68	2.13	6.73
					4	14.06	9.84	8.04	6.77	5.46	4.53	6.19	2.69	2.11	6.70
					1	15.89	11.14	9.11	7.67	6.16	5.18	6.49	3.01	2.39	7.59
					2	16.09	11.29	9.24	7.79	6.25	5.22	3.87	3.08	2.43	7.70
					3	16.19	11.37	9.30	7.85	6.31	5.24	8.28	3.11	2.45	7.75
					4	16.06	11.33	9.28	7.81	6.27	5.23	6.93	3.10	2.44	7.72
5	5	5.5	18.0	68.5	1	7.93	5.09	4.06	3.47	2.92	2.50	1.92	1.70	1.27	3.60
					2	7.93	5.07	4.04	3.45	2.90	2.49	1.93	1.73	1.28	3.59
					3	7.96	5.05	4.04	3.47	2.91	2.49	1.91	1.73	1.27	3.60
					4	8.01	5.08	4.03	3.46	2.92	2.51	1.95	1.76	1.28	3.59
					1	9.81	6.25	5.01	4.30	3.61	3.10	5.28	1.99	1.59	4.42
					2	9.89	6.29	5.05	4.32	3.63	3.16	2.41	1.98	1.60	4.46
					3	9.91	6.30	5.06	4.37	3.62	3.15	2.57	2.00	1.59	4.46
					4	10.03	6.31	5.09	4.38	3.66	3.17	2.47	2.02	1.60	4.49
					1	12.04	7.55	6.11	5.26	4.41	3.78	2.99	2.43	1.94	5.32
					2	12.52	7.65	6.17	5.33	4.47	3.82	3.11	2.44	1.95	5.39
					3	11.91	7.56	6.11	5.27	4.40	3.78	3.03	2.43	1.93	5.32
					4	11.96	7.61	6.15	5.30	4.45	3.82	10.74	2.41	1.94	5.35
					1	14.09	8.81	7.10	6.12	5.12	4.39	10.67	2.82	2.24	6.18
					2	13.94	8.97	7.21	6.21	5.23	4.45	10.29	2.81	2.23	6.25
					3	13.99	8.80	7.16	6.18	5.19	4.43	9.86	2.80	2.24	6.22
					4	13.84	8.86	7.17	6.16	5.19	4.42	10.06	2.82	2.24	6.21
					1	16.11	10.32	8.33	7.17	6.01	5.14	9.57	3.25	2.61	7.20
					2	16.14	10.27	8.35	7.20	6.04	5.15	11.40	3.29	2.60	7.22
					3	15.89	10.15	8.28	7.13	5.96	5.11	9.37	3.18	2.56	7.14
					4	16.14	10.26	8.36	7.20	6.03	5.15	14.07	3.30	2.60	7.22

Table A-1 Continued

Test Section	Test Location	HMA Thickness (in.)	Base Thickness (in.)	Pavement Surface Temperature (°F)	Drop	Load (1000 lb)	Deflection (mils)								
							0 in.	8 in.	12 in.	18 in.	24 in.	36 in.	48 in.	60 in.	-12 in.
6	1	5.5	18.0	66.5	1	7.91	6.42	4.87	4.05	3.21	2.66	1.90	2.37	1.21	4.29
					2	8.06	6.38	4.88	4.07	3.25	2.66	1.89	2.18	1.21	4.29
					3	8.01	6.46	4.90	4.07	3.24	2.67	1.99	2.15	1.24	4.32
					4	8.08	6.43	4.91	4.09	3.28	2.68	1.98	1.86	1.22	4.34
					1	10.11	8.10	6.15	5.13	4.12	3.35	2.54	2.00	1.53	5.34
					2	10.01	7.98	6.12	5.11	4.09	3.32	2.51	2.73	1.51	5.30
					3	9.94	7.85	6.07	5.06	4.06	3.28	2.52	1.99	1.49	5.24
					4	10.01	7.79	6.04	5.02	4.03	3.29	2.50	1.95	1.48	5.23
					1	11.79	9.36	7.19	5.99	4.78	3.89	2.99	2.31	1.77	6.19
					2	11.94	9.68	7.29	6.09	4.88	3.95	3.03	2.30	1.79	6.26
					3	12.01	9.41	7.29	6.10	4.91	3.97	3.05	2.66	1.78	6.27
					4	12.01	9.49	7.38	6.15	4.93	4.00	3.30	2.38	1.82	6.32
					1	13.99	10.93	8.49	7.09	5.68	4.61	3.82	2.74	2.09	7.26
					2	14.16	11.35	8.65	7.23	5.81	4.67	8.87	2.70	2.11	7.39
					3	13.99	11.34	8.60	7.20	5.79	4.66	6.64	2.65	2.07	7.32
					4	14.09	11.21	8.59	7.19	5.75	4.64	4.84	2.70	2.13	7.32
					1	16.02	12.56	9.73	8.14	6.54	5.23	4.82	3.04	2.37	8.28
					2	16.19	12.65	9.84	8.22	6.57	5.29	5.22	3.02	2.38	8.37
					3	15.89	12.80	9.76	8.17	6.49	5.29	5.67	2.95	2.42	8.30
					4	15.99	12.98	9.82	8.19	6.50	5.30	4.93	3.02	2.41	8.32
6	2	5.5	18.0	67.5	1	8.20	5.94	4.66	3.93	3.19	2.66	1.94	1.59	1.31	4.10
					2	7.98	5.73	4.52	3.81	3.10	2.61	1.90	1.65	1.27	3.99
					3	7.98	5.75	4.54	3.84	3.12	2.59	1.91	1.69	1.26	3.99
					4	7.86	5.70	4.50	3.80	3.10	2.58	1.92	1.82	1.24	3.96
					1	10.01	7.15	5.68	4.82	3.91	3.27	7.15	1.97	1.59	4.92
					2	9.99	7.11	5.68	4.80	3.91	3.26	4.96	1.96	1.59	4.92
					3	10.08	7.18	5.72	4.84	3.92	3.30	2.61	1.97	1.58	4.97
					4	10.11	7.21	5.74	4.85	3.93	3.30	2.56	1.98	1.58	4.96
					1	12.21	8.70	6.94	5.89	4.78	3.98	3.05	2.36	1.92	5.98
					2	12.06	8.67	6.94	5.88	4.78	3.97	3.05	2.39	1.92	5.95
					3	12.13	8.67	6.95	5.90	4.78	3.98	6.86	2.40	1.94	5.97
					4	12.01	8.62	6.91	5.85	4.74	3.94	3.46	2.36	1.94	5.88
					1	14.01	10.00	8.03	6.81	5.52	4.58	6.12	2.74	2.20	6.88
					2	14.18	10.15	8.18	6.91	5.60	4.67	3.52	2.77	2.26	6.97
					3	14.06	10.08	8.11	6.87	5.55	4.64	8.94	2.76	2.23	6.92
					4	13.89	10.02	8.08	6.85	5.56	4.62	6.74	2.74	2.22	6.92
					1	16.06	11.47	9.26	7.85	6.34	5.25	7.97	3.09	2.53	7.90
					2	16.11	11.66	9.36	7.92	6.39	5.33	8.45	3.13	2.57	7.94
					3	16.11	11.67	9.37	7.94	6.40	5.33	11.00	3.15	2.57	7.96
					4	16.14	11.67	9.37	7.93	6.39	5.32	5.99	3.17	2.58	7.96

Table A-1 Continued

Test Section	Test Location	HMA Thickness (in.)	Base Thickness (in.)	Pavement Surface Temperature (°F)	Drop	Load (1000 lb)	Deflection (mils)								
							0 in.	8 in.	12 in.	18 in.	24 in.	36 in.	48 in.	60 in.	-12 in.
6	3	5.5	18.0	67.5	1	8.15	5.90	4.72	3.97	3.24	2.77	2.16	1.69	1.31	4.13
					2	8.11	5.82	4.67	3.94	3.21	2.73	2.13	1.69	1.29	4.12
					3	8.06	6.62	4.64	3.91	3.20	2.70	2.23	1.74	1.28	4.08
					4	7.84	5.58	4.49	3.81	3.10	2.66	2.11	2.09	1.25	3.98
					1	9.91	7.00	5.68	4.79	3.91	3.36	5.77	2.12	1.58	4.97
					2	10.01	7.05	5.76	4.87	3.96	3.39	2.74	2.09	1.62	4.98
					3	10.08	7.14	5.83	4.94	4.04	3.42	2.72	2.04	1.62	5.04
					4	10.01	7.07	5.76	4.85	3.99	3.39	2.68	2.05	1.60	4.98
					1	12.18	8.54	7.00	5.91	4.84	4.09	5.41	2.51	1.95	5.99
					2	12.06	8.51	6.98	5.92	4.83	4.10	6.67	2.47	1.95	5.99
					3	12.08	8.56	7.02	5.91	4.82	4.10	6.63	2.48	1.95	5.99
					4	12.06	8.50	6.99	5.91	4.84	4.08	5.84	2.47	1.94	5.97
					1	14.01	9.80	8.07	6.82	5.58	4.73	10.62	2.87	2.24	6.88
					2	14.04	9.95	8.18	6.90	5.62	4.77	8.63	2.93	2.27	6.95
					3	13.99	9.21	8.16	6.89	5.63	4.77	10.31	2.93	2.28	6.94
					4	14.01	9.97	8.17	6.91	5.64	4.75	8.78	2.96	2.27	6.96
					1	16.24	11.46	9.39	7.93	6.46	5.46	11.18	3.27	2.58	7.96
					2	16.26	11.43	9.43	7.97	6.51	5.49	9.79	3.29	2.60	8.01
					3	16.16	11.45	9.43	7.98	6.52	5.51	11.22	3.29	2.61	8.01
					4	16.19	11.41	9.38	7.95	6.48	5.48	11.75	3.27	2.60	8.01
6	4	5.5	18.0	68.5	1	8.79	6.50	5.27	4.48	3.76	3.15	2.32	1.89	1.44	4.58
					2	8.54	6.39	5.15	4.38	3.66	3.08	2.29	2.08	1.41	4.46
					3	8.45	6.22	5.05	4.26	3.53	3.02	2.21	2.40	1.38	4.37
					4	8.33	6.19	4.98	4.23	3.51	2.97	2.21	3.03	1.36	4.34
					1	10.18	7.48	6.09	5.18	4.29	3.66	2.71	2.33	1.67	5.23
					2	10.13	7.54	6.13	5.20	4.27	3.66	2.74	2.17	1.67	5.27
					3	10.08	7.46	6.07	5.17	4.30	3.63	2.69	2.15	1.66	5.24
					4	10.03	7.43	6.05	5.16	4.28	3.61	2.73	2.17	1.65	5.22
					1	11.89	8.78	7.17	6.11	5.13	4.25	7.66	2.49	1.97	6.12
					2	12.06	8.92	7.30	6.23	5.25	4.34	3.22	2.55	2.01	6.24
					3	12.04	8.88	7.30	6.20	5.21	4.34	3.22	2.51	1.98	6.19
					4	11.99	8.88	7.29	6.19	5.16	4.33	3.20	2.53	1.99	6.18
					1	13.67	10.14	8.35	7.09	5.89	4.89	3.73	2.86	2.24	7.09
					2	13.94	10.41	8.58	7.28	6.11	5.06	4.09	2.94	2.30	7.28
					3	14.16	10.53	8.70	7.37	6.17	5.11	3.87	2.97	2.32	7.36
					4	14.09	10.46	8.67	7.34	6.16	5.11	3.87	2.92	2.32	7.33
					1	16.02	11.90	9.87	8.37	6.99	5.78	11.32	3.32	2.72	8.34
					2	16.09	12.04	9.97	8.48	7.09	5.87	11.12	3.42	2.67	8.43
					3	16.21	12.10	9.99	8.52	7.14	5.89	9.10	3.45	2.71	8.48
					4	16.16	12.07	9.94	8.48	7.02	5.86	9.37	3.42	2.77	8.46

Table A-1 Continued

Test Section	Test Location	HMA Thickness (in.)	Base Thickness (in.)	Pavement Surface Temperature (°F)	Drop	Load (1000 lb)	Deflection (mils)								
							0 in.	8 in.	12 in.	18 in.	24 in.	36 in.	48 in.	60 in.	-12 in.
6	5	5.5	18.0	68.5	1	8.13	5.34	4.21	3.57	2.95	2.55	1.88	1.47	1.11	3.70
					2	8.08	5.32	4.19	3.55	2.93	2.55	1.86	1.39	1.08	3.70
					3	8.03	5.31	4.18	3.55	2.93	2.55	1.83	1.38	1.09	3.71
					4	8.08	5.29	4.18	3.52	2.93	2.54	1.83	1.37	1.09	3.68
					1	10.13	6.64	5.30	4.50	3.73	3.19	2.42	1.77	1.41	4.62
					2	10.23	6.69	5.33	4.52	3.74	3.20	2.38	1.82	1.40	4.66
					3	10.13	6.60	5.26	4.48	3.71	3.17	2.36	1.77	1.37	4.59
					4	10.11	6.57	5.25	4.45	3.68	3.16	2.40	1.77	1.37	4.60
					1	12.04	7.85	6.31	5.35	4.45	3.79	6.27	2.16	1.65	5.49
					2	11.96	7.86	6.31	5.36	4.49	3.82	6.61	2.17	1.65	5.47
					3	12.01	7.88	6.31	5.36	4.45	3.82	3.22	2.15	1.64	5.48
					4	12.04	7.89	6.31	5.36	4.46	3.81	3.01	2.13	1.65	5.49
					1	14.11	9.22	7.42	6.31	5.23	4.46	8.96	2.57	1.92	6.43
					2	14.16	9.31	7.52	6.39	5.31	4.51	8.12	2.61	1.94	6.52
					3	14.09	9.29	7.48	6.36	5.27	4.52	7.33	2.57	1.95	6.48
					4	14.11	9.36	7.54	6.40	5.31	4.53	6.83	2.57	1.96	6.50
					1	16.11	10.59	8.55	7.28	6.04	5.12	7.43	2.91	2.22	7.37
					2	16.09	10.58	8.56	7.28	6.03	5.12	10.13	2.90	2.22	7.39
					3	16.14	10.63	8.56	7.30	6.02	5.14	7.31	2.93	2.21	7.40
					4	16.02	10.60	8.54	7.28	6.02	5.13	8.36	2.96	2.23	7.41
7	1	5.5	20.0	67.5	1	8.06	10.39	8.52	7.19	5.77	4.75	3.26	2.44	1.91	7.45
					2	8.03	10.29	8.43	7.11	5.72	4.70	3.23	2.45	1.92	7.35
					3	7.91	10.09	8.33	7.03	5.65	4.60	3.20	2.43	1.89	7.23
					4	7.96	10.15	8.37	7.07	5.72	4.63	3.21	2.42	1.90	7.30
					1	9.89	12.65	10.46	8.88	7.13	5.80	4.09	3.03	2.38	9.08
					2	9.89	12.64	10.47	8.87	7.13	5.77	4.09	3.05	2.39	9.07
					3	9.99	12.73	10.57	8.96	7.21	5.88	4.09	3.05	2.39	9.18
					4	9.99	12.74	10.57	8.98	7.22	5.88	4.07	3.07	2.42	9.18
					1	11.89	15.06	12.55	10.66	8.58	6.98	7.45	3.64	2.87	10.81
					2	11.87	15.22	12.67	10.76	8.69	7.08	5.18	3.67	2.91	10.94
					3	11.89	15.23	12.68	10.79	8.68	7.10	6.50	3.68	2.90	10.96
					4	11.99	15.25	12.73	10.81	8.71	7.11	5.14	3.66	2.86	10.98
					1	13.89	17.68	14.75	12.57	10.15	8.25	5.88	4.28	3.37	12.70
					2	14.04	17.92	14.95	12.74	10.32	8.36	6.24	4.32	3.36	12.88
					3	14.01	17.97	15.01	12.79	10.30	8.39	5.93	4.39	3.36	12.95
					4	13.92	17.95	14.98	12.76	10.29	8.37	5.87	4.38	3.37	12.93
					1	15.97	20.39	17.03	14.52	11.76	9.55	8.37	4.90	3.83	14.66
					2	16.06	20.57	17.21	14.66	11.83	9.66	8.61	4.96	3.96	14.80
					3	15.89	20.60	17.21	14.67	11.88	9.65	6.74	5.04	3.88	14.81
					4	15.97	20.65	17.26	14.72	11.87	9.67	7.10	4.98	3.87	14.85

Table A-1 Continued

Test Section	Test Location	HMA Thickness (in.)	Base Thickness (in.)	Pavement Surface Temperature (°F)	Drop	Load (1000 lb)	Deflection (mils)								
							0 in.	8 in.	12 in.	18 in.	24 in.	36 in.	48 in.	60 in.	-12 in.
7	2	5.5	20.0	66.8	1	7.93	10.34	8.38	7.05	5.58	4.52	3.33	2.42	1.87	7.37
					2	7.93	10.24	8.30	7.00	5.56	4.48	3.34	2.36	1.85	7.33
					3	7.93	10.20	8.32	7.00	5.55	4.46	3.31	2.36	1.86	7.29
					4	7.98	10.18	8.30	6.99	5.57	4.49	3.36	2.38	1.84	7.32
					1	9.91	12.66	10.42	8.78	6.99	5.60	6.31	2.97	2.33	9.02
					2	10.03	12.83	10.55	8.91	7.07	5.69	4.17	3.02	2.40	9.14
					3	9.94	12.76	10.55	8.88	7.06	5.67	4.15	3.03	2.35	9.09
					4	9.96	12.72	10.52	8.89	7.04	5.66	8.08	3.01	2.37	9.10
					1	11.94	15.38	12.74	10.77	8.57	6.86	8.01	3.62	2.86	10.88
					2	11.94	15.37	12.72	10.77	8.57	6.88	9.76	3.69	2.85	10.87
					3	11.96	15.38	12.75	10.77	8.56	6.88	8.87	3.65	2.86	10.89
					4	11.91	15.40	12.79	10.82	8.60	6.90	9.06	3.68	2.87	10.92
					1	13.77	17.77	14.82	12.54	10.00	8.01	15.22	4.24	3.34	12.62
					2	13.94	18.10	15.10	12.78	10.24	8.17	11.09	4.30	3.39	12.85
					3	14.06	18.24	15.21	12.88	10.28	8.23	11.23	4.34	3.42	12.95
					4	14.06	18.22	15.23	12.92	10.28	8.23	16.56	4.33	3.43	12.95
					1	15.97	20.68	17.31	14.66	11.67	9.35	21.33	4.88	3.77	14.68
					2	15.99	20.87	17.43	14.79	11.75	9.43	12.58	4.91	3.82	14.78
					3	16.02	20.88	17.48	14.82	11.84	9.46	14.62	4.98	3.83	14.82
					4	15.92	20.88	17.54	14.84	11.86	9.47	15.02	5.02	3.84	14.85
7	3	5.5	20.0	66.5	1	8.03	7.06	5.62	4.70	3.76	3.12	2.43	2.17	1.46	5.10
					2	8.06	7.20	5.58	4.66	3.74	3.10	2.33	2.01	1.47	5.03
					3	8.06	7.12	5.54	4.63	3.72	3.09	2.29	2.17	1.47	5.01
					4	8.06	7.16	5.56	4.63	3.72	3.10	2.34	2.13	1.45	5.01
					1	10.08	8.88	6.95	5.81	4.65	3.87	3.04	2.39	1.85	6.20
					2	10.08	8.92	6.98	5.86	4.68	3.90	3.07	2.41	1.83	6.22
					3	9.99	8.91	6.95	5.85	4.66	3.90	3.02	2.40	1.83	6.20
					4	9.96	8.80	6.91	5.79	4.67	3.86	2.95	2.38	1.83	6.14
					1	11.94	10.41	8.32	6.98	5.59	4.61	6.27	2.81	2.15	7.27
					2	12.08	10.67	8.42	7.08	5.66	4.69	5.81	2.82	2.19	7.39
					3	12.01	10.63	8.43	7.07	5.67	4.69	6.79	2.81	2.21	7.38
					4	12.06	10.65	8.46	7.09	5.71	4.70	5.44	2.87	2.21	7.42
					1	13.96	12.33	9.81	8.23	6.60	5.45	5.86	3.27	2.53	8.53
					2	14.06	12.47	9.96	8.34	6.70	5.53	12.25	3.29	2.58	8.63
					3	14.06	12.46	9.91	8.31	6.66	5.49	12.02	3.32	2.58	8.62
					4	14.09	12.51	9.98	8.38	6.70	5.54	11.52	3.32	2.60	8.68
					1	16.06	14.35	11.37	9.55	7.63	6.28	20.91	3.74	2.95	9.86
					2	16.19	14.38	11.48	9.65	7.71	6.35	15.83	3.82	2.99	9.93
					3	16.06	13.86	11.47	9.63	7.70	6.34	11.34	3.74	2.97	9.92
					4	15.94	14.35	11.38	9.56	7.66	6.31	16.00	3.71	2.94	9.86

Table A-1 Continued

Test Section	Test Location	HMA Thickness (in.)	Base Thickness (in.)	Pavement Surface Temperature (°F)	Drop	Load (1000 lb)	Deflection (mils)								
							0 in.	8 in.	12 in.	18 in.	24 in.	36 in.	48 in.	60 in.	-12 in.
7	4	5.5	20.0	67.5	1	8.01	7.77	6.10	5.09	4.11	3.43	2.43	2.29	1.49	5.41
					2	7.93	7.59	5.98	5.00	4.02	3.37	2.39	2.87	1.47	5.32
					3	7.89	7.56	5.97	4.98	4.04	3.34	2.50	3.12	1.48	5.30
					4	7.96	7.61	6.02	5.04	4.09	3.39	2.39	2.51	1.47	5.34
					1	10.01	9.53	7.61	6.37	5.15	4.27	3.32	2.72	1.90	6.65
					2	9.94	9.56	7.64	6.41	5.16	4.28	3.33	2.51	1.91	6.64
					3	10.06	9.58	7.67	6.44	5.22	4.34	3.22	2.50	1.91	6.67
					4	9.99	9.55	7.63	6.41	5.14	4.31	3.04	2.52	1.89	6.66
					1	11.96	11.37	9.13	7.66	6.18	5.12	3.86	2.92	2.26	7.88
					2	12.21	11.54	9.28	7.79	6.35	5.20	4.77	2.99	2.30	8.02
					3	11.89	11.37	9.15	7.68	6.21	5.12	3.73	2.88	2.27	7.92
					4	11.99	11.41	9.16	7.69	6.20	5.12	10.06	2.89	2.26	7.89
					1	13.82	13.17	10.61	8.93	7.16	5.93	9.65	3.52	2.64	9.13
					2	14.01	13.45	10.78	9.11	7.32	6.08	9.07	3.53	2.64	9.32
					3	13.96	13.49	10.83	9.14	7.37	6.07	8.98	3.56	2.69	9.34
					4	14.01	13.51	10.91	9.19	7.40	6.07	10.42	3.55	2.71	9.38
					1	15.97	15.26	12.31	10.41	8.37	6.88	10.31	3.79	2.98	10.58
					2	16.02	15.39	12.41	10.48	8.41	6.92	14.27	3.92	3.00	10.66
					3	16.02	15.35	12.39	10.49	8.40	6.94	10.54	3.83	3.04	10.66
					4	16.04	15.38	12.42	10.50	8.38	6.95	13.54	3.86	3.07	10.64
7	5	5.5	20.0	67.5	1	7.86	7.54	5.93	4.98	3.98	3.28	2.29	2.39	1.44	5.34
					2	8.08	7.64	6.06	5.09	4.09	3.32	2.30	1.93	1.48	5.43
					3	8.25	7.64	6.06	5.10	4.12	3.36	2.34	2.07	1.50	5.41
					4	8.18	7.59	6.03	5.07	4.10	3.31	2.34	2.08	1.49	5.37
					1	10.13	9.44	7.53	6.37	5.08	4.18	2.96	2.40	1.89	6.67
					2	9.91	9.29	7.41	6.27	5.00	4.12	2.96	2.33	1.83	6.55
					3	9.96	9.32	7.45	6.31	5.06	4.14	2.89	2.37	1.84	6.60
					4	9.99	9.35	7.45	6.31	5.04	4.16	2.97	2.38	1.85	6.60
					1	12.11	11.25	9.06	7.66	6.17	4.98	3.66	2.84	2.24	7.85
					2	12.06	11.23	9.03	7.65	6.15	4.99	3.55	2.91	2.24	7.85
					3	11.96	11.20	9.03	7.65	6.15	4.99	3.55	2.91	2.23	7.85
					4	12.08	11.25	9.06	7.68	6.18	5.00	3.58	2.93	2.25	7.89
					1	13.94	12.97	10.48	8.90	7.16	5.80	4.08	3.33	2.59	9.08
					2	14.11	13.09	10.61	9.01	7.22	5.86	4.29	3.32	2.63	9.18
					3	14.01	13.08	10.59	8.98	7.21	5.85	4.21	3.31	2.60	9.15
					4	14.11	13.13	10.66	9.04	7.24	5.87	4.14	3.36	2.64	9.17
					1	16.09	14.91	12.14	10.29	8.24	6.70	6.90	3.80	2.92	10.42
					2	16.11	14.98	12.15	10.30	8.26	6.72	4.76	3.77	2.92	10.41
					3	15.97	14.93	12.11	10.29	8.25	6.72	4.76	3.78	2.92	10.40
					4	15.94	14.97	12.10	10.26	8.23	6.69	4.70	3.81	2.94	10.40

Table A-1 Continued

Test Section	Test Location	HMA Thickness (in.)	Base Thickness (in.)	Pavement Surface Temperature (°F)	Drop	Load (1000 lb)	Deflection (mils)								
							0 in.	8 in.	12 in.	18 in.	24 in.	36 in.	48 in.	60 in.	-12 in.
8	1	5.5	20.0	67.5	1	8.18	7.48	6.10	5.09	3.95	3.17	2.01	1.50	1.27	5.18
					2	8.13	7.32	6.00	4.97	3.90	3.11	1.98	1.50	1.27	5.07
					3	8.03	7.22	5.90	4.95	3.86	3.10	1.95	1.49	1.23	5.00
					4	7.96	7.12	5.82	4.88	3.80	3.06	1.90	1.47	1.24	4.95
					1	10.03	9.01	7.42	6.22	4.82	3.85	2.48	1.89	1.58	6.24
					2	10.06	8.98	7.43	6.22	4.82	3.89	2.49	1.90	1.59	6.22
					3	9.99	8.92	7.36	6.17	4.80	3.86	2.48	1.89	1.57	6.19
					4	10.01	8.91	7.38	6.19	4.81	3.86	2.47	1.88	1.57	6.18
					1	11.89	10.62	8.81	7.38	5.76	4.59	2.99	2.25	1.91	7.36
					2	12.04	10.74	8.92	7.49	5.85	4.64	3.03	2.31	1.90	7.45
					3	12.16	10.80	8.98	7.55	5.90	4.68	3.06	2.31	1.94	7.50
					4	12.16	10.80	8.98	7.55	5.90	4.71	3.05	2.31	1.94	7.50
					1	14.11	12.50	10.40	8.76	6.84	5.43	3.53	2.68	2.19	8.67
					2	14.06	12.54	10.45	8.79	6.88	5.45	3.57	2.68	2.26	8.68
					3	14.06	12.54	10.45	8.80	6.86	5.46	3.57	2.70	2.17	8.71
					4	14.01	12.47	10.42	8.77	6.86	5.47	3.56	2.68	2.24	8.67
					1	16.16	14.18	11.78	9.95	7.80	6.16	4.12	3.08	2.50	9.83
					2	15.99	14.18	11.81	9.96	7.79	6.20	4.23	3.08	2.58	9.85
					3	15.97	14.20	11.84	9.99	7.84	6.20	4.10	3.09	2.60	9.87
					4	16.06	14.29	11.91	10.03	7.87	6.26	4.18	3.12	2.51	9.91
8	2	5.5	20.0	68.5	1	8.06	5.29	4.13	3.42	2.70	2.19	1.50	1.36	0.92	3.62
					2	7.91	5.18	4.07	3.39	2.66	2.18	1.50	1.40	0.93	3.53
					3	8.18	5.24	4.14	3.44	2.73	2.23	1.51	1.19	0.92	3.60
					4	8.06	5.20	4.11	3.43	2.71	2.22	1.51	1.19	0.93	3.57
					1	10.08	6.54	5.21	4.35	3.43	2.78	1.93	1.50	1.18	4.45
					2	10.11	6.51	5.18	4.32	3.40	2.79	1.90	1.53	1.18	4.43
					3	9.99	6.49	5.16	4.31	3.42	2.78	1.88	1.51	1.18	4.43
					4	9.99	6.45	5.16	4.32	3.39	2.78	1.86	1.49	1.17	4.41
					1	11.94	7.68	6.15	5.14	4.09	3.29	2.24	1.80	1.39	5.21
					2	11.99	7.75	6.21	5.20	4.12	3.35	2.25	1.84	1.40	5.28
					3	12.01	7.73	6.20	5.20	4.12	3.32	2.25	1.82	1.43	5.26
					4	12.08	7.76	6.23	5.21	4.13	3.33	2.29	1.85	1.43	5.29
					1	13.82	8.87	7.12	5.99	4.74	3.82	2.62	2.11	1.66	6.03
					2	14.09	9.02	7.25	6.08	4.81	3.91	2.69	2.09	1.62	6.12
					3	14.11	9.09	7.33	6.13	4.84	3.94	2.70	2.15	1.69	6.17
					4	14.23	9.14	7.36	6.16	4.89	3.95	2.70	2.18	1.67	6.19
					1	15.89	10.13	8.16	6.84	5.44	4.41	3.02	2.39	1.88	6.87
					2	16.04	10.26	8.25	6.92	5.49	4.47	3.06	2.43	1.91	6.97
					3	16.16	10.33	8.33	7.00	5.55	4.50	3.13	2.51	1.92	7.03
					4	16.11	10.30	8.32	6.98	5.53	4.47	3.14	2.42	1.94	7.00

Table A-1 Continued

Test Section	Test Location	HMA Thickness (in.)	Base Thickness (in.)	Pavement Surface Temperature (°F)	Drop	Load (1000 lb)	Deflection (mils)								
							0 in.	8 in.	12 in.	18 in.	24 in.	36 in.	48 in.	60 in.	-12 in.
8	3	5.5	20.0	68.5	1	7.81	6.62	5.27	4.44	3.57	3.00	2.13	1.95	1.32	4.63
					2	7.98	6.65	5.29	4.47	3.62	3.04	2.16	1.85	1.35	4.68
					3	7.98	6.64	5.30	4.46	3.64	3.00	2.15	1.82	1.37	4.67
					4	8.06	6.63	5.28	4.47	3.62	3.00	2.15	1.74	1.35	4.66
					1	9.86	8.22	6.62	5.60	4.53	3.77	2.78	2.19	1.71	5.76
					2	9.94	8.29	6.67	5.64	4.57	3.81	2.76	2.17	1.72	5.78
					3	10.06	8.31	6.73	5.69	4.61	3.85	2.76	2.23	1.74	5.85
					4	10.01	8.25	6.70	5.65	4.59	3.83	2.75	2.23	1.74	5.81
					1	11.72	9.68	7.91	6.66	5.42	4.49	3.41	2.60	2.03	6.80
					2	11.87	9.81	8.01	6.77	5.49	4.56	7.95	2.66	2.04	6.88
					3	11.89	9.85	8.06	6.82	5.54	4.58	3.46	2.67	2.07	6.92
					4	11.99	9.96	8.10	6.84	5.59	4.63	3.38	2.70	2.08	6.96
					1	13.77	11.40	9.34	7.92	6.45	5.31	4.67	3.15	2.39	7.98
					2	14.09	11.67	9.59	8.14	6.62	5.48	12.23	3.18	2.48	8.19
					3	14.01	11.65	9.59	8.13	6.62	5.45	3.93	3.19	2.47	8.19
					4	14.04	11.66	9.63	8.17	6.65	5.47	3.98	3.20	2.46	8.22
					1	15.87	13.02	10.75	9.13	7.43	6.15	10.25	3.59	2.78	9.19
					2	15.75	13.00	10.75	9.12	7.43	6.13	7.72	3.56	2.77	9.16
					3	15.82	13.11	10.82	9.19	7.49	6.15	8.06	3.59	2.77	9.22
					4	15.97	13.23	10.91	9.28	7.54	6.24	7.83	3.64	2.83	9.27
8	4	5.5	20.0	68.5	1	7.91	7.00	5.48	4.64	3.74	3.12	2.24	1.68	1.33	4.94
					2	7.91	6.97	5.49	4.63	3.74	3.10	2.25	1.62	1.30	4.91
					3	7.93	6.94	5.50	4.65	3.75	3.09	2.28	1.63	1.31	4.90
					4	7.91	6.92	5.48	4.64	3.75	3.09	2.30	1.62	1.31	4.88
					1	9.84	8.56	6.85	5.79	4.67	3.89	2.92	2.08	1.65	6.04
					2	9.84	8.59	6.89	5.83	4.70	3.94	2.92	2.13	1.68	6.07
					3	10.01	8.70	6.99	5.94	4.77	4.00	2.97	2.15	1.70	6.14
					4	9.94	8.65	6.95	5.90	4.73	3.97	2.95	2.11	1.69	6.08
					1	12.01	10.33	8.38	7.12	5.74	4.77	13.26	2.53	2.03	7.21
					2	11.99	10.35	8.41	7.17	5.76	4.77	7.21	2.55	2.03	7.26
					3	11.91	10.36	8.42	7.18	5.76	4.80	12.36	2.56	2.03	7.26
					4	11.94	10.37	8.41	7.16	5.78	4.77	13.43	2.55	2.03	7.26
					1	13.77	11.82	9.65	8.21	6.61	5.48	18.00	2.95	2.34	8.22
					2	13.96	12.05	9.81	8.38	6.73	5.60	16.74	2.97	2.39	8.40
					3	14.14	12.14	9.93	8.46	6.79	5.68	17.31	3.02	2.46	8.48
					4	14.09	12.15	9.96	8.47	6.81	5.69	17.04	2.96	2.42	8.50
					1	15.77	13.51	11.09	9.46	7.63	6.33	21.45	3.35	2.72	9.44
					2	15.89	13.62	11.21	9.54	7.69	6.44	22.96	3.41	2.75	9.54
					3	15.92	13.68	11.25	9.63	7.72	6.44	21.13	3.45	4.61	9.59
					4	16.02	13.74	11.32	9.66	7.79	6.49	20.95	3.44	5.91	9.64

Table A-1 Continued

Test Section	Test Location	HMA Thickness (in.)	Base Thickness (in.)	Pavement Surface Temperature (°F)	Drop	Load (1000 lb)	Deflection (mils)								
							0 in.	8 in.	12 in.	18 in.	24 in.	36 in.	48 in.	60 in.	-12 in.
8	5	5.5	20.0	69.0	1	7.93	7.98	6.21	5.19	4.15	3.39	2.29	2.20	1.36	5.43
					2	7.98	7.95	6.19	5.19	4.14	3.38	2.27	2.05	1.38	5.42
					3	8.08	7.97	6.22	5.21	4.17	3.40	2.29	1.82	1.38	5.42
					4	8.03	7.93	6.21	5.20	4.18	3.39	2.30	1.83	1.40	5.42
					1	9.99	9.86	7.76	6.51	5.20	4.26	2.91	2.35	1.78	6.66
					2	9.91	9.77	7.71	6.49	5.16	4.24	2.94	2.36	1.75	6.64
					3	10.03	9.84	7.79	6.55	5.23	4.30	2.97	2.34	1.77	6.68
					4	10.03	9.83	7.79	6.56	5.24	4.30	2.95	2.36	1.77	6.68
					1	11.89	11.61	9.27	7.82	6.25	5.05	3.50	2.69	2.02	7.84
					2	12.13	11.86	9.45	7.97	6.35	5.16	3.54	2.80	2.08	8.02
					3	11.94	11.68	9.32	7.85	6.29	5.10	4.28	2.82	2.12	7.90
					4	12.01	11.72	9.35	7.89	6.30	5.12	3.53	2.79	2.11	7.94
					1	13.96	13.50	10.86	9.16	7.34	5.93	4.10	3.20	2.38	9.16
					2	14.11	13.67	11.02	9.28	7.45	6.05	7.76	3.28	2.41	9.27
					3	14.01	13.66	10.99	9.28	7.42	6.02	4.24	3.27	2.52	9.27
					4	14.04	13.75	11.04	9.31	7.45	6.02	7.56	3.29	2.43	9.30
					1	16.02	15.44	12.48	10.52	8.39	6.83	5.89	3.74	2.75	10.43
					2	16.24	15.77	12.69	10.71	8.59	6.94	8.98	3.86	2.82	10.60
					3	16.14	15.63	12.65	10.67	8.54	6.91	9.35	3.80	2.77	10.56
					4	16.14	15.61	12.64	10.65	8.54	6.91	4.83	3.75	2.77	10.56
9	1	5.5	14.0	70.5	1	7.93	10.99	9.02	7.70	6.17	4.93	3.27	2.39	1.77	8.16
					2	8.08	10.98	9.00	7.71	6.19	4.96	3.33	2.42	1.78	8.18
					3	7.98	10.86	8.98	7.68	6.16	4.93	3.30	2.39	1.77	8.10
					4	7.98	10.80	8.90	7.64	6.14	4.89	3.27	2.39	1.77	8.08
					1	10.06	13.84	11.52	9.90	7.94	6.35	4.27	3.08	2.29	10.30
					2	9.96	13.77	11.47	9.87	7.90	6.35	4.28	3.08	2.27	10.26
					3	10.03	13.82	11.52	9.92	7.94	6.36	4.24	3.14	2.29	10.28
					4	10.06	13.86	11.57	9.97	7.98	6.40	4.30	3.13	2.30	10.33
					1	11.91	16.70	14.01	12.07	9.71	7.73	5.47	3.78	2.76	12.45
					2	11.96	16.89	14.19	12.22	9.83	7.87	5.36	3.78	2.72	12.59
					3	12.01	16.86	14.21	12.25	9.84	7.87	5.22	3.78	2.71	12.56
					4	11.99	16.91	14.26	12.30	9.88	7.88	5.23	3.79	2.83	12.63
					1	13.89	19.54	16.50	14.25	11.45	9.15	7.03	4.41	3.13	14.59
					2	14.01	19.91	16.83	14.53	11.66	9.35	7.83	4.51	3.21	14.84
					3	13.96	19.96	16.86	14.58	11.70	9.36	7.15	4.47	3.20	14.89
					4	14.06	20.08	16.97	14.67	11.78	9.42	7.12	4.46	3.22	14.97
					1	15.75	22.48	19.04	16.45	13.23	10.62	9.44	4.99	3.63	16.81
					2	15.92	22.96	19.43	16.77	13.46	10.83	9.79	5.14	3.67	17.09
					3	16.02	23.14	19.55	16.90	13.63	10.89	9.58	5.25	3.71	17.22
					4	15.94	23.15	19.61	16.93	13.63	10.94	9.02	5.23	3.71	17.26

Table A-1 Continued

Test Section	Test Location	HMA Thickness (in.)	Base Thickness (in.)	Pavement Surface Temperature (°F)	Drop	Load (1000 lb)	Deflection (mils)								
							0 in.	8 in.	12 in.	18 in.	24 in.	36 in.	48 in.	60 in.	-12 in.
9	2	5.5	14.0	68.5	1	7.98	10.55	8.27	6.86	5.37	4.32	2.90	2.32	1.62	7.30
					2	8.01	10.48	8.25	6.86	5.42	4.29	2.91	2.25	1.63	7.30
					3	7.98	10.36	8.20	6.81	5.34	4.24	2.93	2.28	1.62	7.25
					4	8.01	10.36	8.20	6.83	5.36	4.28	3.02	2.23	1.63	7.25
					1	10.08	13.31	10.66	8.88	6.92	5.52	3.89	2.99	2.12	9.25
					2	10.18	13.29	10.68	8.90	6.95	5.53	3.73	2.95	2.14	9.22
					3	9.96	13.12	10.57	8.80	6.89	5.48	3.77	2.95	2.08	9.18
					4	10.03	13.22	10.66	8.89	6.94	5.52	3.89	2.98	2.09	9.20
					1	12.04	16.16	13.10	10.95	8.58	6.81	6.80	3.62	2.59	11.27
					2	11.99	16.20	13.17	11.00	8.60	6.86	5.57	3.63	2.61	11.31
					3	11.91	16.03	13.03	10.91	8.53	6.79	4.73	3.56	2.51	11.20
					4	12.04	16.03	13.06	10.90	8.55	6.81	6.19	3.58	2.57	11.23
					1	14.11	19.17	15.62	13.12	10.29	8.15	7.13	4.29	3.01	13.39
					2	14.11	19.25	15.72	13.20	10.36	8.24	8.22	4.28	3.10	13.43
					3	14.09	19.27	15.75	13.20	10.35	8.22	7.23	4.27	3.09	13.43
					4	14.04	19.22	15.69	13.17	10.32	8.20	8.87	4.28	3.00	13.40
					1	16.11	22.06	18.01	15.15	11.89	9.44	8.34	5.05	3.50	15.39
					2	15.94	21.98	17.97	15.14	11.91	9.44	10.33	4.95	3.43	15.36
					3	15.97	22.12	18.02	15.21	11.93	9.45	11.87	4.91	3.46	15.40
					4	15.87	21.99	17.97	15.15	11.90	9.42	11.93	4.81	3.43	15.36
9	3	5.5	14.0	69.5	1	8.01	8.72	6.98	5.96	4.82	3.99	2.78	2.03	1.55	6.33
					2	8.11	8.65	6.96	5.94	4.84	3.99	2.87	2.11	1.56	6.32
					3	7.98	8.49	6.84	5.85	4.77	3.96	2.76	2.00	1.55	6.22
					4	8.01	8.44	6.81	5.83	4.75	3.93	2.72	2.00	1.56	6.17
					1	9.96	10.75	8.78	7.52	6.07	5.01	3.52	2.62	1.99	7.82
					2	10.06	10.83	8.87	7.59	6.13	5.06	3.59	2.65	1.99	7.87
					3	9.94	10.78	8.86	7.57	6.13	5.07	3.61	2.67	1.98	7.82
					4	10.08	10.82	8.87	7.61	6.14	5.09	3.61	2.66	2.00	7.85
					1	11.99	13.07	10.79	9.26	7.55	6.15	4.94	3.19	2.40	9.46
					2	12.06	13.13	10.86	9.33	7.58	6.18	4.56	3.20	2.44	9.52
					3	11.96	13.08	10.83	9.29	7.57	6.19	4.35	3.19	2.41	9.49
					4	11.96	13.10	10.86	9.33	7.58	6.18	4.98	3.22	2.44	9.51
					1	13.89	15.21	12.64	10.89	8.89	7.23	5.74	3.71	2.82	11.04
					2	14.04	15.52	12.89	11.10	9.03	7.40	10.25	3.72	2.89	11.24
					3	14.06	15.55	12.96	11.15	9.03	7.43	8.68	3.75	2.89	11.28
					4	14.14	15.57	12.97	11.18	9.06	7.47	5.30	3.77	2.89	11.30
					1	16.06	17.80	14.84	12.78	10.40	8.55	8.35	4.46	3.33	12.94
					2	16.06	17.88	14.95	12.86	10.49	8.61	11.43	4.45	3.36	12.98
					3	16.02	17.90	14.95	12.86	10.54	8.60	13.50	4.45	3.37	12.98
					4	16.04	17.94	14.98	12.92	10.54	8.61	10.46	4.51	3.37	13.03

Table A-1 Continued

Test Section	Test Location	HMA Thickness (in.)	Base Thickness (in.)	Pavement Surface Temperature (°F)	Drop	Load (1000 lb)	Deflection (mils)								
							0 in.	8 in.	12 in.	18 in.	24 in.	36 in.	48 in.	60 in.	-12 in.
9	4	5.5	14.0	70.0	1	7.91	8.11	6.63	5.70	4.66	3.91	2.79	2.12	1.61	5.99
					2	8.15	8.21	6.70	5.76	4.71	3.93	2.74	2.15	1.62	6.05
					3	8.08	8.09	6.65	5.72	4.70	3.92	2.73	2.12	1.62	5.99
					4	7.96	7.98	6.57	5.66	4.63	3.89	2.69	2.18	1.60	5.91
					1	10.03	10.21	8.41	7.26	5.92	4.97	3.47	2.69	2.05	7.56
					2	9.96	10.13	8.39	7.25	5.91	4.92	3.46	2.66	2.05	7.48
					3	10.08	10.24	8.50	7.32	5.98	5.00	3.51	2.76	2.08	7.58
					4	9.99	10.20	8.45	7.29	5.96	4.98	3.51	2.74	2.06	7.53
					1	12.21	12.55	10.43	9.04	7.36	6.12	4.37	3.30	2.54	9.27
					2	12.01	12.46	10.39	8.96	7.33	6.08	4.34	3.30	2.51	9.17
					3	12.04	12.50	10.39	8.98	7.33	6.06	4.36	3.28	2.49	9.17
					4	12.11	12.50	10.42	9.00	7.36	6.10	4.32	3.24	2.51	9.21
					1	14.11	14.74	12.28	10.63	8.70	7.20	5.09	3.84	2.94	10.91
					2	14.01	14.73	12.29	10.65	8.70	7.22	5.08	3.89	2.95	10.87
					3	14.11	14.80	12.35	10.72	8.75	7.24	5.19	3.90	2.98	10.91
					4	13.99	14.72	12.28	10.62	8.69	7.22	5.10	3.84	2.98	10.87
					1	16.02	16.91	14.13	12.22	10.00	8.28	7.34	4.49	3.39	12.45
					2	16.14	17.09	14.26	12.37	10.11	8.35	5.96	4.55	3.38	12.60
					3	15.97	17.00	14.21	12.30	10.09	8.34	7.17	4.49	3.42	12.59
					4	15.94	17.11	14.19	12.32	10.08	8.32	7.34	4.58	3.43	12.54
9	5	5.5	14.0	69.5	1	8.01	9.03	7.22	6.03	4.73	3.95	2.82	2.39	1.62	6.31
					2	8.01	8.94	7.17	5.99	4.68	3.91	2.72	2.14	1.61	6.26
					3	7.89	8.81	7.11	5.92	4.68	3.87	2.73	2.52	1.63	6.19
					4	8.01	8.91	7.17	5.99	4.71	3.92	2.80	2.14	1.61	6.25
					1	9.94	11.26	9.15	7.65	5.95	4.93	3.53	2.69	2.03	7.87
					2	9.99	11.29	9.19	7.69	5.98	4.97	3.47	2.68	2.04	7.86
					3	9.96	11.33	9.20	7.70	6.00	4.95	3.48	2.70	2.05	7.89
					4	9.99	11.34	9.21	7.71	5.98	4.96	3.49	2.71	2.06	7.93
					1	11.84	13.63	11.16	9.36	7.27	5.98	4.27	3.15	2.45	9.49
					2	11.94	13.82	11.34	9.50	7.41	6.07	4.26	3.20	2.51	9.59
					3	11.91	13.83	11.35	9.53	7.44	6.08	4.31	3.22	2.48	9.61
					4	11.91	13.85	11.38	9.54	7.45	6.08	4.32	3.21	2.48	9.62
					1	13.92	16.19	13.31	11.17	8.73	7.09	10.01	3.76	2.90	11.24
					2	13.99	16.50	13.57	11.39	8.91	7.26	6.04	3.78	2.94	11.45
					3	13.89	16.45	13.57	11.39	8.89	7.26	6.70	3.77	2.96	11.46
					4	13.94	16.48	13.60	11.42	8.94	7.29	7.54	3.77	2.97	11.47
					1	15.84	18.79	15.48	13.00	10.16	8.28	11.88	4.28	3.40	13.04
					2	15.99	19.13	15.72	13.22	10.34	8.44	6.89	4.46	3.46	13.24
					3	15.97	19.12	15.74	13.26	10.40	8.42	10.08	4.43	3.42	13.28
					4	15.99	19.20	15.82	13.32	10.42	8.48	7.06	4.47	3.43	13.33

Table A-1 Continued

Test Section	Test Location	HMA Thickness (in.)	Base Thickness (in.)	Pavement Surface Temperature (°F)	Drop	Load (1000 lb)	Deflection (mils)								
							0 in.	8 in.	12 in.	18 in.	24 in.	36 in.	48 in.	60 in.	-12 in.
10	1	5.5	14.0	69.0	1	8.03	6.20	4.53	3.62	2.74	2.05	1.32	1.49	0.75	4.13
					2	8.06	6.10	4.46	3.57	2.69	2.04	1.31	1.58	0.88	4.08
					3	8.15	6.11	4.49	3.61	2.71	2.07	1.30	1.57	0.85	4.08
					4	8.01	6.01	4.44	3.55	2.69	2.03	1.29	1.62	0.96	4.00
					1	10.08	7.78	5.85	4.71	3.51	2.68	1.71	1.52	0.99	5.11
					2	9.99	7.69	5.79	4.67	3.49	2.65	1.68	2.08	0.98	5.06
					3	9.99	7.70	5.80	4.68	3.48	2.65	1.66	1.44	0.99	5.05
					4	9.99	7.67	5.79	4.66	3.47	2.65	1.66	1.51	0.98	5.04
					1	12.06	9.32	7.11	5.73	4.31	3.23	2.02	1.59	1.18	6.06
					2	12.11	9.35	7.15	5.77	4.33	3.25	2.03	1.59	1.16	6.09
					3	11.96	9.27	7.08	5.72	4.32	3.24	2.06	1.63	1.15	6.06
					4	11.94	9.25	7.09	5.72	4.28	3.25	2.03	1.62	1.17	6.03
					1	13.75	10.64	8.16	6.60	4.99	3.74	2.32	1.82	1.33	6.91
					2	14.09	10.96	8.44	6.82	5.13	3.85	2.38	1.84	1.38	7.12
					3	14.21	11.07	8.53	6.92	5.23	3.92	2.39	1.92	1.39	7.20
					4	14.18	11.08	8.54	6.91	5.22	3.92	5.70	1.88	1.39	7.19
					1	16.14	12.64	9.76	7.91	5.98	4.48	7.37	2.21	1.57	8.16
					2	16.11	12.66	9.79	7.95	5.99	4.49	2.76	2.16	1.57	8.17
					3	16.09	12.67	9.79	7.95	5.98	4.50	2.78	2.15	1.57	8.16
					4	15.92	12.51	9.70	7.88	5.92	4.47	2.76	2.10	1.56	8.10
10	2	5.5	14.0	70.5	1	8.18	6.78	4.99	3.98	2.89	2.12	1.43	1.32	0.73	4.42
					2	8.18	6.69	4.96	3.94	2.89	2.11	1.37	1.21	0.72	4.34
					3	7.98	6.49	4.81	3.83	2.80	2.07	1.31	1.32	0.82	4.21
					4	7.98	6.48	4.81	3.81	2.78	2.05	1.32	1.24	0.71	4.17
					1	10.40	8.38	6.27	5.02	3.67	2.72	1.82	1.20	0.90	5.41
					2	9.86	8.06	6.02	4.83	3.51	2.62	1.72	1.16	0.86	5.24
					3	9.84	8.11	6.07	4.86	3.52	2.62	1.73	1.22	0.87	5.27
					4	9.86	8.12	6.07	4.87	3.54	2.63	1.72	1.21	0.86	5.26
					1	11.96	9.89	7.44	5.98	4.40	3.22	2.11	1.41	1.05	6.36
					2	12.08	9.98	7.51	6.03	4.42	3.25	2.18	1.42	1.05	6.45
					3	11.96	9.88	7.46	6.00	4.39	3.24	2.15	1.43	1.05	6.38
					4	12.01	9.87	7.45	5.99	4.39	3.20	2.18	1.42	1.05	6.40
					1	13.94	11.48	8.70	7.00	5.14	3.79	2.48	1.61	1.22	7.38
					2	14.04	11.56	8.79	7.08	5.18	3.83	3.22	1.63	1.24	7.43
					3	14.06	11.59	8.80	7.10	5.21	3.85	2.76	1.66	1.24	7.45
					4	14.06	11.60	8.84	7.11	5.22	3.85	5.62	1.70	1.24	7.45
					1	16.19	13.30	10.13	8.16	6.00	4.42	9.77	1.84	1.42	8.56
					2	15.99	13.21	10.06	8.08	5.94	4.40	6.02	1.91	1.41	8.51
					3	15.94	13.17	10.02	8.07	5.93	4.40	8.99	1.91	1.39	8.47
					4	15.94	13.16	10.02	8.08	5.93	4.37	8.83	1.89	1.41	8.46

Table A-1 Continued

Test Section	Test Location	HMA Thickness (in.)	Base Thickness (in.)	Pavement Surface Temperature (°F)	Drop	Load (1000 lb)	Deflection (mils)								
							0 in.	8 in.	12 in.	18 in.	24 in.	36 in.	48 in.	60 in.	-12 in.
10	3	5.5	14.0	69.0	1	8.18	7.34	5.53	4.33	3.08	2.27	1.35	1.09	0.76	4.54
					2	8.30	7.31	5.50	4.33	3.06	2.25	1.33	1.15	0.80	4.53
					3	8.30	7.23	5.45	4.30	3.04	2.24	1.33	1.10	0.75	4.50
					4	8.20	7.17	5.43	4.26	3.02	2.22	1.29	1.09	0.74	4.45
					1	10.06	8.91	6.77	5.32	3.80	2.80	1.63	1.22	0.95	5.53
					2	10.06	8.83	6.71	5.31	3.77	2.79	1.66	1.18	0.93	5.51
					3	10.01	8.84	6.74	5.31	3.76	2.79	1.66	1.21	0.94	5.49
					4	10.23	8.90	6.79	5.35	3.81	2.81	1.66	1.19	0.95	5.59
					1	12.06	10.59	8.16	6.44	4.59	3.38	1.99	1.41	1.14	6.58
					2	12.04	10.64	8.20	6.46	4.63	3.37	2.00	1.43	1.15	6.63
					3	11.96	10.60	8.17	6.44	4.59	3.38	1.98	1.42	1.16	6.59
					4	11.89	10.50	8.11	6.40	4.57	3.36	1.95	1.42	1.12	6.54
					1	14.06	12.42	9.58	7.57	5.45	3.95	2.33	1.64	1.32	7.68
					2	14.11	12.44	9.61	7.60	5.44	3.98	2.33	1.62	1.32	7.69
					3	14.11	12.43	9.62	7.60	5.46	4.01	2.35	1.61	1.34	7.73
					4	13.92	12.32	9.55	7.55	5.41	3.98	2.33	1.60	1.34	7.67
					1	15.94	14.09	10.88	8.63	6.22	4.56	2.74	1.88	1.59	8.76
					2	16.09	14.24	11.01	8.74	6.27	4.60	2.70	1.92	1.56	8.86
					3	16.04	14.21	11.00	8.72	6.27	4.61	2.68	1.92	1.55	8.86
					4	16.06	14.25	11.03	8.76	6.25	4.60	2.69	1.93	1.49	8.87
10	4	5.5	14.0	67.5	1	8.03	6.97	4.87	3.79	2.74	2.06	1.33	1.16	0.78	4.52
					2	8.01	6.82	4.78	3.74	2.70	2.04	1.33	1.27	0.80	4.44
					3	8.11	6.85	4.83	3.78	2.73	2.07	1.35	1.22	0.77	4.46
					4	8.03	6.75	4.77	3.72	2.70	2.04	1.31	1.26	0.77	4.38
					1	9.86	8.54	6.10	4.77	3.45	2.60	1.69	1.24	0.95	5.49
					2	9.91	8.54	6.13	4.79	3.48	2.59	1.71	1.42	0.98	5.49
					3	9.89	8.58	6.15	4.82	3.47	2.59	1.73	1.33	0.96	5.49
					4	10.01	8.71	6.21	4.88	3.56	2.66	1.73	1.29	0.99	5.57
					1	11.84	10.50	7.56	5.94	4.31	3.20	2.11	1.50	1.16	6.60
					2	11.89	10.51	7.64	5.99	4.36	3.26	2.12	1.54	1.18	6.65
					3	11.84	10.47	7.65	6.01	4.36	3.25	2.05	1.60	1.18	6.64
					4	11.94	10.52	7.70	6.05	4.41	3.28	2.17	1.55	1.17	6.66
					1	13.94	12.36	9.12	7.19	5.20	3.86	6.68	1.82	1.39	7.82
					2	13.96	12.52	9.20	7.27	5.26	3.89	10.31	1.83	1.38	7.87
					3	14.04	12.62	9.23	7.29	5.27	3.90	2.51	1.81	1.40	7.92
					4	13.96	12.48	9.21	7.26	5.28	3.91	9.29	1.81	1.39	7.89
					1	15.94	14.32	10.63	8.39	6.08	4.51	10.57	2.11	1.60	9.02
					2	16.02	14.52	10.73	8.47	6.12	4.52	12.97	2.40	1.61	9.08
					3	16.04	14.44	10.77	8.51	6.18	4.56	11.18	2.23	1.63	9.11
					4	16.09	14.48	10.81	8.54	6.21	4.58	11.83	2.18	1.62	9.15

Table A-1 Continued

Test Section	Test Location	HMA Thickness (in.)	Base Thickness (in.)	Pavement Surface Temperature (°F)	Drop	Load (1000 lb)	Deflection (mils)								
							0 in.	8 in.	12 in.	18 in.	24 in.	36 in.	48 in.	60 in.	-12 in.
10	5	5.5	14.0	67.5	1	8.08	8.56	6.41	5.23	3.93	3.01	1.93	1.80	1.11	5.98
					2	7.93	8.47	6.39	5.20	3.91	3.00	1.96	1.84	1.13	5.91
					3	8.01	8.42	6.35	5.18	3.90	3.02	1.95	1.89	1.13	5.89
					4	8.11	8.51	6.44	5.26	3.97	3.06	1.96	1.52	1.13	5.95
					1	9.99	10.64	8.07	6.62	4.98	3.80	2.49	1.91	1.41	7.42
					2	10.01	10.64	8.11	6.65	4.99	3.83	2.53	1.91	1.42	7.42
					3	9.96	10.59	8.08	6.61	4.98	3.80	2.54	1.90	1.42	7.36
					4	9.96	10.63	8.11	6.65	5.00	3.81	2.56	1.93	1.43	7.39
					1	11.87	12.85	9.90	8.13	6.16	4.67	3.08	2.33	1.71	8.86
					2	11.91	12.96	10.01	8.22	6.22	4.71	5.97	2.34	1.73	8.93
					3	11.91	12.99	10.02	8.25	6.24	4.72	3.11	2.34	1.75	8.95
					4	11.89	12.94	10.02	8.24	6.22	4.71	4.04	2.31	1.73	8.91
					1	13.92	15.14	11.77	9.70	7.32	5.52	12.05	2.74	1.97	10.43
					2	13.94	15.34	11.93	9.84	7.42	5.62	10.11	2.76	2.06	10.54
					3	13.99	15.41	11.97	9.87	7.44	5.64	6.42	2.79	2.05	10.60
					4	14.06	15.41	12.01	9.90	7.45	5.67	11.25	2.77	2.06	10.60
					1	15.89	17.47	13.63	11.25	8.50	6.43	10.74	3.19	2.26	11.99
					2	15.99	17.70	13.78	11.38	8.59	6.51	10.49	3.33	2.35	12.12
					3	16.06	17.79	13.84	11.44	8.63	6.55	13.08	3.35	2.35	12.18
					4	15.89	17.68	13.79	11.38	8.60	6.52	10.75	3.27	2.29	12.11

APPENDIX B DYNAMIC CONE PENETROMETER DATA

Table B-1 presents the individual DCP test values collected in this research, and Figures B-1 through B-16 provide corresponding DCP profiles for test locations at which the base layer was fully penetrated by the DCP; in many cases, the base layer was too stiff to be fully penetrated, resulting in refusal as indicated by a hyphen in Table B-1.

Table B-1: DCP Data for October 10, 2015, at Wells Draw Road

Test Section	Layer	Measurement	Test Location		
			1	3	5
1	Base	Penetration Rate (mm/blow)	1.41	0.99	1.30
		CBR (%)	199	294	218
	Subgrade	Penetration Rate (mm/blow)	8.05	7.14	5.84
		CBR (%)	28	32	40
2	Base	Penetration Rate (mm/blow)	-	-	2.46
		CBR (%)	-	-	106
	Subgrade	Penetration Rate (mm/blow)	-	-	10.60
		CBR (%)	-	-	21
3	Base	Penetration Rate (mm/blow)	-	-	1.04
		CBR (%)	-	-	278
	Subgrade	Penetration Rate (mm/blow)	-	-	11.94
		CBR (%)	-	-	18
4	Base	Penetration Rate (mm/blow)	1.42	-	-
		CBR (%)	197	-	-
	Subgrade	Penetration Rate (mm/blow)	8.63	-	-
		CBR (%)	26	-	-

Table B-1 Continued

Test Section	Layer	Measurement	Test Location		
			1	3	5
5	Base	Penetration Rate (mm/blow)	-	1.13	-
		CBR (%)	-	255	-
	Subgrade	Penetration Rate (mm/blow)	-	5.71	-
		CBR (%)	-	41	-
6	Base	Penetration Rate (mm/blow)	-	-	-
		CBR (%)	-	-	-
	Subgrade	Penetration Rate (mm/blow)	-	-	-
		CBR (%)	-	-	-
7	Base	Penetration Rate (mm/blow)	2.03	1.47	1.45
		CBR (%)	132	190	193
	Subgrade	Penetration Rate (mm/blow)	7.09	4.52	2.35
		CBR (%)	33	54	112
8	Base	Penetration Rate (mm/blow)	1.49	-	1.05
		CBR (%)	186	-	276
	Subgrade	Penetration Rate (mm/blow)	3.63	-	2.27
		CBR (%)	69	-	117
9	Base	Penetration Rate (mm/blow)	2.83	-	1.82
		CBR (%)	91	-	149
	Subgrade	Penetration Rate (mm/blow)	10.64	-	3.77
		CBR (%)	21	-	66
10	Base	Penetration Rate (mm/blow)	-	1.56	1.80
		CBR (%)	-	178	151
	Subgrade	Penetration Rate (mm/blow)	-	3.83	6.41
		CBR (%)	-	65	36

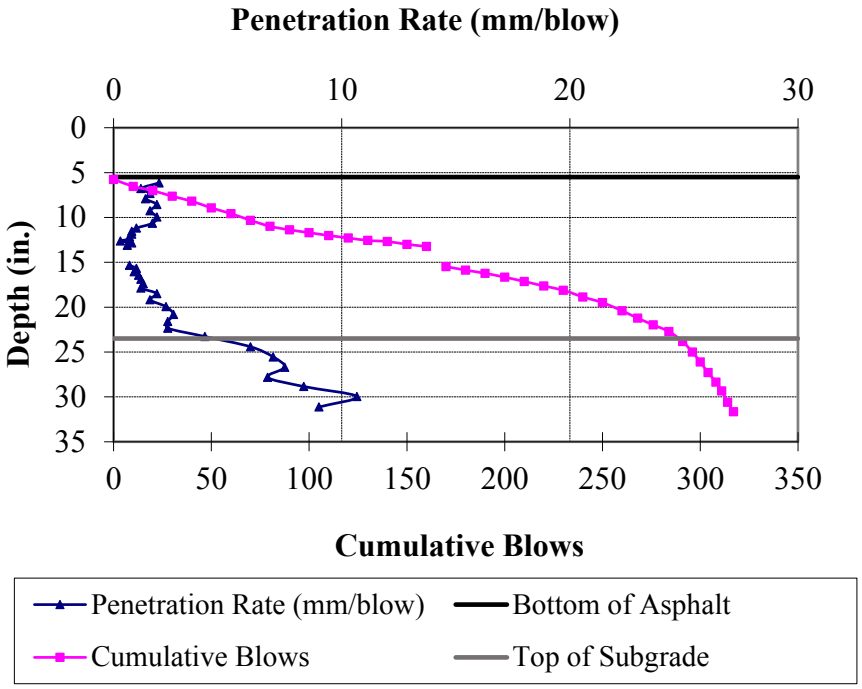

Figure B-1: DCP profile for test location 1 in test section 1.

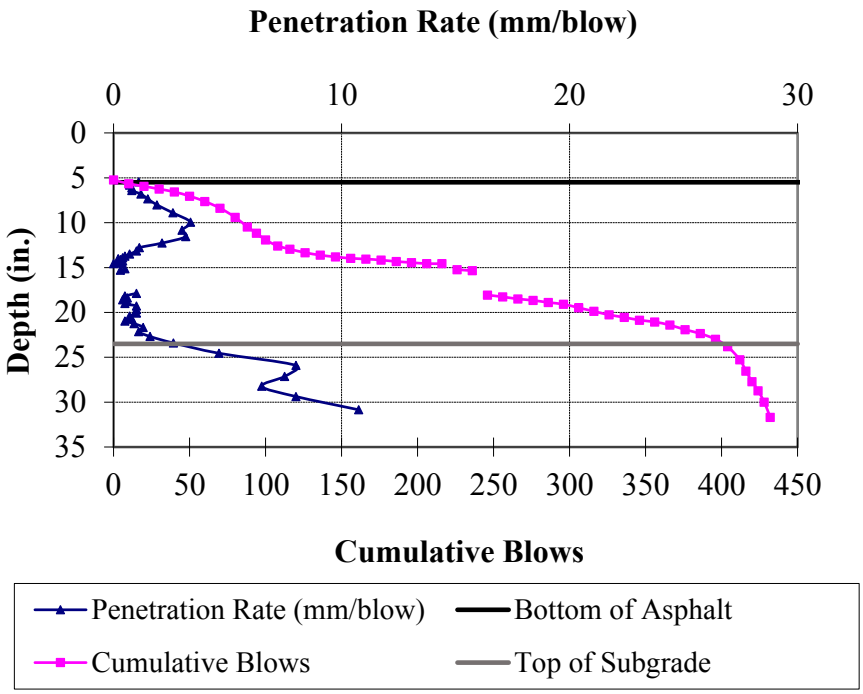

Figure B-2: DCP profile for test location 3 in test section 1.

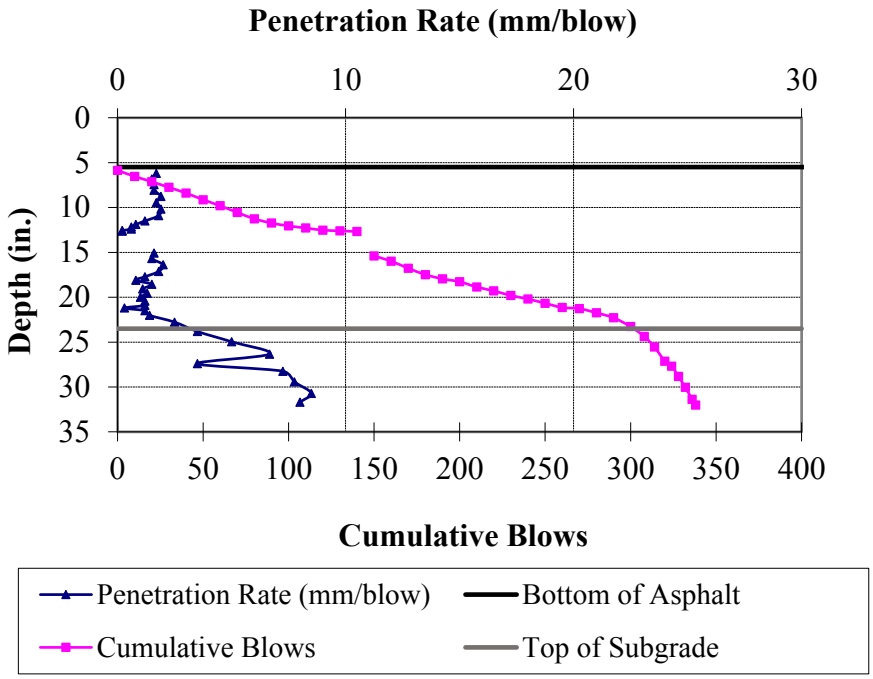

Figure B-3: DCP profile for test location 5 in test section 1.

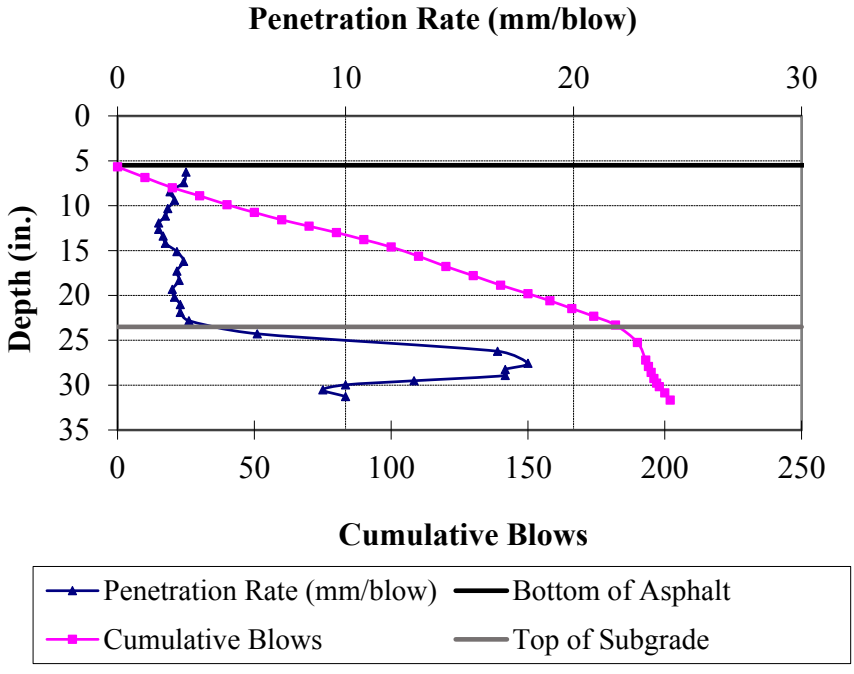

Figure B-4: DCP profile for test location 5 in test section 2.

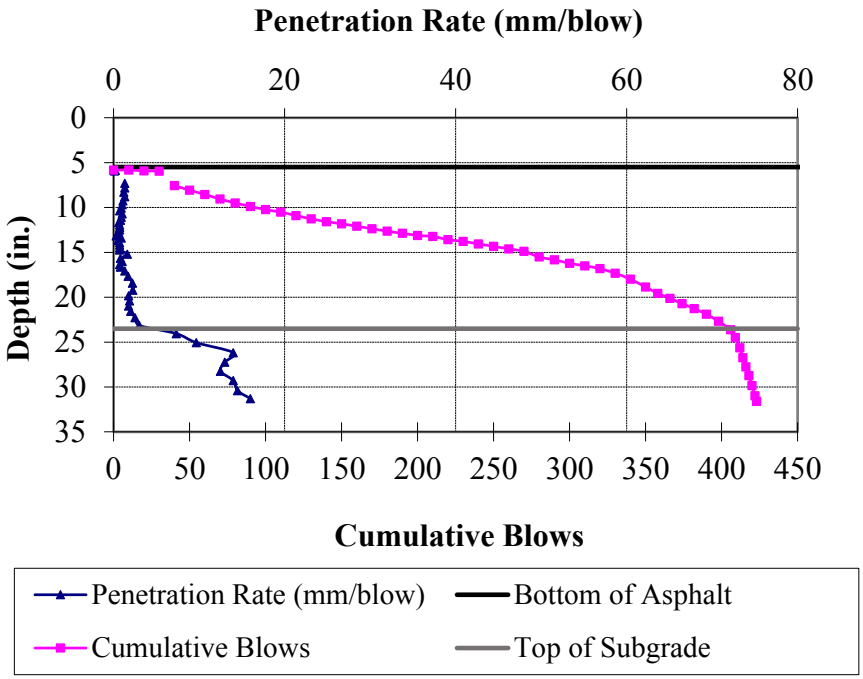

Figure B-5: DCP profile for test location 5 in test section 3.

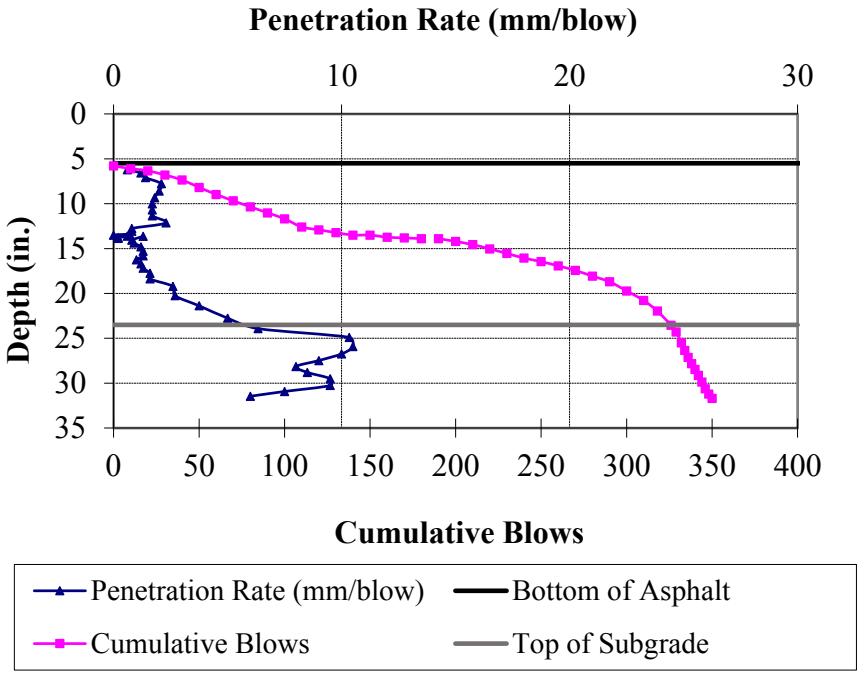

Figure B-6: DCP profile for test location 1 in test section 4.

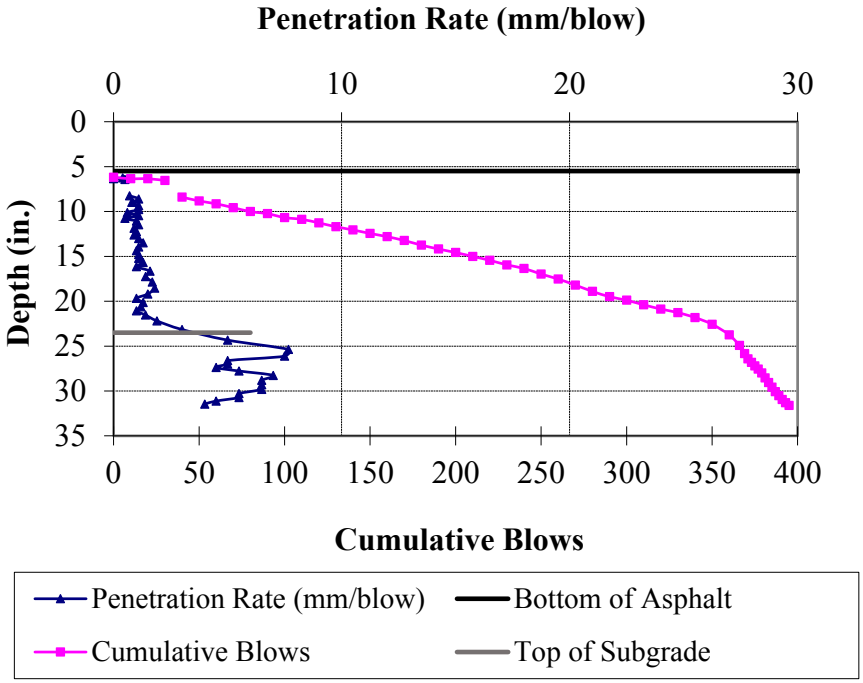

Figure B-7: DCP profile for test location 3 in test section 5.

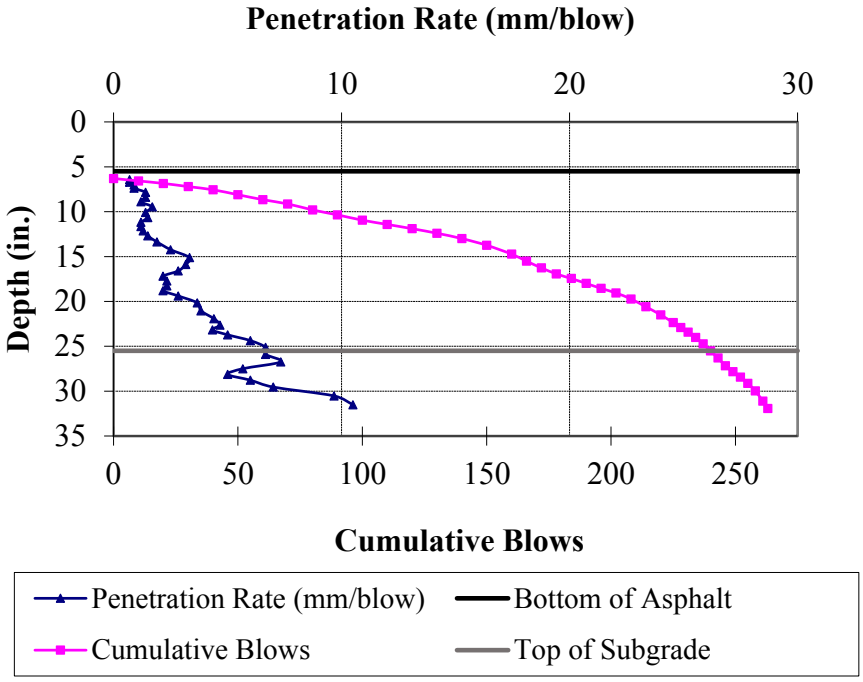

Figure B-8: DCP profile for test location 1 in test section 7.

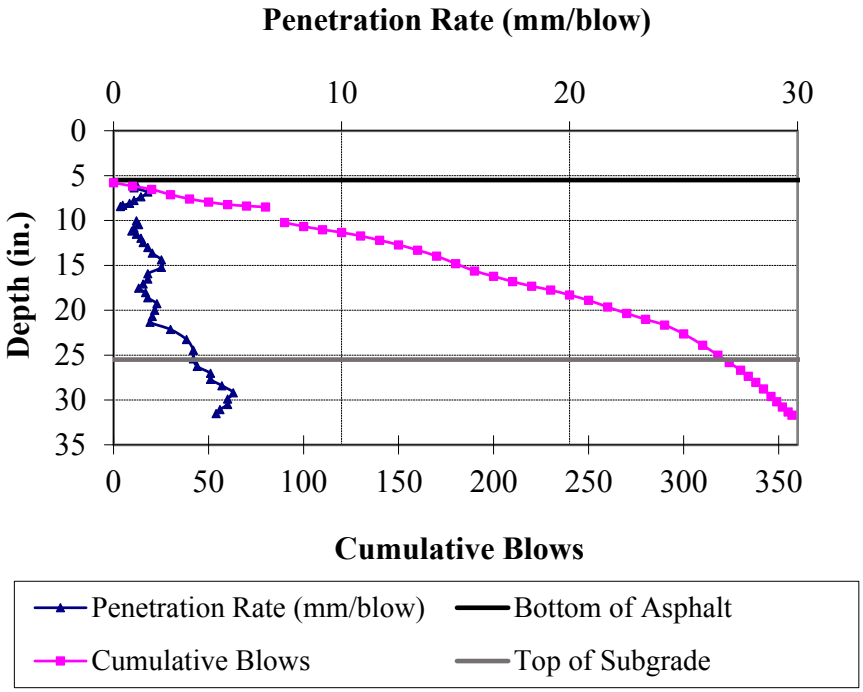

Figure B-9: DCP profile for test location 3 in test section 7.

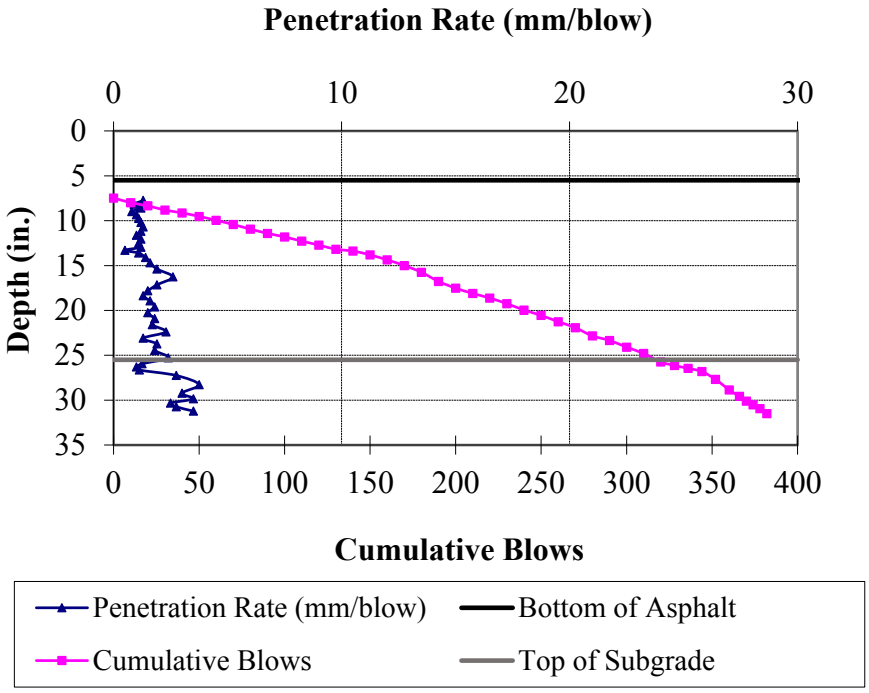

Figure B-10: DCP profile for test location 5 in test section 7.

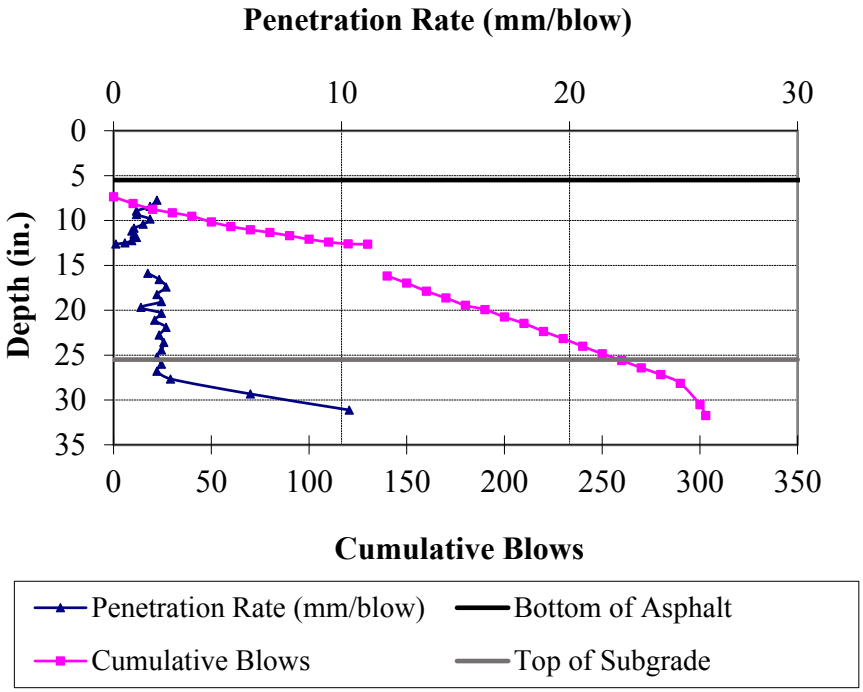

Figure B-11: DCP profile for test location 1 in test section 8.

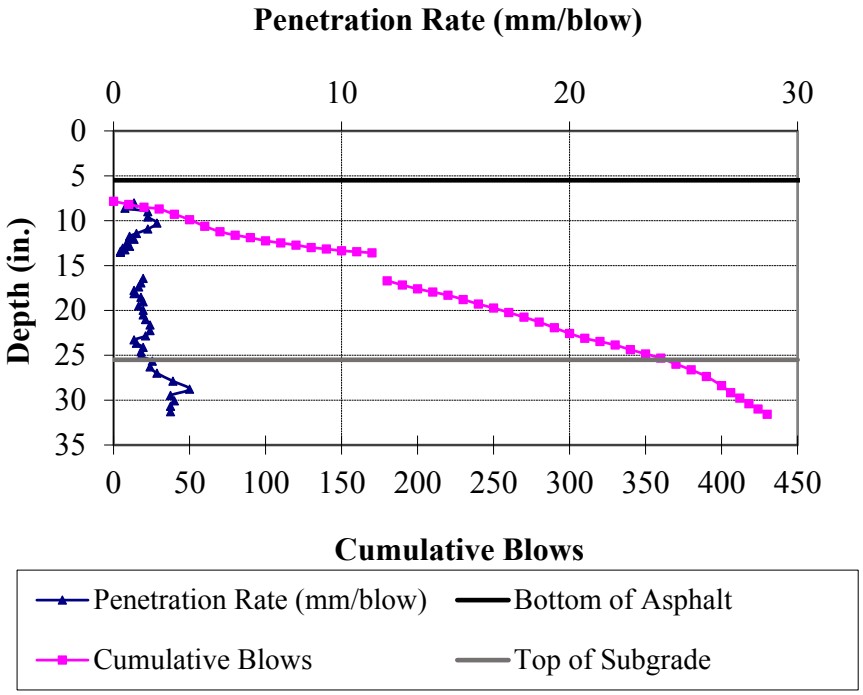

Figure B-12: DCP profile for test location 5 in test section 8.

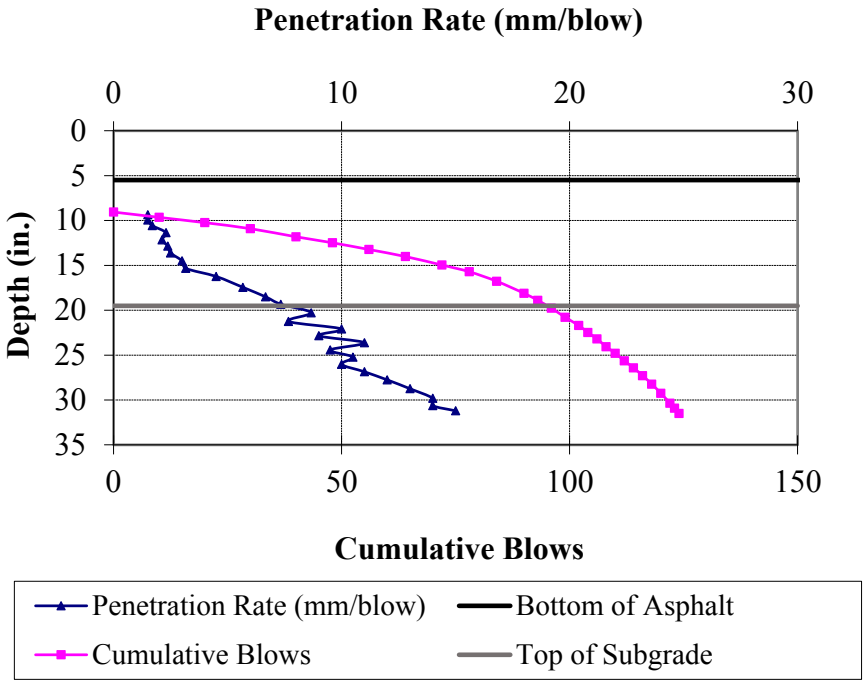

Figure B-13: DCP profile for test location 1 in test section 9.

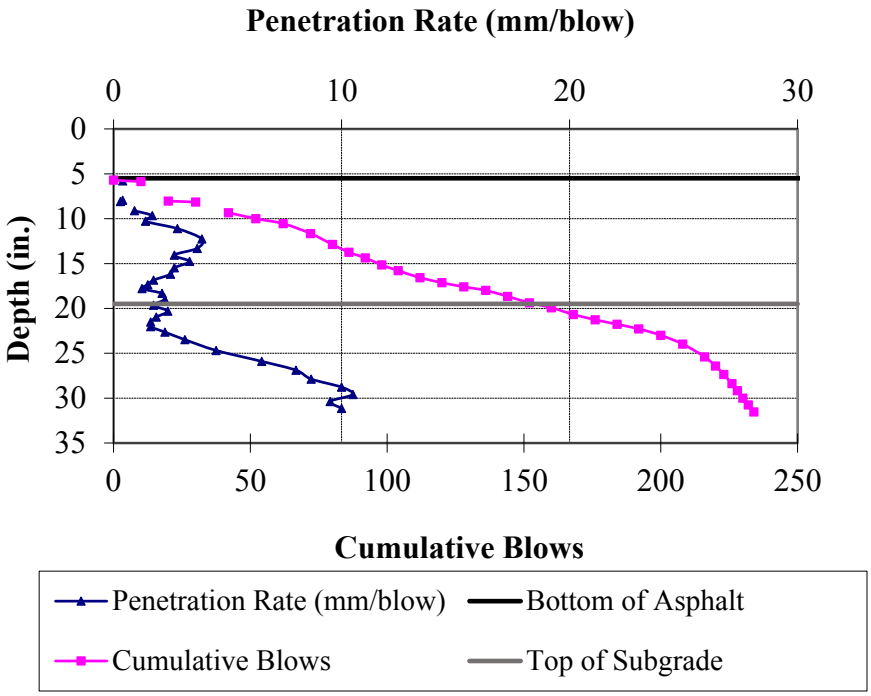

Figure B-14: DCP profile for test location 5 in test section 9.

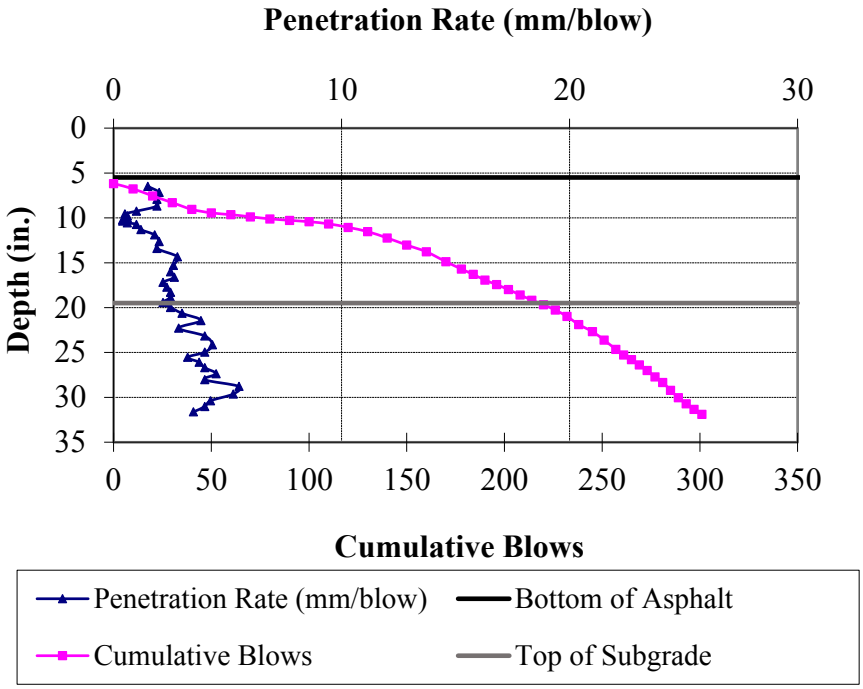

Figure B-15: DCP profile for test location 3 in test section 10.

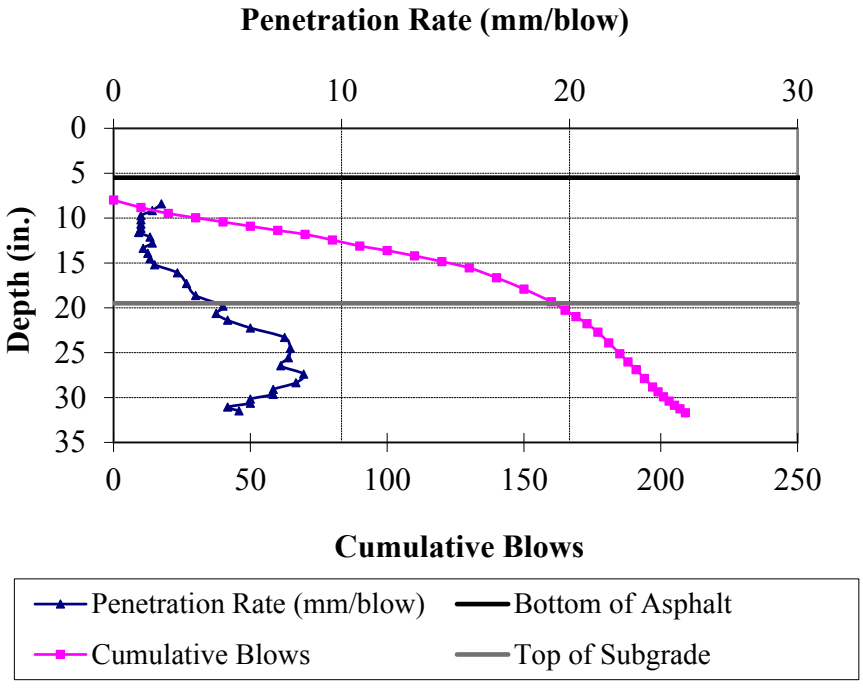

Figure B-16: DCP profile for test location 5 in test section 10.

APPENDIX C PAVEMENT ANALYSES

Tables C-1 and C-2 present the results of pavement analyses performed on the base layer coefficients and AUPP values obtained using the Rohde's method and the AUPP method, respectively.

Table C-1. Pavement Analysis for Rohde's Method

Test Section	a_2	Allowable ESALs
1	0.15	10,623,700
2	0.14	8,389,300
3	0.17	17,037,900
4	0.15	10,623,700
5	0.17	17,037,900
6	0.18	19,190,900
7	0.15	10,623,700
8	0.16	14,078,500
9	0.13	7,064,100
10	0.12	5,866,900

Table C-2. Pavement Analysis for AUPP Method

Test Section	AUPP, mm (in.)	Allowable ESALs
1	229 (9.02)	13,557,287
2	264 (10.41)	8,425,145
3	220 (8.66)	15,522,497
4	260 (10.22)	8,942,616
5	224 (8.82)	14,633,752
6	213 (8.38)	17,341,642
7	273 (10.76)	7,536,431
8	231 (9.11)	13,145,985
9	303 (11.94)	5,345,294
10	340 (13.37)	3,663,279